**Atmospheric and
Environmental Research, Inc.**

PERFORMANCE EVALUATION OF CMAQ AND PM-CAMx
FOR THE JULY 1999 SOS EPISODE

CRC Project Number A-40-1

Prepared by

Yang Zhang, Betty Pun, Shiang-Yuh Wu, Krish Vijayaraghavan, Gopi K. Yelluru, and
Christian Seigneur
Atmospheric & Environmental Research, Inc.
2682 Bishop Drive, Suite 120
San Ramon, CA

Prepared for

Coordinating Research Council, Inc.
Alpharetta, GA

Document Number CP131-03-02
October 2003

TABLE OF CONTENTS

TABLE OF CONTENTS (CONTINUED)

LIST OF FIGURES

LIST OF FIGURES (CONTINUED)

LIST OF TABLES

ACKNOWLEDGMENTS

LEGAL NOTICE

GLOSSARY OF ABBREVIATIONS

2-D: Two-Dimensional

3-D: Three-Dimensional

AER: Atmospheric & Environmental Research, Inc.

AIRS: Aerometric Information Reporting System monitoring network

BC: Black Carbon

BCs: Boundary Conditions

BHM: Birmingham, AL

BRAVO: Big Bend Regional Aerosol and Visibility Observational Study

CDT: Central Day Time

CBM-IV: Carbon-bond mechanism version IV

CF: Cornelia Fort, TN

CMAQ: EPA Models-3 Community Multiscale Air Quality Modeling System

CMC: Chemical Mechanism Compiler

CMU: Carnegie-Mellon University

CO: Carbon monoxide

CPU: Central Processing Unit

CRC: Coordinating Research Council

CRPAQS: California Regional PM Air Quality Study

CTR: Centreville, AL

DI: Dickson, Tennessee

EC: Elemental Carbon

ENVIRON: ENVIRON International Corporation

EPA: United States Environmental Protection Agency

EPRI: formerly Electric Power Research Institute

GRSM: Great Smoky Mountains National Park

HEN: Hendersonville, Tennessee

ICs: Initial Conditions

IMPROVE:	Interagency Monitoring of Protected Visual Environments
ISORROPIA:	Equilibrium in Greek
JPROC:	Preprocessor for photolytic rate
JST:	Jefferson Street, Atlanta, Georgia
MACA:	Mammoth Cave National Park
MEBI:	Modified Euler Backward Iterative algorithm
MM5:	Mesoscale Meteorological model 5th generation
NARSTO:	formerly North American Research Strategy for Tropospheric Ozone
netCDF:	Network Common Data Format
MADRID:	Model of Aerosol Dynamics, Reaction, Ionization, and Dissolution
MCIP:	Meteorology-Chemistry Interface Processor
MCNC:	formerly Microelectronics Center of North Carolina
MM5CAMx:	CAMx pre-processor for MM5
MNB:	Mean Normalized Bias
MNGE:	Mean Normalized Gross Error
OC:	Organic Carbon
OI:	Other inorganic species
OM:	Organic Material
PAVE:	Package for Analysis and Visualization of Environmental Data
PBL:	Planetary Boundary Layer
PM:	Particulate Matter
$PM_{2.5}$:	PM with aerodynamic diameter less than 2.5 μm
PM_{10}:	PM with aerodynamic diameter less than 10 μm
PM-CAMx:	Particulate Matter Comprehensive Air Quality Model with Extensions
RADM:	Regional Acid Deposition Model chemical kinetic mechanism
RADM2:	Regional Acid Deposition Model chemical kinetic mechanism version 2
REMSAD:	Regional Modeling System for Aerosols and Deposition
SEARCH:	Southeastern Aerosol Research and Characterization study

SHRO:	Shining Rock Wilderness Area
SIPS:	Sipsey Wilderness Area, AL
SMOKE:	Sparse Matrix Operator Kernel Emissions System
SOS:	Southern Oxidants Study
TEOM:	Tapered Element Oscillating Microbalance
TKE:	Turbulent Kinetic Energy
TVA:	Tennessee Valley Authority
UAM-IV:	Urban Airshed Model, version IV
UAM-VPM:	Variable-Grid Urban Airshed Model with Particulate Matter
U.S.	United State of America
VOC:	Volatile organic compounds
YRK:	Yorkville, Georgia

EXECUTIVE SUMMARY

CMAQ (EPA July 2002 version) and PM-CAMx (version 3.01) were applied to simulate the 29 June – 11 July 1999 episode of the Southern Oxidants Study (SOS). Both models used the Carbon-Bond Mechanism version IV for gas-phase chemistry. The modeling domain consists of two nested grids: the outer grid covers the contiguous United States (U.S.) with a 32 km horizontal resolution; the inner grid covers an area of the southeastern U.S. that includes Atlanta and Nashville with an 8 km horizontal resolution. Nineteen layers were used for both grids. The simulation results were evaluated with available data following a modeling protocol developed earlier.

E.1 Model Performance for Ozone Mixing Ratios

The spatial distributions of O_3 mixing ratios predicted by CMAQ and PM-CAMx are somewhat different, especially over the eastern and southeastern U.S., where PM-CAMx tends to overpredict O_3 mixing ratios.

Over the southeastern U.S. domain, the mean normalized gross error (MNGE) and mean normalized bias (MNB) for CMAQ using the 8 km resolution results with a 60 ppb threshold for observed O_3 values were 17% and -1%, respectively. The corresponding MNGE and MNB for PM-CAMx were 24% and 10%, respectively. With a 40 ppb threshold for observed O_3 values, the MNGE and MNB were 27% and 16% for CMAQ, and 41% and 33% for PM-CAMx, respectively. Model performance for CMAQ and PM-CAMx (using a 60 ppb threshold for observed O_3 concentrations) is, therefore, considered satisfactory according to EPA guidance.

E.2 Model Performance for PM Concentrations

The spatial variations of $PM_{2.5}$ and PM_{10} concentrations in the rural areas from the western to the eastern U.S. predicted by both models are generally similar. The two models, however, differ significantly in their predictions over some urban/suburban areas in the U.S., especially in the southeastern, eastern and central U.S. Those differences

between the $PM_{2.5}$ and PM_{10} predictions by the two models with the fine and coarse grids can be explained by differences in the predicted PM composition in the corresponding areas.

In the coarse grid domain, CMAQ predicts that sulfate and organic material (OM) are the largest and the second largest contributors to $PM_{2.5}$ concentrations for the eastern and southeastern U.S.; nitrate and OM tend to dominate in California. PM-CAMx predicts that sulfate is the largest contributor to $PM_{2.5}$ concentrations for the eastern and southeastern U.S., followed by either OM or ammonium or both. PM-CAMx predicts high nitrate concentrations of 5-20 μg m^{-3} in several areas including Houston, TX; southern Louisiana, Monroe, LA; Los Angeles, CA; Fort Worth, TX; Atlanta, GA; North Birmingham, AL and the adjacent area of South Dakota, Nebraska, and Iowa.

In the fine grid of the southeastern U.S. domain, CMAQ predicts sulfate to be the largest contributor in the northern portion of the domain on July 5, the northeastern portion on July 6, and the eastern and southern portions on July 7. OM is predicted to be the second largest contributor in the eastern portion on July 5 and the eastern and southern portions on July 7. The concentrations of black carbon (BC), nitrate and ammonium are below 5 μg m^{-3} in many areas of the domain. PM-CAMx predicts sulfate to be the largest contributor in the northern and eastern portions on July 5 and 6 and almost the entire domain except for a small area in the northern portion of the domain on July 7. The second largest contributor is OM in a small area in the southeastern corner on July 6 or ammonium in the northeastern portion on July 5-6 or both OM and ammonium in the southeastern portion on July 7. While the concentrations of BC are below 5 μg m^{-3} in many areas of the domain, those of nitrate can be as high as 11 μg m^{-3} in several areas including Louisville, KY on July 5 and Memphis, TN on July 6-7.

Model performance statistics for the southeastern U.S. domain with the fine grid resolution are summarized in Table E-1. The PM components (sulfate, nitrate, ammonium, OM and BC) refer to the $PM_{2.5}$ fraction. Over the southeastern U.S. domain, CMAQ with the fine grid predicts MNGEs of $\leq$ 50% and MNBs of -31 to 9% for PM_{10}, $PM_{2.5}$, $PM_{2.5}$ sulfate and $PM_{2.5}$ ammonium and MNGEs of 71-98% and MNBs of -50 to 68% for other PM components. These statistics for CMAQ are generally consistent with the performance of other current PM models.

Table E-1. Performance statistics over the fine grid domain.

Species	CMAQ		PM-CAMx	
	Mean normalized gross error (MNGE)	Mean normalized bias (MNB)	Mean normalized gross error (MNGE)	Mean Normalized bias (MNB)
PM_{10}	42.7	-17.3	58.7	14.4
$PM_{2.5}$	37.7	-6.5	49.7	9.0
Sulfate	44.8	8.7	51.7	22.9
Nitrate	97.8	-49.5	138.0	98.6
Ammonium	50.4	-30.7	90.1	49.7
BC	71.3	19.8	88.2	63.8
OM	83.9	68.2	60.1	10.3

PM-CAMx with the fine grid predicts MNGEs and MNBs of 59% and 14% for PM_{10}, 50% and 9% for $PM_{2.5}$ and 51-138% and 23-99% for PM components. The predictions of $PM_{2.5}$ nitrate have the largest MNGEs and MNBs. The significant overpredictions in PM predictions by PM-CAMx may be attributed to several major reasons including (1) the lack of wet removal for PM species in the current version of PM-CAMx; (2) a likely underprediction in the vertical mixing during the daytime; (3) the uncertainties in the gas/particle partitioning under some conditions in PM-CAMx.

For the 12-day 1999 SOS episode, CMAQ is computationally more efficient that PM-CAMx by a factor of 2.1-2.5. PM-CAMx requires more memory than CMAQ, due primarily to the use of more PM size sections (10 size sections in PM-CAMx vs. 3 modes in CMAQ).

E.3   Recommendations

The performance of CMAQ for O_3 and PM is consistent with the performance that we can currently expect for air quality models. There are, however, significant uncertainties in the chemical composition of $PM_{2.5}$ that will require further diagnostic investigations. In particular, spikes were sometimes predicted in nitrate concentrations due possibly to the inaccuracies in the aerosol activity coefficients under some conditions. Future areas of improvements in the model inputs and /or model formulation should then be identified.

The performance of PM-CAMx for both O_3 and PM is lower than that of CMAQ. The overpredictions of O_3 mixing ratios appear to be due primarily to the vertical diffusion algorithm selected for this study. The treatment of vertical diffusion also leads to overpredictions of PM concentrations. In addition, the lack of treatment for wet deposition of PM and the inaccuracies in the aerosol activity coefficients under some conditions may contribute significantly to PM overpredictions.

We recommend that (1) wet deposition of PM be incorporated into PM-CAMx, (2) a different algorithm be used for vertical diffusion (e.g., TKE) in PM-CAMx (in this case, a new MM5 simulation for the July 1999 episode will need to be conducted to output TKE values that can be used to generate vertical diffusion coefficients for input

into PM-CAMx), and (3) calculations of aerosol activity coefficients be conducted on-line (instead of using a look-up table) in both PM-CAMx and CMAQ. Such an on-line calculation can be implemented easily in ISORROPIA. PM-CAMx performance should then be reevaluated following those improvements.

1.   INTRODUCTION

Several air quality models for particulate matter (PM) are being applied to the eastern United States (U.S.) for the 29 June-11 July 1999 episode of the Southern Oxidants Study (SOS). The Tennessee Valley Authority (TVA) is applying the Environmental Protection Agency (EPA) version of the Community Multiscale Air Quality model (CMAQ) with the Regional Acid Deposition Model, Version 2 (RADM2) gas-phase chemistry. Under separate contracts, Atmospheric & Environmental Research, Inc. (AER) is applying CMAQ with two versions of the Model of Aerosol Dynamics, Reaction, Ionization, and Dissolution (MADRID). ICF Consulting is applying the Variable-Grid Urban Airshed Model with Particulate Matter (UAM-VPM) and the Regional Modeling System for Aerosols and Deposition (REMSAD). Under CRC Project Number A-40-1, AER has applied the EPA June 2002 version of CMAQ with the Carbon Bond Mechanism version IV (CBM-IV) gas-phase chemistry and PM-CAMx.

A protocol for modeling and evaluating model performance has been developed (Seigneur et al., 2002). The protocol for performance evaluation follows the general guidance provided by EPA (2001) and Seigneur et al. (2000), and is consistent with the protocol prepared by AER under a separate contract for the evaluation of the first five models mentioned above. The simulation results predicted by CMAQ and PM-CAMx have been evaluated with ambient air quality data of PM, precursors and oxidants. In this report, we present the performance evaluation for the two models. We describe first the configurations of CMAQ and PM-CAMx that are used in this study, along with the description of the modeling domain and the preparation of the input files. We describe then the results from the model performance evaluation. Finally, we summarize the performance evaluation results and provide recommendations for PM-CAMx improvements.

2.   CONFIGURATION OF THE MODELS AND INPUT FILES

2.1   Configuration of the Models

It is important when conducting a performance evaluation of several models against the same data base to maintain as much consistency as possible among the models. For example, if several options are available to simulate a given process (e.g., gas-phase chemistry), it is preferable to select the same option for both CMAQ and PM-CAMx (here, CBM-IV) to minimize the possible sources of difference between the two models. Table 2-1 summarizes the options that were selected for CMAQ and PM-CAMx. The same or similar modules are used for gas-phase chemistry, horizontal advection, dry deposition for both gaseous and particulate matter (PM) species, and wet deposition for gaseous species (Note that wet deposition of PM species is currently not treated in PM-CAMx). Differences exist in the treatment of aqueous-phase chemistry, subgrid-scale convective transport, vertical advection, horizontal diffusion, vertical diffusion, and all aspects of aerosol microphysical processes.

As a default, the particle size distribution is represented in the current version of PM-CAMx using ten sections over a size range of 0.039 to 20 μm in diameter. The developer recommends using this particle size representation for all PM-CAMx simulations (Yarwood, 2002). CMAQ uses three (Aitken, accumulation, and coarse) modes to represent the size distribution of particles.

2.2   Modeling Domain

The modeling domain consists of two nested grid domains with horizontal resolutions of 32 and 8 km, respectively (see Figure 2-1). The coarse grid domain covers the entire contiguous U.S. and the fine grid domain covers an area of the southeast U.S. that includes Atlanta and Nashville. The coarse grid and fine grid domains include 160 x 106 grid cells and 100 x 100 grid cells, respectively. For PM CAMx, the number of grid cells is increased by two in each direction due to the use of boundary grid cells. The vertical resolution includes 19 layers from the surface to the tropopause, corresponding to

Table 2-1.   Configurations of CMAQ and PM-CAMx for the major processes.

Process	CMAQ	PM-CAMx
Gas-phase chemistry	CBM-IV	CBM-IV
Gas-phase chemistry solver	Modified Euler Backward Iterative (MEBI) solver	Environ Chemical Mechanism Compiler (CMC) solver
Aqueous-phase chemistry	RADM	CMU
Horizontal advection	Piecewise parabolic method	Piecewise parabolic method
Vertical advection	Piecewise parabolic method	Crank-Nicholson scheme
Convective transport	Subgrid-scale parameterization at both 32 and 8 km horizontal resolutions with K-diffusion coefficient	None
Horizontal diffusion	K theory	K theory using Smagorinsky (1963)
Vertical diffusion	K theory, with PBL similarity method for K_{zz} calculation (online calculation)	K theory, with the O'Brien scheme for K_{zz} calculation (precalculated)
Dry Deposition	Resistance transfer approach	Resistance transfer approach
Wet deposition	Henry's law equilibrium for gases. Complete scavenging for accumulation and coarse mode particles; transient scavenging for Aitken mode particles	Scavenging rate parameterization for gases. Scavenging of particles is not treated.

Table 2-1.   Configurations of CMAQ and PM-CAMx for the major processes (continued).

Process	CMAQ	PM-CAMx
Aerosol processes		
size distribution	Three modes	Ten sections
inorganic species	Thermodynamic equilibrium with ISORROPIA	Thermodynamic equilibrium with ISORROPIA
organic species	Reversible absorption parameterization for products of 8 classes of VOC precursors	Reversible absorption parameterization for products of 6 VOC precursors
coagulation	Modal approach of Binkowski and Shankar (1995)	Sectional approach of Seinfeld (1986)
nucleation	Parameterization of Harrington and Kreidenweis (1998)	Parameterization of Russell et al. (1994)
condensational growth/shrinkage by volatilization	Modal approach of Binkowski and Shankar (1995)	Sectional approach of Pandis et al. (1993)
gas/particle mass transfer	Full equilibrium approach	Full equilibrium approach* of Capaldo et al. (2000)

*The approach of Capaldo et al. (2000) includes three options, bulk equilibrium, hybrid, and dynamic. Only the bulk equilibrium option is operational in the current version of PM-CAMx.
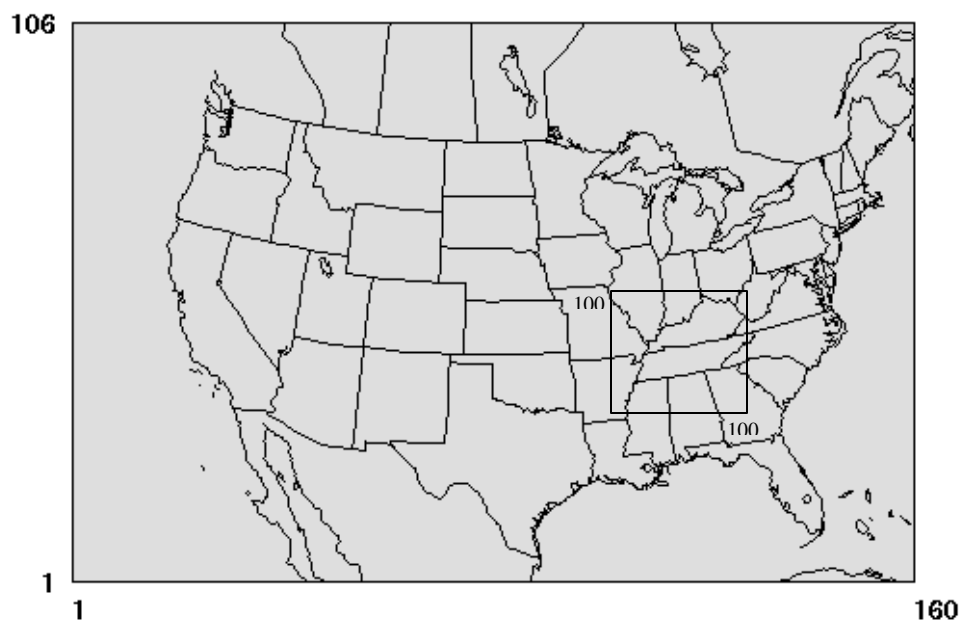
Figure 2-1.   Modeling domains (32 km and 8 km horizontal resolution).

sigma levels of 1.00, 0.998, 0.995, 0.990, 0.985, 0.980, 0.970, 0.960, 0.945, 0.930, 0.910, 0.890, 0.865, 0.840, 0.810, 0.740, 0.650, 0.500, 0.200, and 0.00 at the boundaries.

2.3   Meteorological Files

A simulation with the meteorological Mesoscale Model (MM5) version 3 for the coarse domain with a grid resolution of 32 km and the nested fine domain with a grid resolution of 8 km were conducted by TVA. A preliminary performance evaluation of MM5 has been conducted by TVA (TVA, 2003). The model behavior of the 32-km and 8 km grids was basically consistent. Differences in the results with the two grids could be due to their different responses to certain physics schemes used in the model, although the same types of physics options were applied to both grids. The MM5 output files had already been processed with the Meteorology-Chemistry Interface Processor (MCIP) version 2.2 for CMAQ. We processed these files with the CAMx pre-processor (MM5CAMx) for the PM-CAMx application. The fine grid domain size to be used for the MM5CAMx processing is 102 x 102 grid cells, including two boundary cells in each of the x and y directions.

Meteorological inputs required by PM-CAMx include winds, pressure, temperature, water vapor, cloud, rain, and vertical diffusivity (K_v or K_{zz}). Several options are available to derive K_v fields from MM5 output. One requires turbulent kinetic energy (TKE), which was not available in the MM5 output. The O'Brien scheme implemented in PM-CAMx (ENVIRON, 2000, 2002) was thus selected to calculate K_v (Emery, 2002); this method requires the planetary boundary layer (PBL) depth as an input.

2.4   Emission Files

A gridded emission inventory for the contiguous United States, southern Canada and northern Mexico was prepared by TVA. This inventory was compiled based on EPA's NET'96 emission inventory that contains county-level emissions from different emission source categories. Differences in weekday-weekend or holiday emissions are taken into account in the gridded emission inventory. This emission inventory was

processed with the Sparse Matrix Operator Kernel Emissions system (SMOKE) for the U.S. sources and for the Canadian area, mobile and biogenic sources for both the 32-km and the 8 km grids using a spatial surrogate file of 4-km grid that is available from the State University of New York at Albany. Other processors were used to incorporate Canadian point sources and Mexican sources from a global inventory. SMOKE was run with the CBM-IV VOC speciation file for U.S. and Canadian sources (except Canadian point sources). For Mexican sources and Canadian point sources, the RADM2 speciation was converted into a CBM-IV speciation using the conversion parameters provided in Table 2-2.

Emission inputs for PM-CAMx are provided in an upper level point source file and a lower level point/area/mobile/biogenic file. The upper level point source file contains the emissions strengths, locations and stack characteristics of major point sources. The lower level file represents the 2-D surface emissions of the remaining sources. The gaseous emission files are generated using SMOKE for U.S. sources and Canadian non-point sources. For Canadian point sources and Mexican sources a processor from TVA was adapted to generate CBM-IV speciated emissions. The size-resolved PM emissions for PM-CAMx were obtained by integrating the three-mode lognormal size distribution used in CMAQ. PM speciation includes sulfate, nitrate, black carbon (or elemental carbon) (BC or EC), organic materials (OM = organic carbon (OC) x 1.4), and other inorganic species (OI).

The emissions of sea salt particles, including coarse and fine sodium, chloride, and sulfate, were calculated using a preprocessor developed at MCNC and merged with the SMOKE-generated emissions for the application of PM-CAMx. The current version of CMAQ treats particulate sodium and chloride but only in the coarse mode; fine sea salt particles were added to the other fine particulate species category so that CMAQ and PM-CAMx have consistent total fine mass.

Table 2-2.   Conversion of VOC chemical speciation from RADM2 to CBM-IV (Byun and Ching, 1999).

CBM-IV Functional Groups	RADM2 VOC Surrogates
PAN	PAN
FACD	ORA1
AACD	ORA2
PACD	PAA
UMHP	OP1
MGLY	MGLY
OPEN	DCB
CRES	CSL
FORM	HCHO + 1.0 * GLY
ALD2	1.0 * ALD + 2.0 * OLI
PAR	0.4 * ETH + 2.9 * HC3 + 4.8 * HC5 + 7.9 * HC8 + 0.8 * OLT + 0.8 OLI + 3.9 * KET
OLE	OLT
TOL	TOL
ISOP	ISO
ETH	OL2
XYL	XYL
TERP	TERP

2.5   Initial and Boundary Conditions

The CMAQ default values were used for both initial conditions (ICs) and boundary conditions (BCs). A spin-up period of three days is used to minimize the influence of IC. In this spin-up period, the first day of the episode is run twice to allow the build-up of a representative concentration field. The default IC can be found in Byun and Ching (1999). Since the 36 km resolution domain extends beyond most populated and industrial areas (except for some parts of Mexico), it is appropriate to use default concentrations typical of a clean background atmosphere at the boundaries. BCs were added for seasalt particles. Seasalt is only treated in the coarse mode in CMAQ, but sodium and chloride are represented in all sections in PM-CAMx. Over the ocean, sodium and chloride BCs at the surface and aloft were derived from the results of a simulation conducted for the Big Bend Regional Aerosol and Visibility Observational (BRAVO) study. No sodium and chloride BCs were applied over land. The average of all BCs were used as ICs for sodium and chloride species.

2.6   Photolysis Inputs

A photolytic rate lookup table is needed for CMAQ CBM-IV. This table is generated by the JPROC preprocessor to provide photolysis rates by hour of day, latitude, and altitude. For PM-CAMx, photolysis rates are looked up based on zenith angle, altitude, O_3 column, haze, and albedo. The input files are generated using processors that were distributed with the PM-CAMx source code. Two options are available to calculate radiative transfer: a pseudo-spherical two-stream delta-Eddington method and a discrete ordinates method. The delta-Eddington two-stream radiative transfer method is used in the JPROC processor for CMAQ photolysis inputs; therefore, the pseudo-spherical two-stream delta-Eddington method was used to process photolysis rates for PM-CAMx.

3. PERFORMANCE EVALUATION

During the 1999 Nashville SOS study and the subsequent Atlanta study, late June-early July was the only period with regional buildup of O_3 and PM, therefore, it was selected for the modeling study. The observed O_3 and PM data were available on July 1-6 and the buildup of O_3 and PM started on July 5. We, therefore, focus our analyses of results for July 5, 6 and 7 (e.g., analyses of spatial distribution of O_3 and PM and PM compositions). We describe first the spatial distributions of O_3 mixing ratios and concentrations of PM_{10}, $PM_{2.5}$ and $PM_{2.5}$ chemical components predicted by CMAQ and PM-CAMx. Next, we describe the temporal distributions of predicted O_3 mixing ratios and concentrations of PM_{10}, $PM_{2.5}$ and $PM_{2.5}$ chemical components at selected sites. Finally, the performance statistics for both models are discussed.

3.1 Spatial Distributions of O_3 and PM

3.1.1 O_3 Mixing Ratios Over the U.S. and the Southeastern U.S.

Figure 3-1 shows the spatial distribution of hourly O_3 mixing ratios predicted by CMAQ and PM-CAMx at 5:00 p.m. (CDT), the peak O_3 time for the southeastern U.S. predicted by PM-CAMx, on July 5, 1999 under the base emission scenario, with horizontal resolutions of 32 km and 8 km. For the coarse grid simulation over the U.S., CMAQ predicts high O_3 mixing ratios of > 80 ppb in most areas in the eastern U.S., CA in the western U.S., with the highest O_3 mixing ratio of 163 ppb occurring near the Atlantic coast off Norfolk, VA. On the other hand, PM-CAMx predicts high O_3 mixing ratios of > 80 ppb in larger areas in the eastern and the southeastern U.S., with the highest O_3 mixing ratio of 168 ppb occurring in southern Rhode Island. For the fine grid simulation over the southeastern U.S., CMAQ predicts high O_3 mixing ratios of > 80 ppb in the northeastern corner that covers southeastern Ohio and Indiana, northern Kentucky, the Nashville and Knoxville areas in Tennessee, and the Atlanta area in Georgia, with the highest O_3 mixing ratio of 126 ppb occurring about 25 miles northwest of Charleston, WV. PM-CAMx predicts high O_3 mixing ratios of > 80 ppb in many locations in the

Figure 3-1.   The spatial distribution of hourly average O_3 mixing ratios at 5:00 p.m. (CDT), the peak O_3 time for the southeastern U.S. predicted by PM-CAMx, on July 5, 1999 under the TVA base emission scenario by (a) CMAQ (32 km), (b) PM-CAMx (32 km); (c) CMAQ (8 km); and (d) PM-CAMx (8 km).

southeast domain, with the highest O_3 mixing ratio of 156 ppb occurring about 33 miles northwest of Atlanta, Georgia. The observed maximum O_3 mixing ratio recorded in the Aerometric Information Reporting System (AIRS) monitoring network in the southeastern U.S. modeling domain was 136 ppb. Compared to CMAQ, PM-CAMx simulations with both fine and coarse grids tend to give larger overpredictions for O_3 in many locations in the southeastern U.S. (see Section 3.3 for a statistical performance evaluation). The NO_x mixing ratios predicted by PM-CAMx are also higher than those predicted by CMAQ in the southeastern U.S. (figures not shown). Since O_3 chemistry is generally NO_x-limited during summer time in many areas in the southeastern U.S. (e.g., Atlanta), O_3 formation is mainly controlled by the abundance of NO_x, which can be affected by many atmospheric processes including emissions, chemical transformation, horizontal and vertical transport, and dry and wet deposition.

Both CMAQ and PM-CAMx use the same emission inventory, the same horizontal advection scheme, similar gas-phase chemical mechanism (i.e., modified CBM-IV) and similar dry and wet deposition treatment for gaseous species. They both use K theory for horizontal and vertical diffusion, but differ in their algorithms. For example, for horizontal diffusion, a constant (i.e., space-independent) horizontal eddy diffusivity (i.e., K_{xx} and K_{yy}) of 500 m^2 s^{-1} is assumed in CMAQ, whereas PM-CAMx uses the Smagorinsky approach (Smagorinsky, 1963) to calculate K_{xx} and K_{yy} that account for diffusion due to distortion or stress in the horizontal wind fields. For vertical diffusion, CMAQ directly calculates the vertical diffusivities (i.e., K_{zz}) with Planetary Boundary Layer (PBL) similarity theory in its vertical diffusion module using the PBL thickness generated by MM5, whereas PM-CAMx uses a pre-processor to calculate K_{zz} values which are then used for the model simulations. Several options are available to derive K_{zz} fields from MM5 output in the pre-processor for PM-CAMx. The O'Brien K_{zz} scheme is the closest one to the PBL similarity theory used in CMAQ, as it requires PBL thickness from MM5 file; it was used in the PM-CAMx simulations following recommendation from the model developer (Emery, 2002). As shown below through the analyses of the spatial distribution of CO, the differences in calculating the horizontal and vertical diffusivities between CMAQ and PM-CAMx contribute to differences in the

temporal and spatial abundance of O_3 precursors such as NO_x and VOCs, thus in O_3 formation predicted by the two models.

The spatial distribution of CO at 5:00 p.m. (CDT), on July 5, 1999 is shown in Figure 3-2 to demonstrate the differences in the abundance of species predicted by CMAQ and PM-CAMx. The CO mixing ratios predicted by CMAQ are generally less than 200 ppb for many areas in the U.S. (with a domain-wide maximum of 927 ppb and 759 ppb for the coarse and fine grids, respectively), whereas those predicted by PM-CAMx range from 200 ppb to 1901 ppb for the coarse grid simulation and from 200 ppb to 1344 ppb for the fine grid simulation in many cities in the eastern and the southeastern U.S. Compared to fast-reacting species such as NO_x and many VOCs, CO is a slow-reacting species; its abundance is mainly controlled by emission, transport and deposition processes. Since both models use the same emission inventory and similar dry and wet deposition schemes, the significant differences in CO mixing ratios predicted by the two models are, therefore, most likely caused by different treatments in transport processes. Jang et al. (1995) have shown that CO is mainly affected by vertical transport and the contribution from horizontal transport is negligible; therefore, the differences in predicted CO mixing ratios reflect the differences in vertical transport treatment between the two models. Possible underpredictions in vertical mixing during daytime or other mispredicted transport parameters in PM-CAMx may lead to mispredictions in the temporal and spatial abundance of O_3 precursors such as NO_x and VOCs. These mispredictions may in turn result in significant overpredictions in O_3 mixing ratios during daytime in many areas in the southeastern U.S. Differences in other model formulations such as aqueous-phase chemistry, subgrid-scale convective transport and vertical advection scheme may also contribute to the differences in the predicted abundance of O_3 and its precursors. Figures 3-1 and 3-2 also show the different effects of grid resolution on fast- and slow-reacting species. The spatial distribution of CO predicted by both models with the fine grid (i.e., Figure 3-2 (c) and (d)) is similar to that with the coarse grid (i.e., Figure 3-2 (a) and (b)), implying that for slow-reacting species, the average transport affecting a coarse grid cell is comparable to that affecting the same area with a higher grid resolution. The differences in the magnitudes of the predicted CO mixing
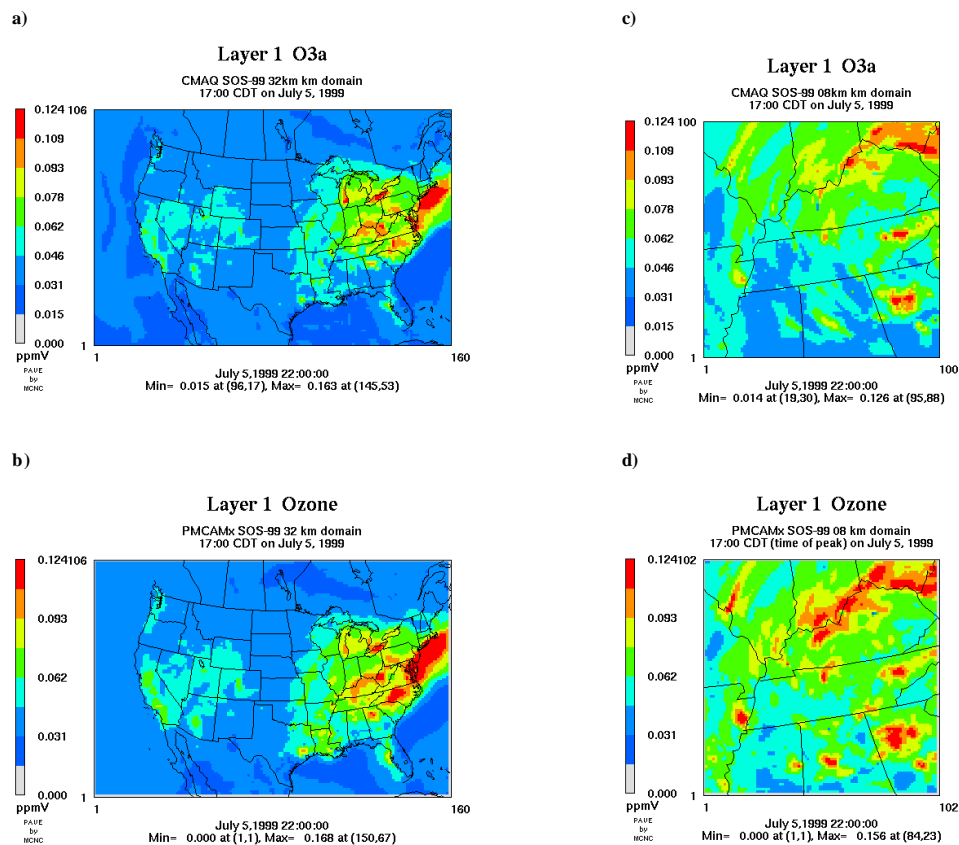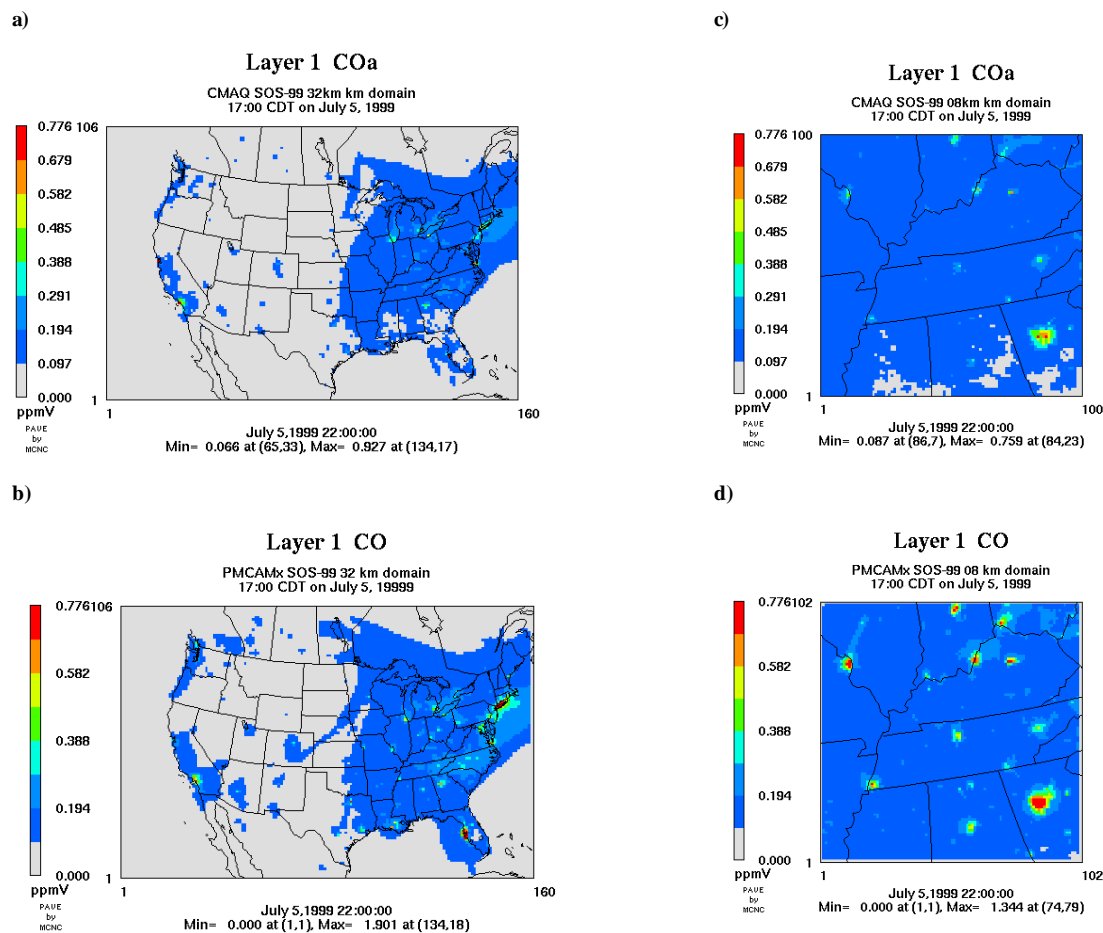
Figure 3-2.   The spatial distribution of hourly average CO mixing ratios at 5:00 p.m. (CDT), the peak O_3 time for the southeastern U.S. predicted by PM-CAMx, on July 5, 1999 under the TVA base emission scenario by (a) CMAQ (32 km), (b) PM-CAMx (32 km); (c) CMAQ (8 km); and (d) PM-CAMx (8 km).

ratios between the two grids are mainly caused by differences in the emissions resolved at a different grid resolution. By contrast, for fast-reacting species such as O_3, the predicted mixing ratios differ appreciably in terms of both magnitude and spatial distribution between the two different grid resolutions, thereby indicating that the nonlinearity of chemical reactions and inhomogeneity associated with precursor emissions have a significant impact on model predictions.

3.1.2   PM Concentrations Over the U.S. and the Southeastern U.S.

3.1.2.1 PM Concentrations Over the U.S.

Figures 3-3 to 3-8 show the spatial distribution of 24-hour average $PM_{2.5}$ and PM_{10} concentrations predicted by CMAQ and PM-CAMx on July 5-7, 1999 under the base emission scenario with both 32 km and 8 km horizontal resolutions. On July 5-7, CMAQ predicts the area of maximum concentrations to be over eastern U.S. and the area of minimum concentrations to be over western U.S., with a factor of 2-8 difference between the maxima and minima in the 24-hour average $PM_{2.5}$ and PM_{10} concentrations. PM-CAMx predicts the area of maximum $PM_{2.5}$ and PM_{10} concentrations to be in southern Louisiana and the Houston area in Texas, respectively; an area of high PM concentrations applies also in the eastern U.S. The area of minimum PM concentrations is in the western U.S. There is a factor of 5-10 between the maximum and the minimum PM concentrations. The spatial variations of $PM_{2.5}$ and PM_{10} concentrations in the rural areas from the western to the eastern U.S. predicted by both models are generally similar. The two models, however, differ significantly in their predictions over some urban/suburban areas in the U.S., especially in the southeastern, eastern and central U.S.

On July 5 (Figures 3-3 (a) vs. 3-3 (b)), while CMAQ predicts the highest $PM_{2.5}$ concentrations of 25-39 $\mu g\ m^{-3}$ in northern Kentucky, southern Virginia, central North Carolina, and off the northeastern coast of the U.S., PM-CAMx predicts the highest $PM_{2.5}$ concentrations of 25-59 $\mu g\ m^{-3}$ in southern Louisiana, Houston, TX and also in the aforementioned areas but extending farther south into northeastern Tennessee and west into western North Carolina. In the western U.S., CMAQ and PM-CAMx predict the

Figure 3-3. The spatial distribution of 24-hour average PM$_{2.5}$ concentrations on July 5, 1999 under the TVA base emission scenario with 32 km and 8 km horizontal resolutions predicted by (a) CMAQ (32 km), (b) PM-CAMx (32 km), (c) CMAQ (8 km), and (d) PM-CAMx (8 km).
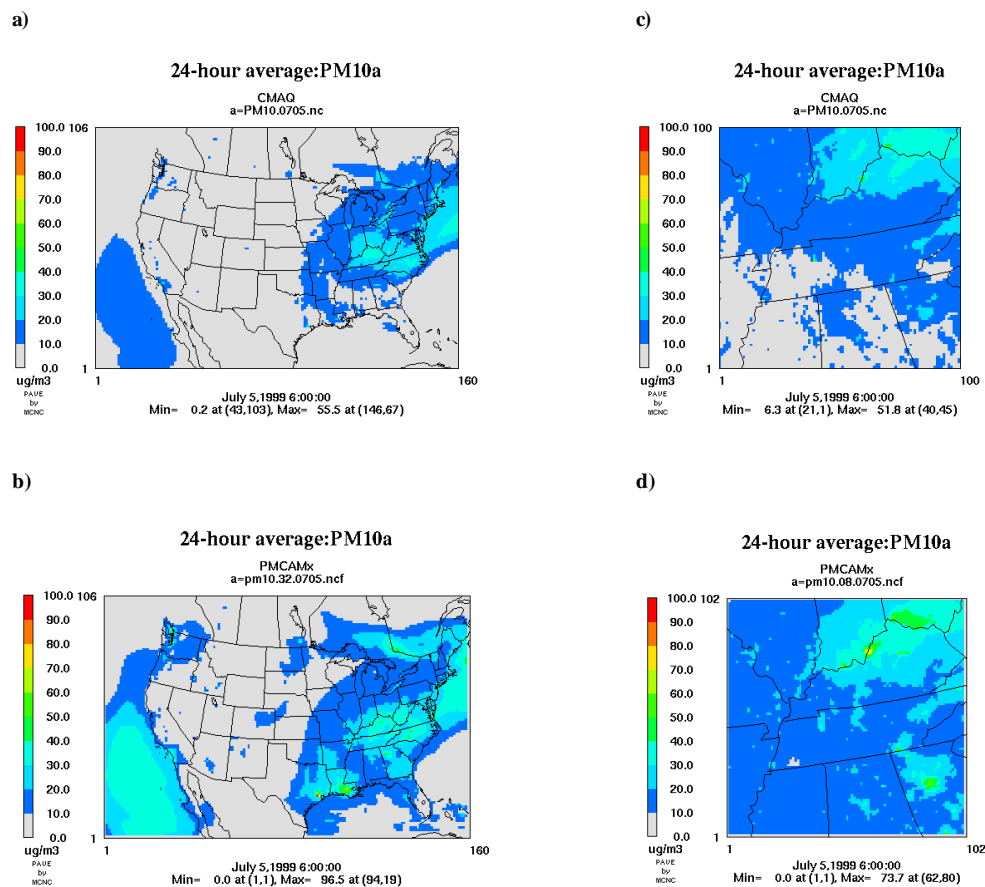
Figure 3-4. The spatial distribution of 24-hour average PM_{10} concentrations on July 5, 1999 under the TVA base emission scenario with 32 km and 8 km horizontal resolutions predicted by (a) CMAQ (32 km), (b) PM-CAMx (32 km), (c) CMAQ (8 km), and (d) PM-CAMx (8 km).
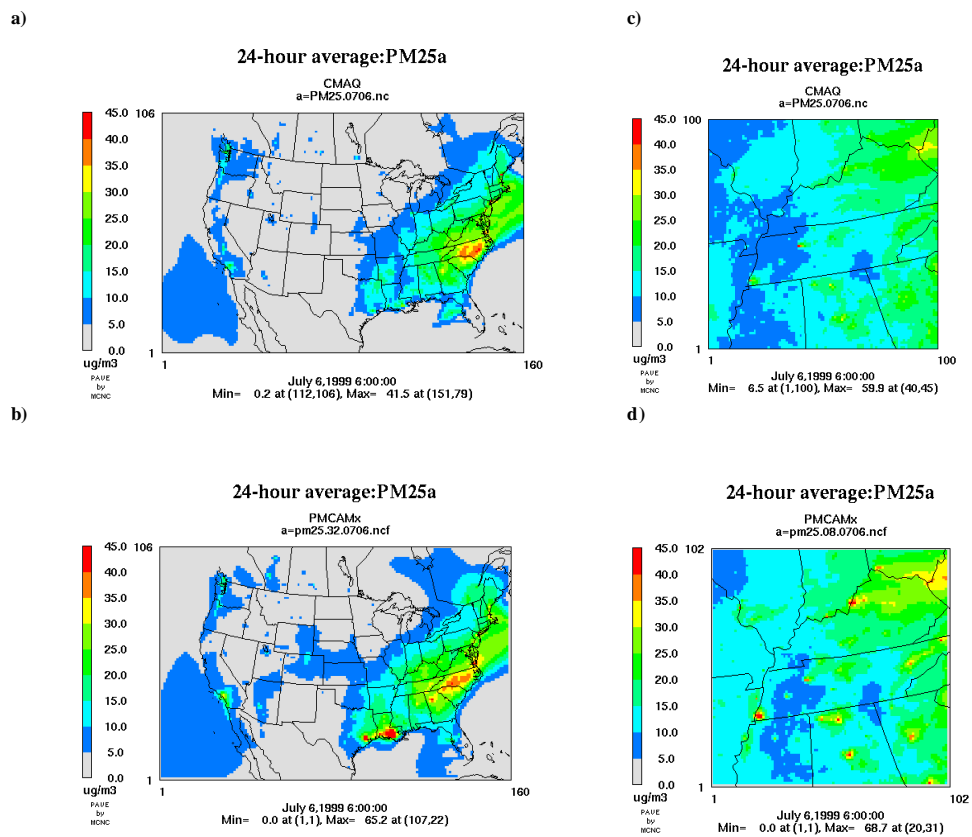
Figure 3-5. The spatial distribution of 24-hour average PM$_{2.5}$ concentrations on July 6, 1999 under the TVA base emission scenario with 32 km and 8 km horizontal resolutions predicted by (a) CMAQ (32 km), (b) PM-CAMx (32 km), (c) CMAQ (8 km), and (d) PM-CAMx (8 km).

a)

c)

(b)

(d)
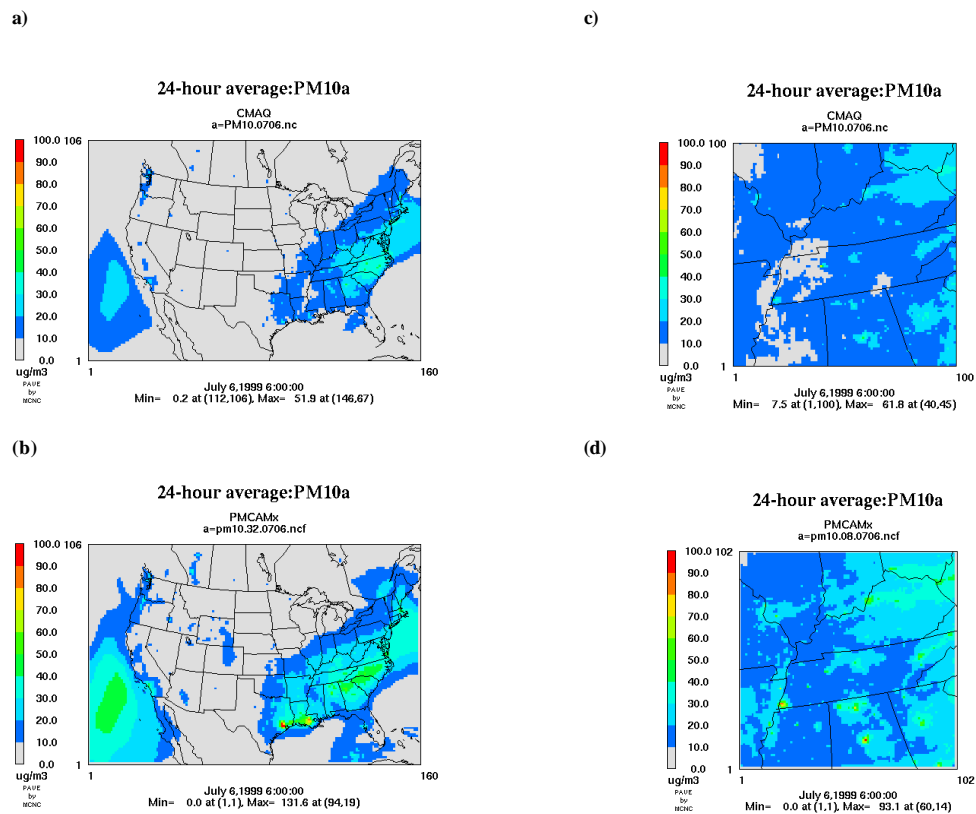
Figure 3-6.   The spatial distribution of 24-hour average PM$_{10}$ concentrations on July 6, 1999 under the TVA base emission scenario with 32 km and 8 km horizontal resolutions predicted by (a) CMAQ (32 km), (b) PM-CAMx (32 km), (c) CMAQ (8 km), and (d) PM-CAMx (8 km).
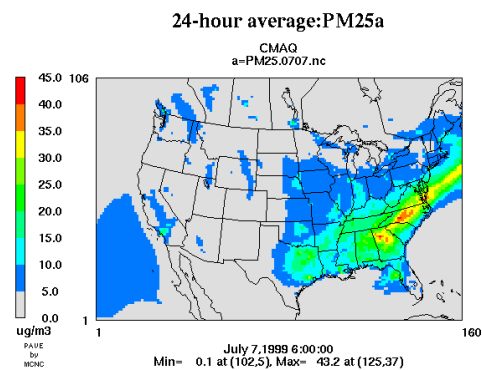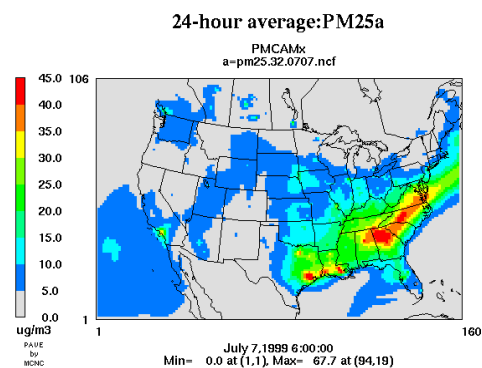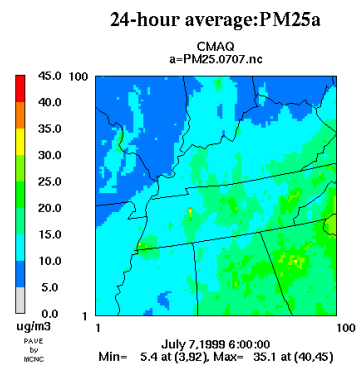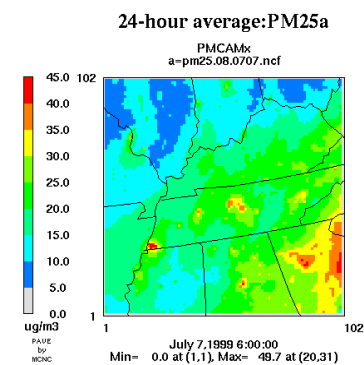
Figure 3-7.   The spatial distribution of 24-hour average PM$_{2.5}$ concentrations on July 7, 1999 under the TVA base emission scenario with 32 km and 8 km horizontal resolutions predicted by (a) CMAQ (32 km), (b) PM-CAMx (32 km), (c) CMAQ (8 km), and (d) PM-CAMx (8 km).
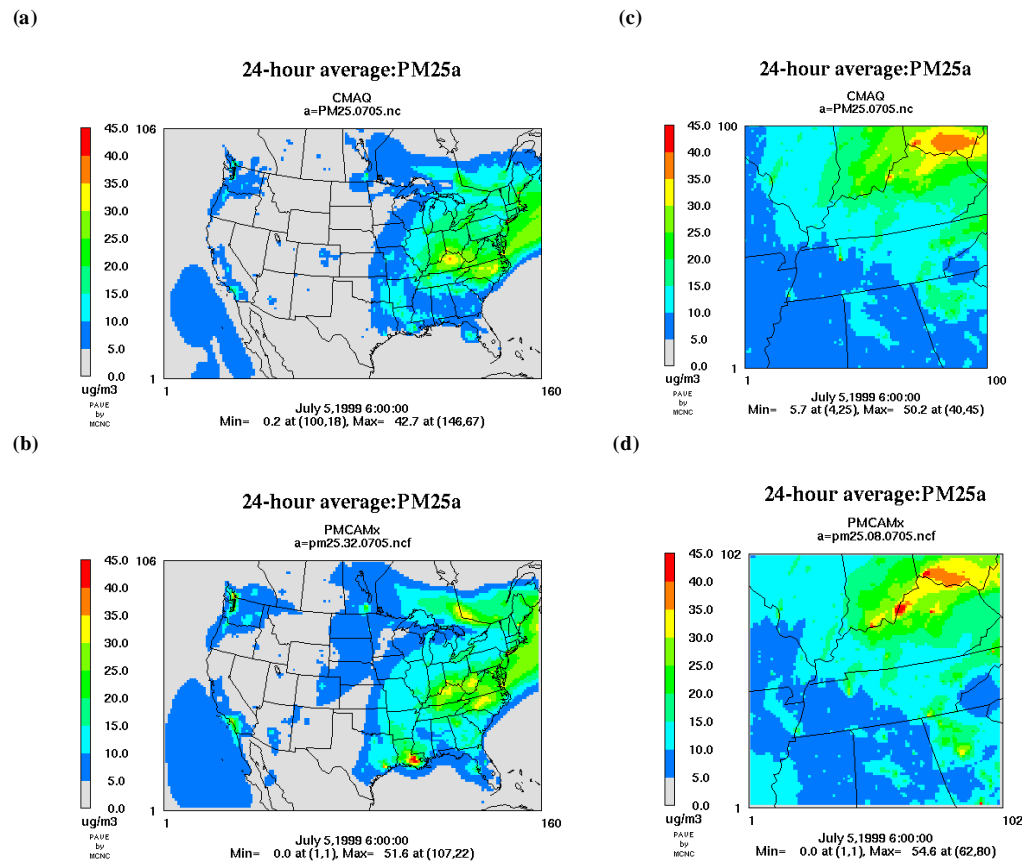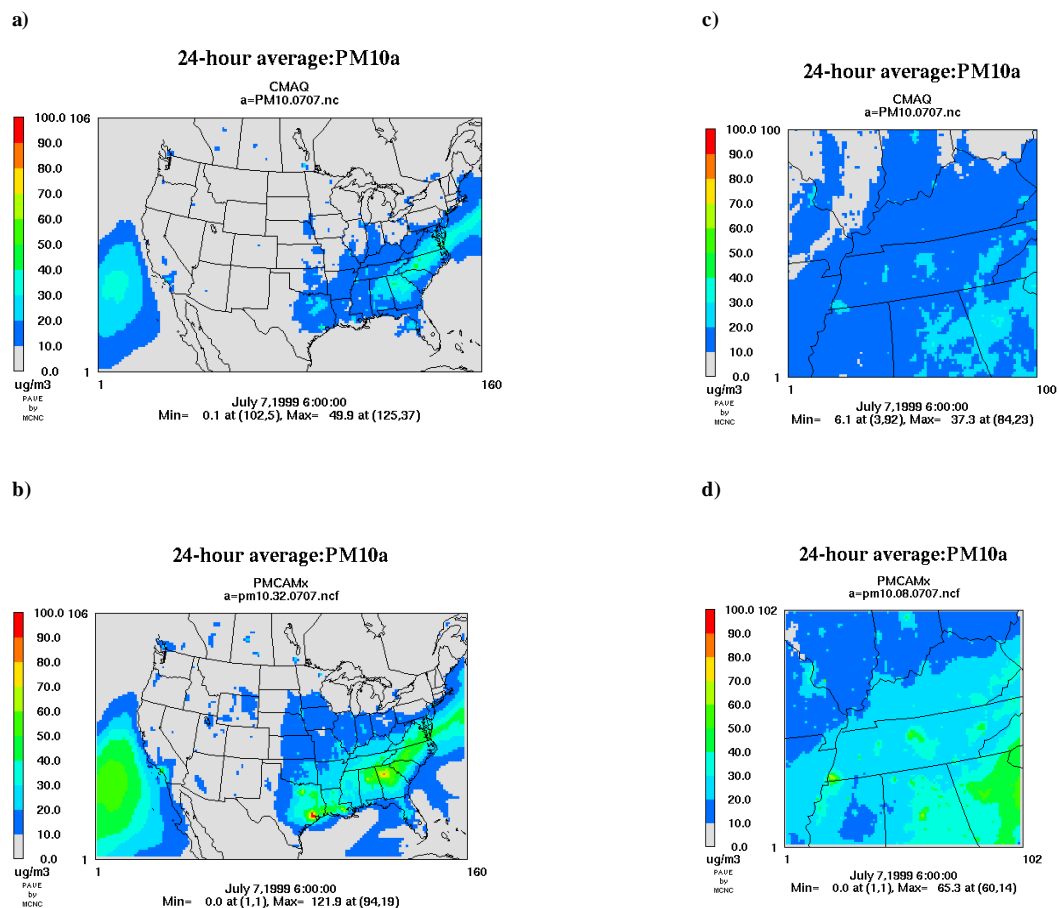
Figure 3-8.   The spatial distribution of 24-hour average PM$_{10}$ concentrations on July 7, 1999 under the TVA base emission scenario with 32 km and 8 km horizontal resolutions predicted by (a) CMAQ (32 km), (b) PM-CAMx (32 km), (c) CMAQ (8 km), and (d) PM-CAMx (8 km).

highest $PM_{2.5}$ concentrations of 10-15 μg m^{-3} and 30-35 μg m^{-3}, respectively, in the border area between Bellingham, Washington and Vancouver, British Columbia and the second highest concentrations of 20-30 μg m^{-3} in the Los Angeles basin, CA. In the central U.S., CMAQ predicts $PM_{2.5}$ concentrations of 5-15 μg m^{-3} in some areas in Colorado and several states in the eastern portion of the central region (e.g., Illinois, Missouri, Arkansas, Mississippi, Alabama, Tennessee and most of Wisconsin, Iowa and Louisiana). PM-CAMx predicts $PM_{2.5}$ concentrations of 5-20 μg m^{-3} in most states in the central U.S. except Montana, central and western Wyoming, and most areas in Idaho and Utah.

On July 6 and 7 (Figures 3-5 (a) vs. 3-5 (b), 3-7(a) vs. 3-7(b)), the spatial distributions of $PM_{2.5}$ concentrations in most of the U.S. predicted by both models are similar to those on July 5 with a few exceptions. First, the area of maximum $PM_{2.5}$ concentrations in the eastern U.S. predicted by CMAQ is centered in central North Carolina on both days. It extends into northern South Carolina on July 6 and extends southwestward into northern Georgia and northeastward into the Atlantic Ocean on July 7. The area of maximum $PM_{2.5}$ concentrations predicted by PM-CMAx is in southern Louisiana and extends westward into Houston, Texas on July 6 and in Houston on July 7, forming a high $PM_{2.5}$ concentration band along the coast of the Gulf of Mexico on both days. Another area of high PM concentrations predicted by PM-CAMx in the eastern U.S. moves southeastward, covering a large area of North Carolina, northwestern South Carolina, and northern Georgia, Alabama and Mississippi on both days. Second, both models predict that the highest $PM_{2.5}$ concentrations in the western U.S. occurred in the Los Angeles areas, CA on both days. Third, CMAQ predicts that $PM_{2.5}$ concentrations in most areas in the central U.S. and over three of the five Great Lakes (i.e., Lakes Superior, Huron, and Michigan) were below 5 μg m^{-3} on both days. On the other hand, PM-CAMx predicts that the areas with $PM_{2.5}$ concentrations of 5-10 μg m^{-3} in the central U.S. extend northward and westward to cover more areas (e.g., Arizona, Utah and Wyoming on both days and eastern Montana and southern Nevada on July 7). The $PM_{2.5}$ concentrations in many areas in North Dakota, Wisconsin and Michigan, central and northern Minnesota and areas around the aforementioned Great Lakes are below 5 μg m^{-3} on both days.

The differences in the PM_{10} concentrations predicted by the two models during July 5-7, 1999 for the entire U.S. domain are quite similar to those in the $PM_{2.5}$ concentrations, as shown in Figures 3-4 (a) vs. 3-4 (b), 3-6 (a) vs. 3-6 (b), 3-8 (a) vs. 3-8 (b).

3.1.2.2 PM Concentrations Over the Southeastern U.S.

As shown in Figures 3-3 (c), 3-3 (d), 3-5 (c), 3-5 (d), 3-7 (c) and 3-7 (d) for $PM_{2.5}$ and Figures 3-4 (c), 3-4 (d), 3-6 (c), 3-6 (d), 3-8 (c) and 3-8 (d) for PM_{10}, the $PM_{2.5}$ and PM_{10} concentrations predicted by both models with an 8 km resolution over the southeastern domain are generally consistent with those predicted for the same area with a 32 km resolution. The differences in the PM_{10} concentrations predicted by the two models during July 5-7, 1999 for the southeastern U.S. domain are quite similar to those in the $PM_{2.5}$ concentrations. However, some noticeable differences do exist between the results obtained with the two different grids. For example, CMAQ with the fine grid predicts the highest $PM_{2.5}$ concentrations of 25-30 μg m^{-3} on July 5 in the northeastern corner of the southeastern U.S. domain (Figure 3-3 (c)), which covers southern Ohio, southeastern Indiana, northern Kentucky and a small portion of northwestern Virginia. For comparison (Figure 3-3 (a)), it predicts $PM_{2.5}$ concentrations of 25-35 μg m^{-3} over most of the same area on July 5 when a coarse grid is used. On July 6 (Figure 3-5 (a) and (c)), CMAQ predicts similar spatial distributions with both grids in the southeastern U.S., with exceptions at two locations, Waverly (about 15 km west of Dickson), TN and Memphis, TN. The $PM_{2.5}$ concentrations predicted with the fine grid at Waverly and Memphis are significantly higher (by 20-30 μg m^{-3}) than those with the coarse grid. On July 7 (Figure 3-7 (a) and (c)), CMAQ with the fine grid predicts $PM_{2.5}$ concentrations of 20-30 μg m^{-3} in some areas in the southeastern corner of the southeastern U.S. domain, whereas CMAQ with the coarse grid predicts higher $PM_{2.5}$ concentrations (in the range of 25-43 μg m^{-3}) in the same area.

As shown later in Figures 3-9 to 3-20, the differences between the $PM_{2.5}$ and PM_{10} predictions in the southeastern U.S. by the two models with the fine and coarse grids can be explained by the differences in the predicted PM composition in the

a)

24-hour average:PM25a

b)

24-hour average:SO4a

c)

24-hour average:NO3a

d)

24-hour average:NH4a

e)

24-hour average:ECa

f)

24-hour average:OMa

Figure 3-9.   The spatial distribution of 24-hour average concentrations of (a) PM$_{2.5}$, (b) sulfate, (c) nitrate, (d) ammonium, (e) OM and (f) BC predicted by CMAQ on July 5, 1999 under the TVA base emission scenario with a 32 km horizontal resolution.
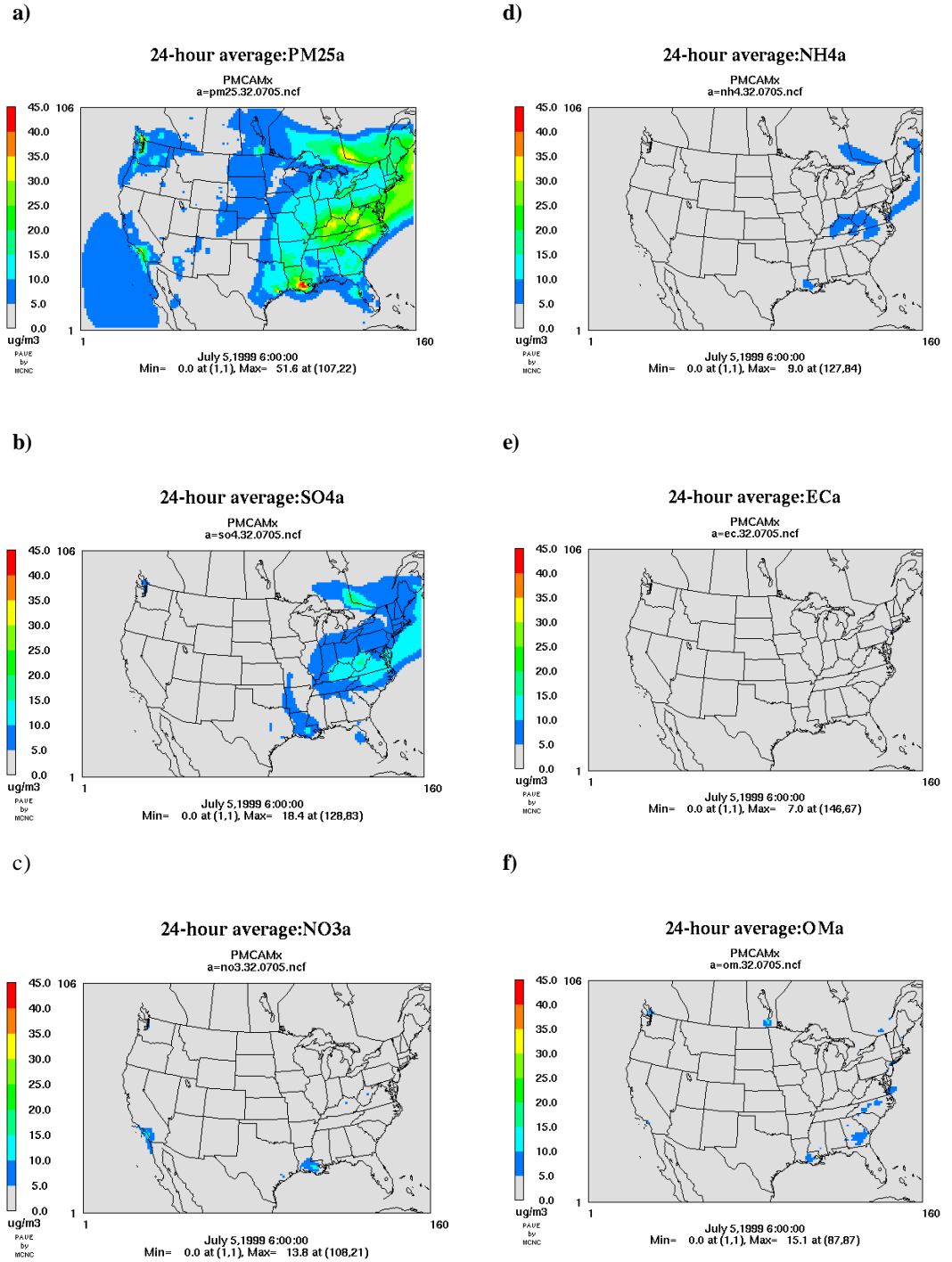
Figure 3-10. The spatial distribution of 24-hour average concentrations of (a) PM$_{2.5}$, (b) sulfate, (c) nitrate, (d) ammonium, (e) OM and (f) BC predicted by PM-CAMx on July 5, 1999 under the TVA base emission scenario with a 32 km horizontal resolution.
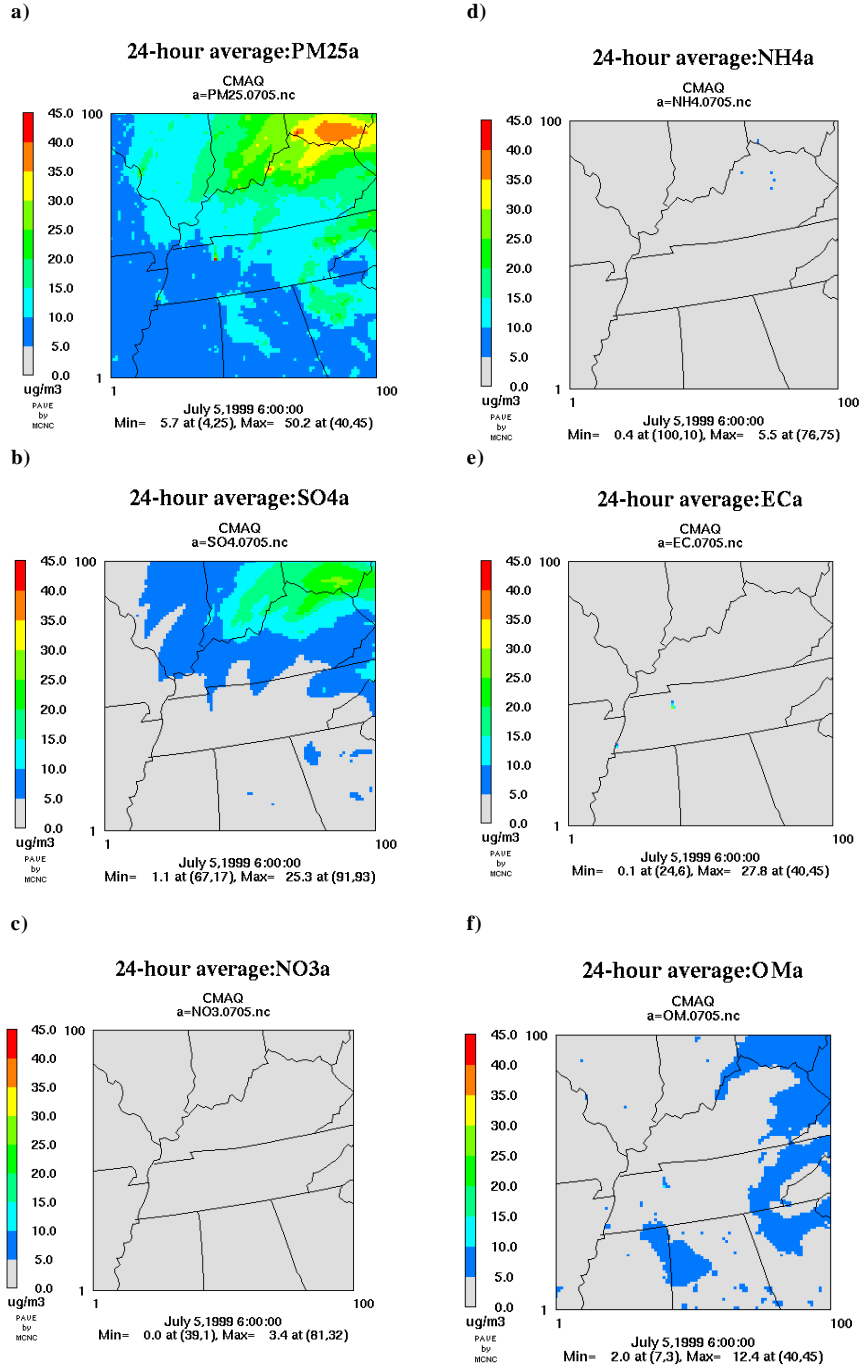
Figure 3-11.   The spatial distribution of 24-hour average concentrations of (a) PM$_{2.5}$, (b) sulfate, (c) nitrate, (d) ammonium, (e) OM and (f) BC predicted by CMAQ on July 5, 1999 under the TVA base emission scenario with an 8 km horizontal resolution.

a)

24-hour average:PM25a

PMCAMx
a=pm25.08.0705.ncf

July 5,1999 6:00:00
Min= 0.0 at (1,1), Max= 54.6 at (62,80)

d)

24-hour average:NH4a

PMCAMx
a=nh4.08.0705.ncf

July 5,1999 6:00:00
Min= 0.0 at (1,1), Max= 8.5 at (83,91)

b)

24-hour average:SO4a

PMCAMx
a=so4.08.0705.ncf

July 5,1999 6:00:00
Min= 0.0 at (1,1), Max= 19.0 at (84,91)

e)

24-hour average:ECa

PMCAMx
a=ec.08.0705.ncf

July 5,1999 6:00:00
Min= 0.0 at (1,1), Max= 12.6 at (20,31)

c)

24-hour average:NO3a

PMCAMx
a=no3.08.0705.ncf

July 5,1999 6:00:00
Min= 0.0 at (1,1), Max= 8.4 at (62,80)

f)

24-hour average:OMa

PMCAMx
a=om.08.0705.ncf

July 5,1999 6:00:00
Min= 0.0 at (1,1), Max= 7.6 at (98,9)

Figure 3-12.   The spatial distribution of 24-hour average concentrations of (a) $PM_{2.5}$, (b) sulfate, (c) nitrate, (d) ammonium, (e) OM and (f) BC predicted by PM-CAMx on July 5, 1999 under the TVA base emission scenario with an 8 km horizontal resolution.

Figure 3-13.   The spatial distribution of 24-hour average concentrations of (a) PM$_{2.5}$, (b) sulfate, (c) nitrate, (d) ammonium, (e) OM and (f) BC predicted by CMAQ on July 6, 1999 under the TVA base emission scenario with a 32 km horizontal resolution.

a)

24-hour average:PM25a

PMCAMx
a=pm25.32.0706.ncf

July 6,1999 6:00:00
Min= 0.0 at (1,1), Max= 65.2 at (107,22)

d)

24-hour average:NH4a

PMCAMx
a=nh4.32.0706.ncf

July 6,1999 6:00:00
Min= 0.0 at (1,1), Max= 12.1 at (107,21)

b)

24-hour average:SO4a

PMCAMx
a=so4.32.0706.ncf

July 6,1999 6:00:00
Min= 0.0 at (1,1), Max= 19.4 at (107,22)

e)

24-hour average:ECa

PMCAMx
a=ec.32.0706.ncf

July 6,1999 6:00:00
Min= 0.0 at (1,1), Max= 7.2 at (146,67)

c)

24-hour average:NO3a

PMCAMx
a=no3.32.0706.ncf

July 6,1999 6:00:00
Min= 0.0 at (1,1), Max= 20.1 at (107,21)

f)

24-hour average:OMa

PMCAMx
a=om.32.0706.ncf

July 6,1999 6:00:00
Min= 0.0 at (1,1), Max= 9.5 at (106,20)

Figure 3-14.   The spatial distribution of 24-hour average concentrations of (a) PM$_{2.5}$, (b) sulfate, (c) nitrate, (d) ammonium, (e) OM and (f) BC predicted by PM-CAMx on July 6, 1999 under the TVA base emission scenario with a 32 km horizontal resolution.
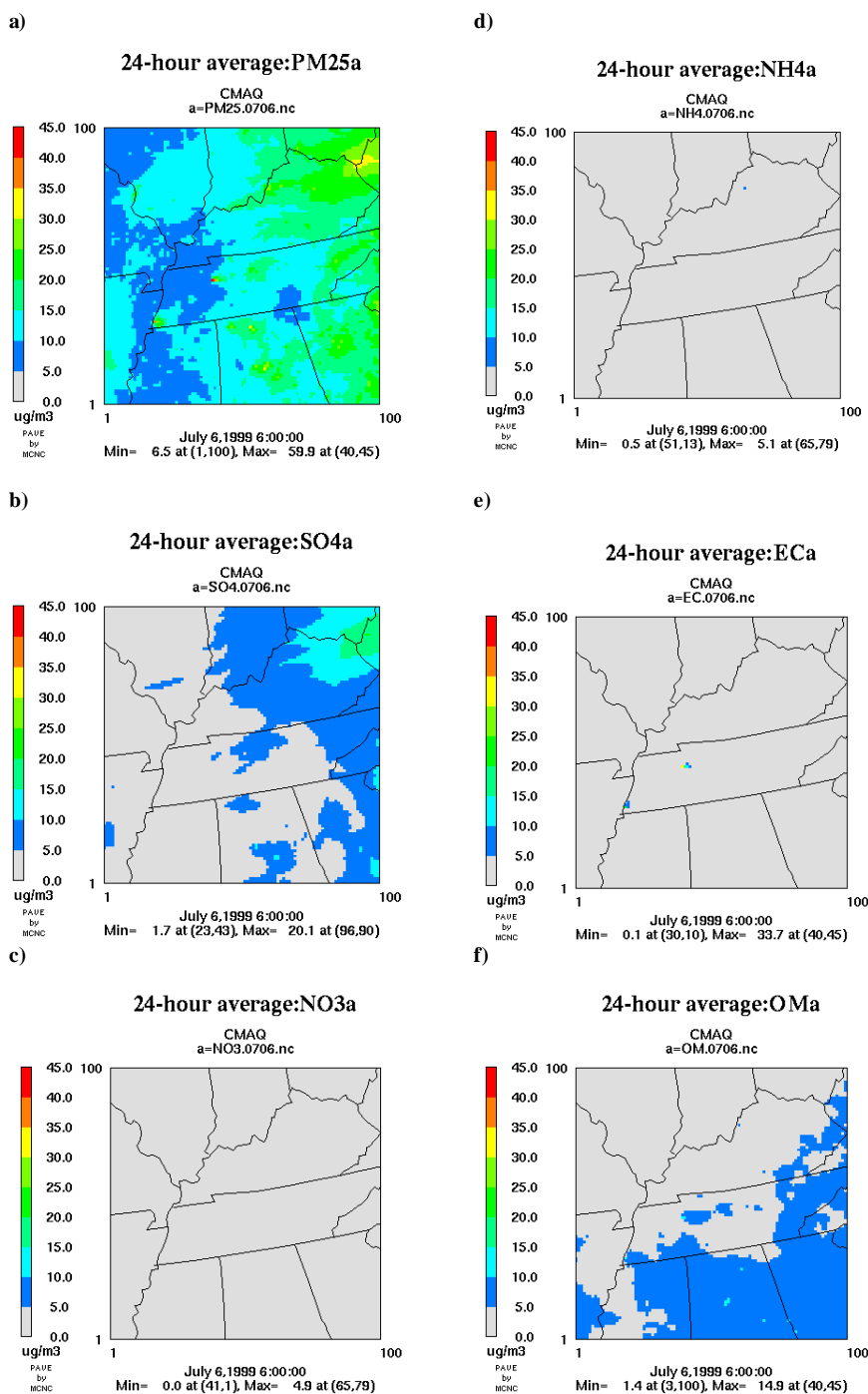
Figure 3-15.   The spatial distribution of 24-hour average concentrations of (a) PM$_{2.5}$, (b) sulfate, (c) nitrate, (d) ammonium, (e) OM and (f) BC predicted by CMAQ on July 6, 1999 under the TVA base emission scenario with an 8 km horizontal resolution.

a) 24-hour average:PM25a

b) 24-hour average:SO4a

c) 24-hour average:NO3a

d) 24-hour average:NH4a

e) 24-hour average:ECa
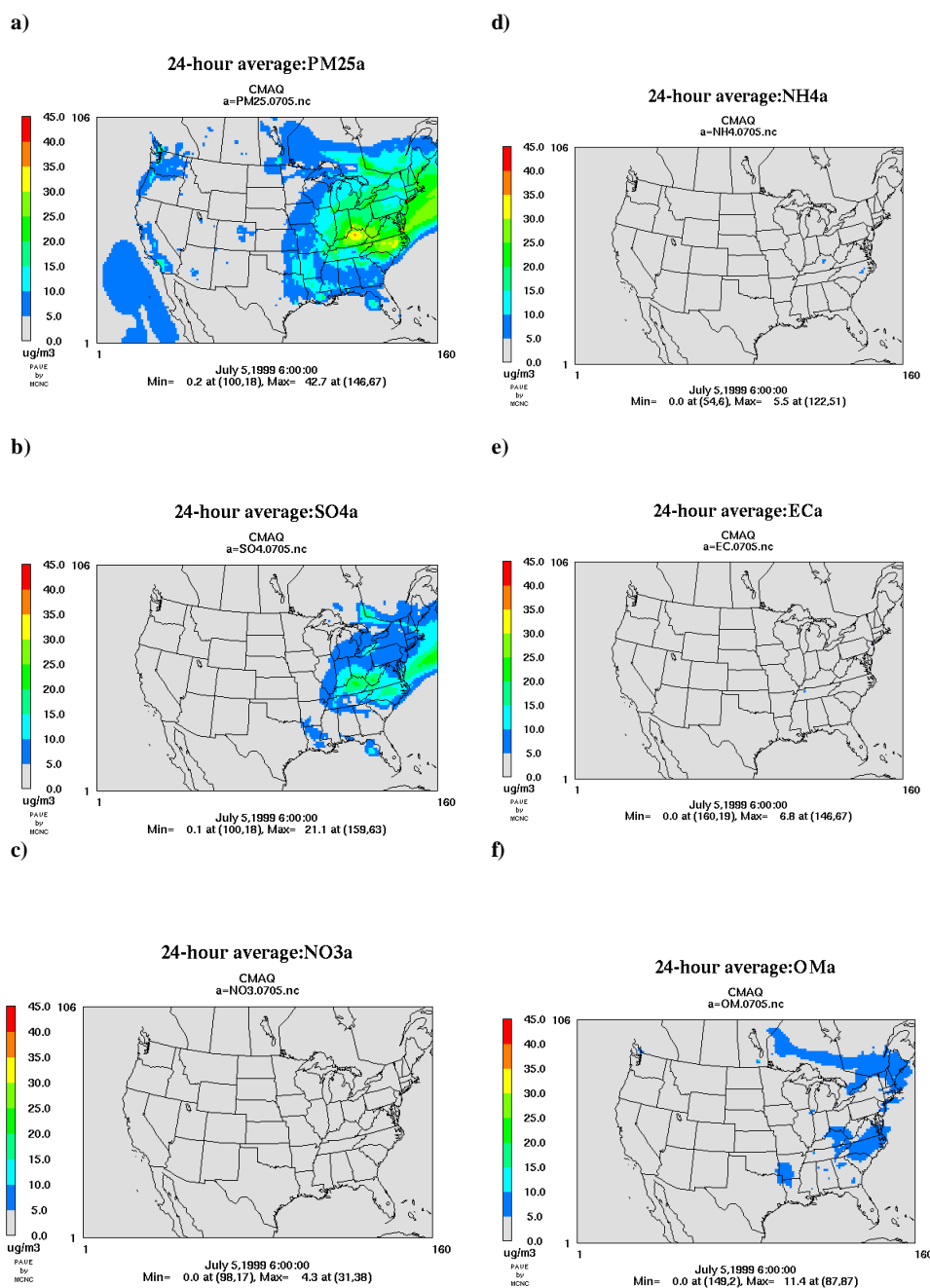
f) 24-hour average:OMa
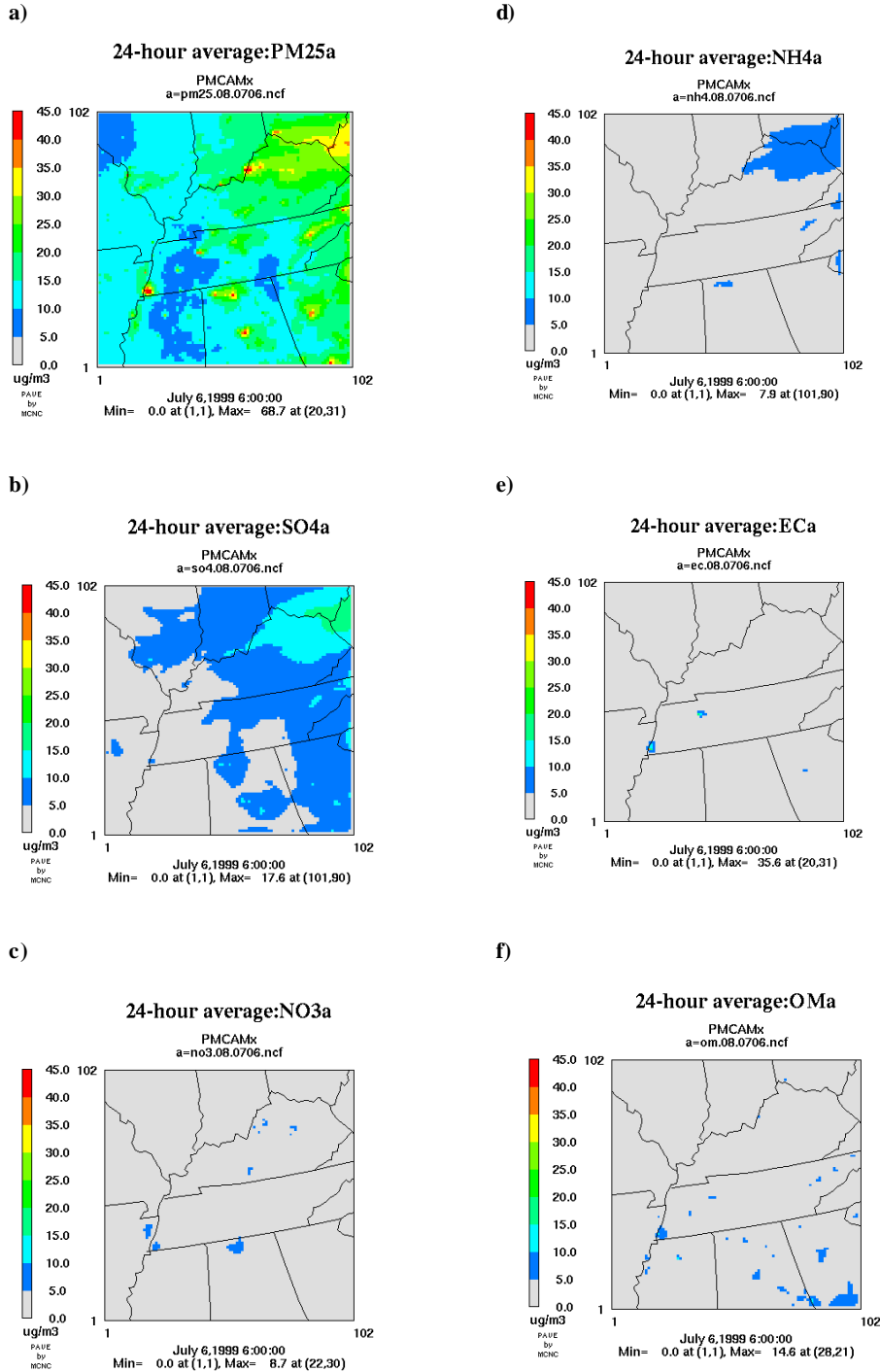
Figure 3-16. The spatial distribution of 24-hour average concentrations of (a) PM$_{2.5}$, (b) sulfate, (c) nitrate, (d) ammonium, (e) OM and (f) BC predicted by PM-CAMx on July 6, 1999 under the TVA base emission scenario with an 8 km horizontal resolution.

a)

24-hour average:PM25a

CMAQ
a=PM25.0707.nc

July 7,1999 6:00:00
Min= 0.1 at (102,5), Max= 43.2 at (125,37)

d)

24-hour average:NH4a

CMAQ
a=NH4.0707.nc

July 7,1999 6:00:00
Min= 0.0 at (142,7), Max= 5.7 at (108,21)

b)

24-hour average:SO4a

CMAQ
a=SO4.0707.nc

July 7,1999 6:00:00
Min= 0.1 at (102,5), Max= 23.8 at (134,45)

e)

24-hour average:ECa

CMAQ
a=EC.0707.nc

July 7,1999 6:00:00
Min= 0.0 at (160,14), Max= 6.0 at (146,67)

c)

24-hour average:NO3a

CMAQ
a=NO3.0707.nc

July 7,1999 6:00:00
Min= 0.0 at (142,7), Max= 5.1 at (31,39)

f)

24-hour average:OMa

CMAQ
a=OM.0707.nc

July 7,1999 6:00:00
Min= 0.0 at (143,7), Max= 13.2 at (87,87)

Figure 3-17.   The spatial distribution of 24-hour average concentrations of (a) $PM_{2.5}$, (b) sulfate, (c) nitrate, (d) ammonium, (e) OM and (f) BC predicted by CMAQ on July 7, 1999 under the TVA base emission scenario with a 32 km horizontal resolution.
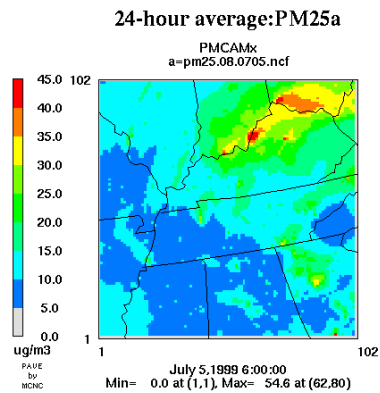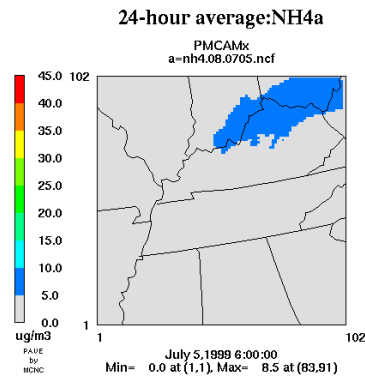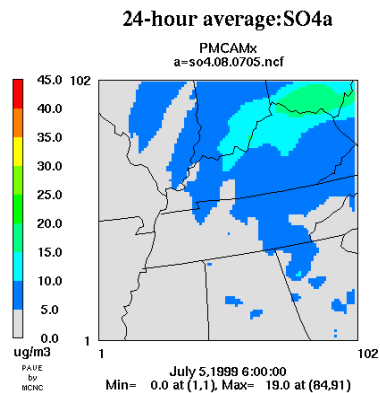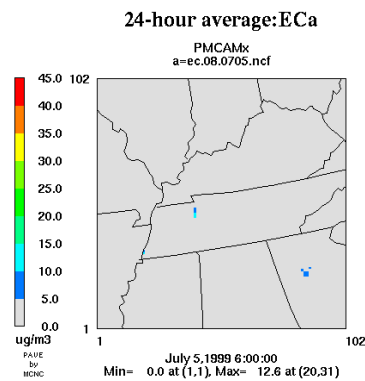
a)

24-hour average:PM25a

PMCAMx
a=pm25.32.0707.ncf

July 7,1999 6:00:00
Min= 0.0 at (1,1), Max= 67.7 at (94,19)

d)

24-hour average:NH4a

PMCAMx
a=nh4.32.0707.ncf

July 7,1999 6:00:00
Min= 0.0 at (1,1), Max= 11.3 at (125,37)

b)

24-hour average:SO4a

PMCAMx
a=so4.32.0707.ncf

July 7,1999 6:00:00
Min= 0.0 at (1,1), Max= 20.7 at (108,21)

e)

24-hour average:ECa

PMCAMx
a=ec.32.0707.ncf

July 7,1999 6:00:00
Min= 0.0 at (1,1), Max= 6.6 at (146,67)

c)

24-hour average:NO3a

PMCAMx
a=no3.32.0707.ncf

July 7,1999 6:00:00
Min= 0.0 at (1,1), Max= 15.8 at (94,19)

f)

24-hour average:OMa

PMCAMx
a=om.32.0707.ncf
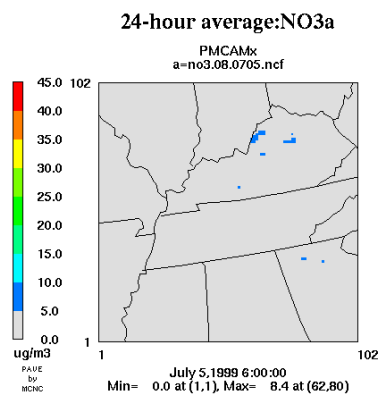
July 7,1999 6:00:00
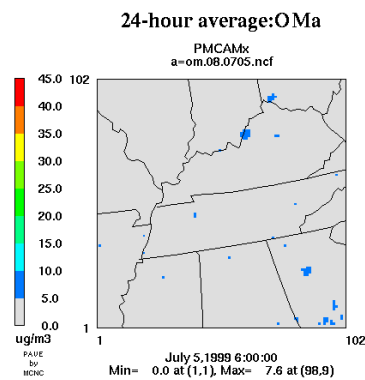Min= 0.0 at (1,1), Max= 11.8 at (87,87)

Figure 3-18.   The spatial distribution of 24-hour average concentrations of (a) PM$_{2.5}$, (b) sulfate, (c) nitrate, (d) ammonium, (e) OM and (f) BC predicted by PM-CAMx on July 7, 1999 under the TVA base emission scenario with a 32 km horizontal resolution.
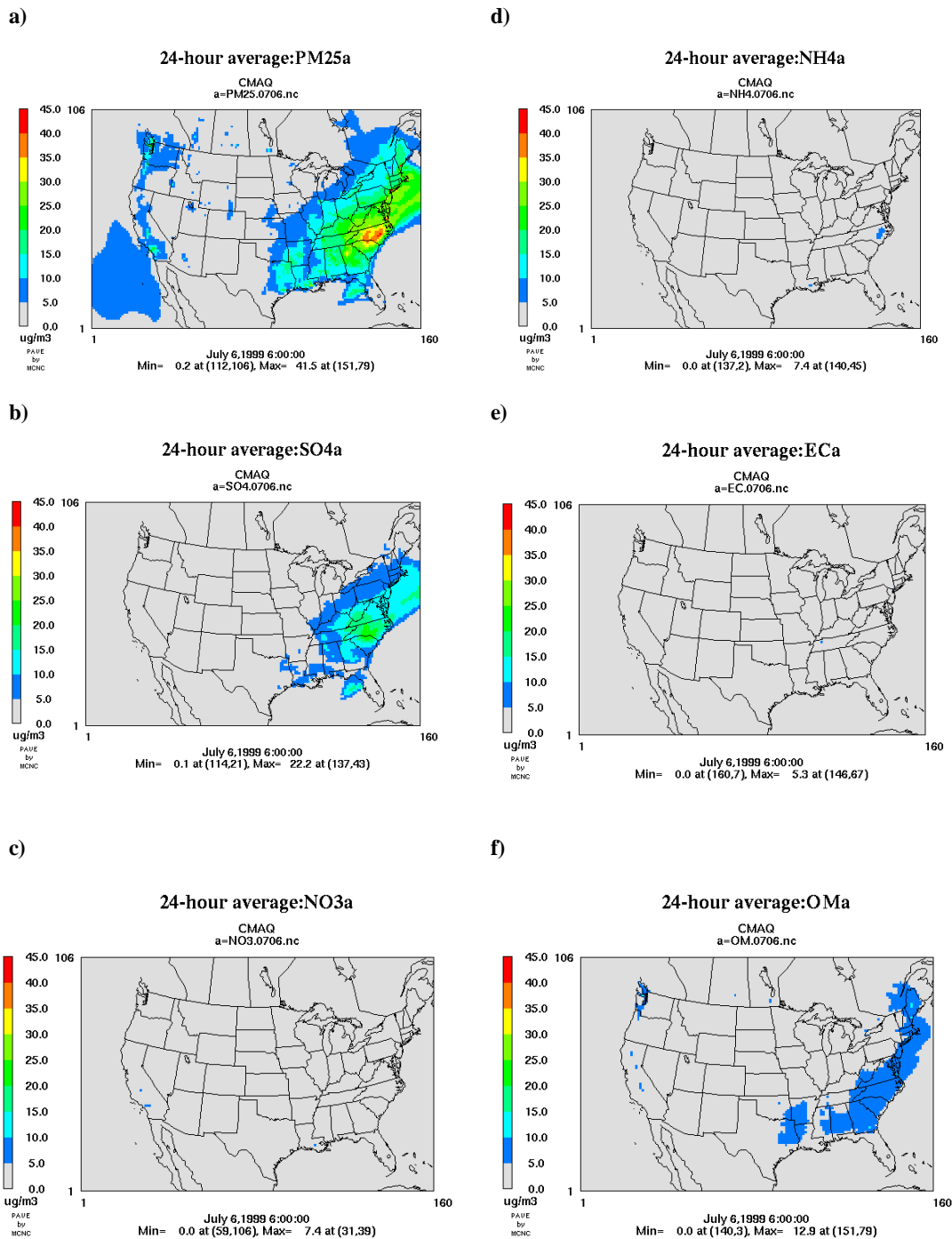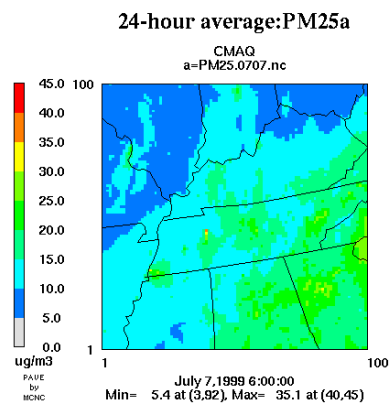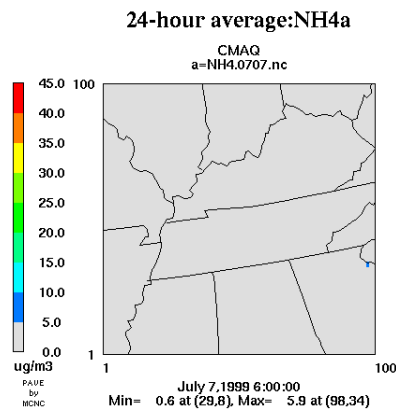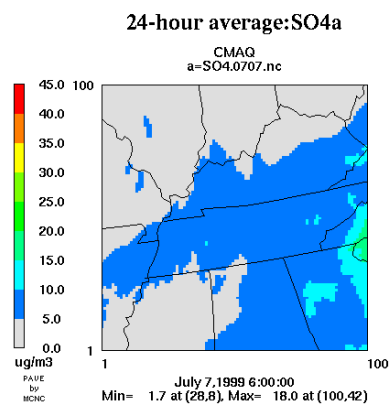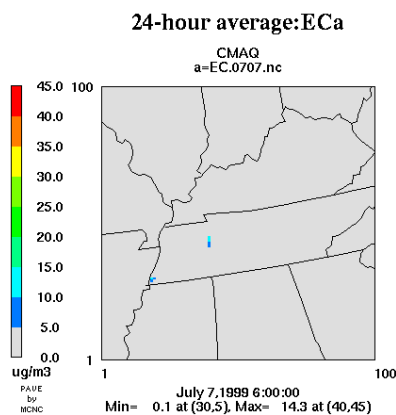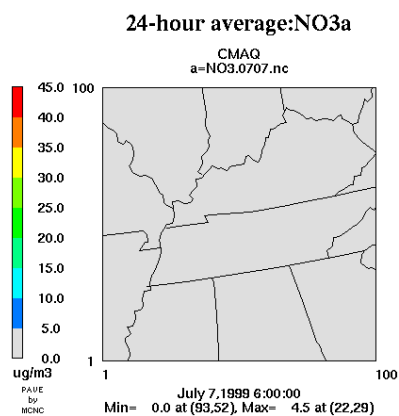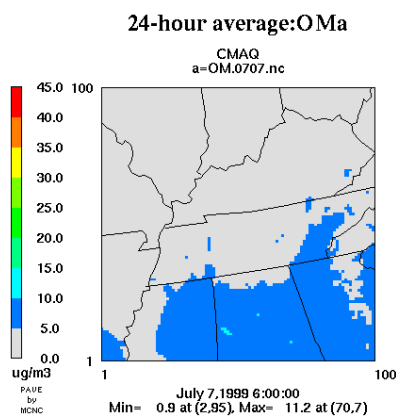
Figure 3-19. The spatial distribution of 24-hour average concentrations of (a) PM$_{2.5}$, (b) sulfate, (c) nitrate, (d) ammonium, (e) OM and (f) BC predicted by CMAQ on July 7, 1999 under the TVA base emission scenario with an 8 km horizontal resolution.
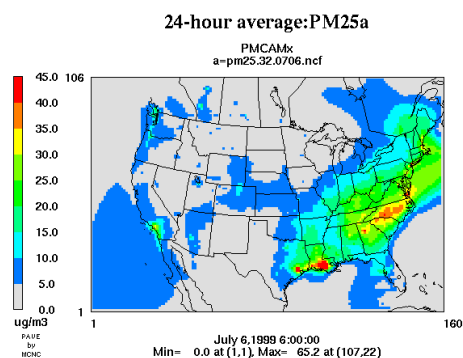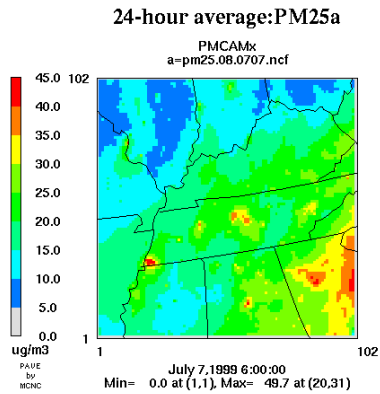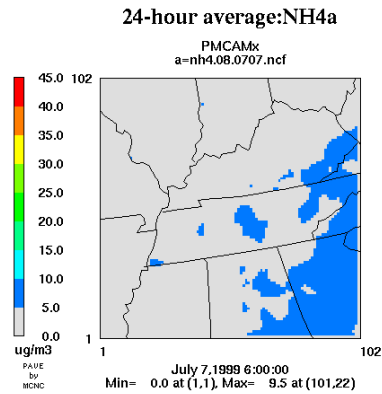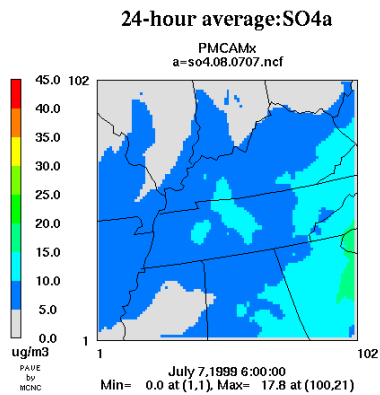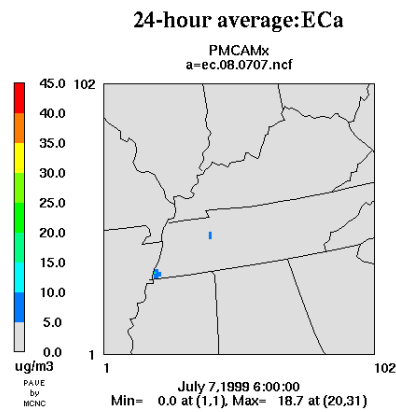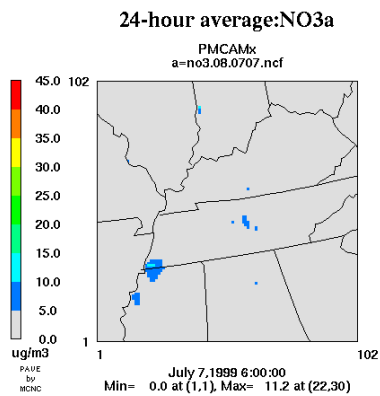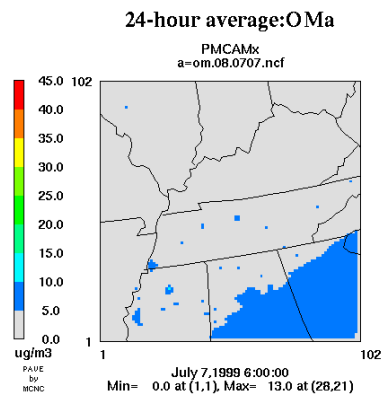
Figure 3-20.   The spatial distribution of 24-hour average concentrations of (a) PM$_{2.5}$, (b) sulfate, (c) nitrate, (d) ammonium, (e) OM and (f) BC predicted by PM-CAMx on July 7, 1999 under the TVA base emission scenario with an 8 km horizontal resolution.
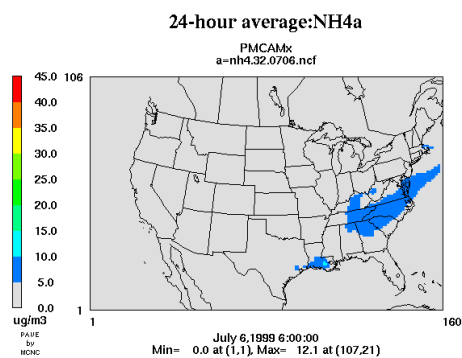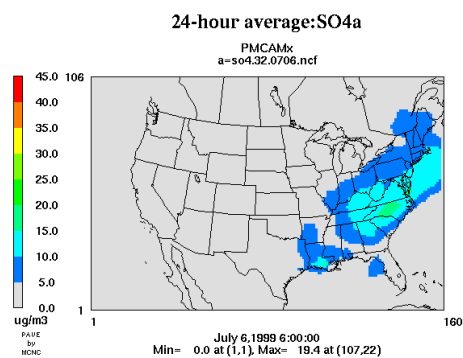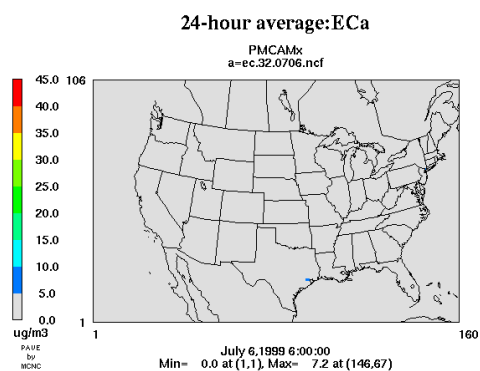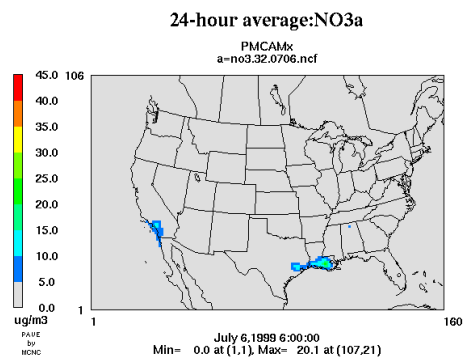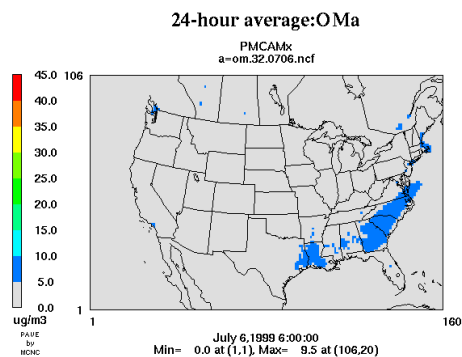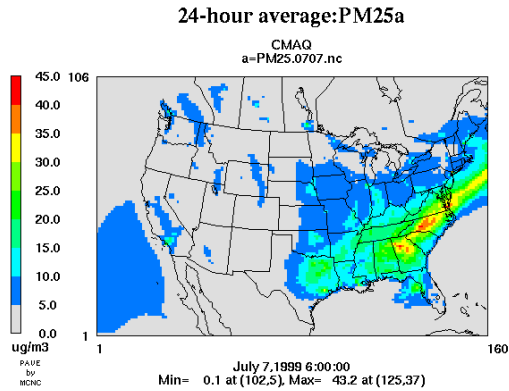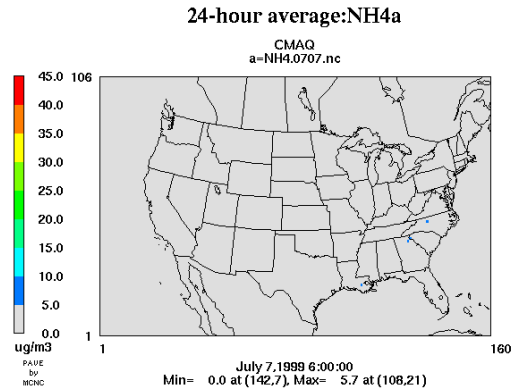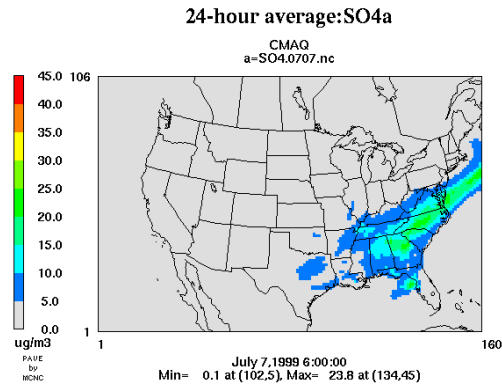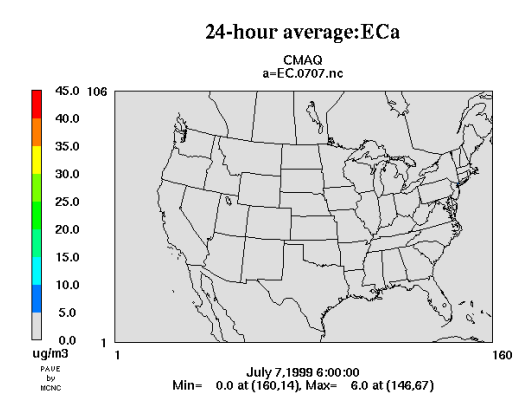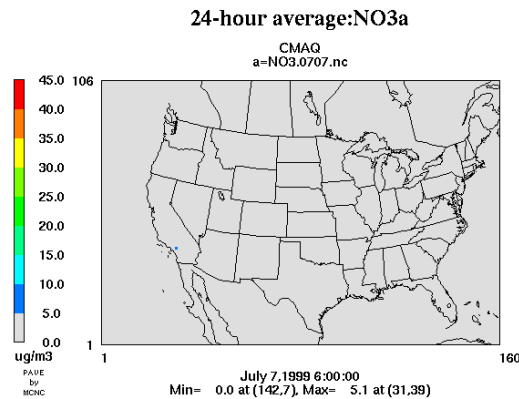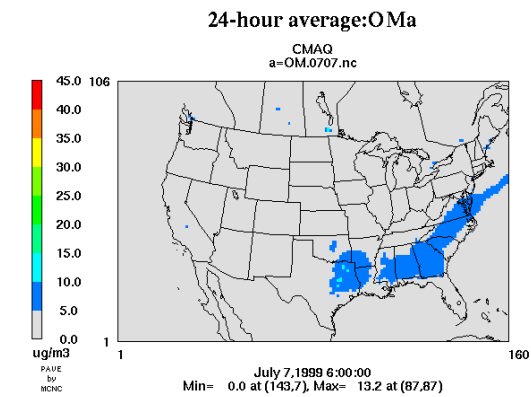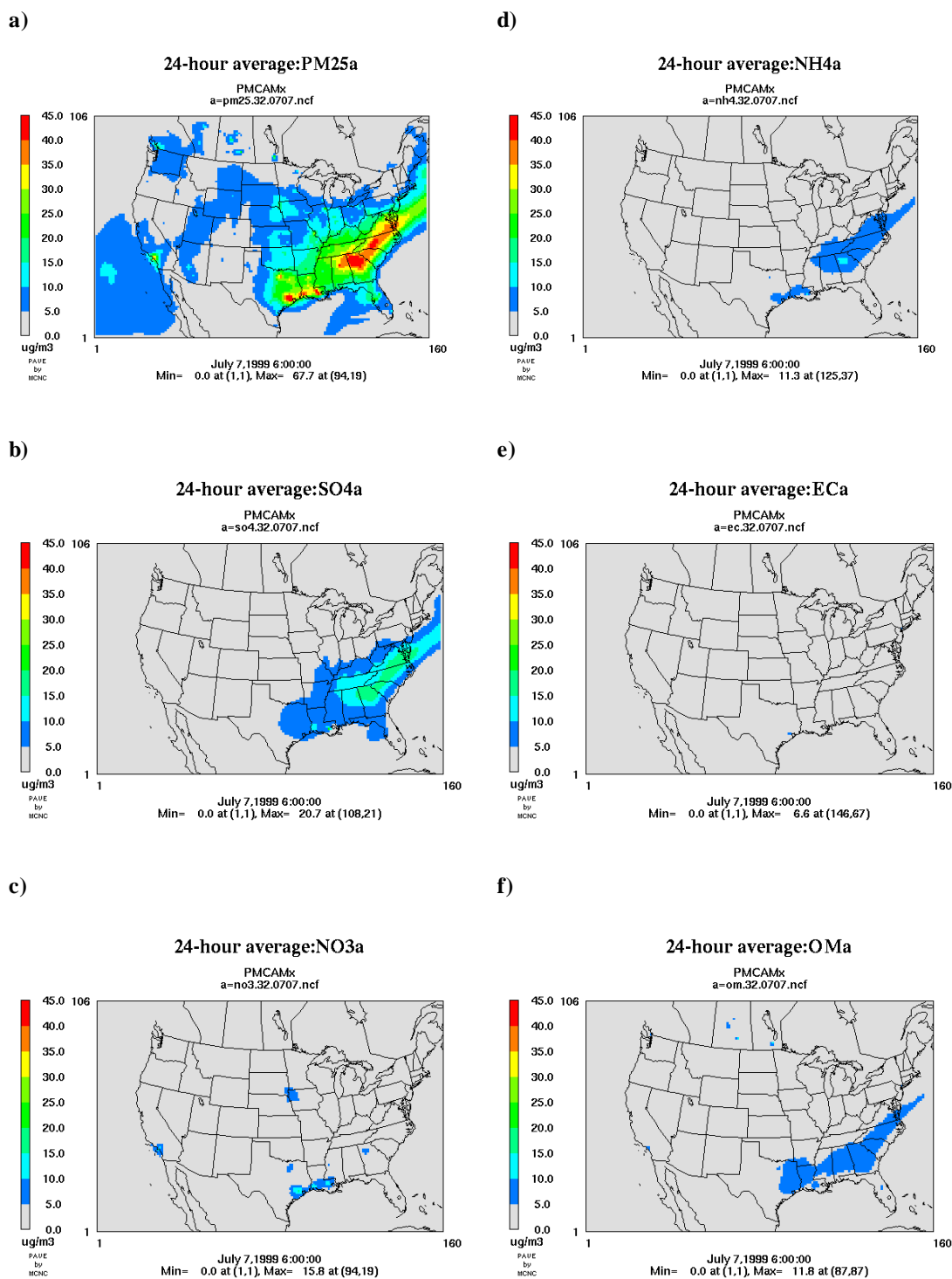
corresponding areas. We discuss below the concentrations of the following $PM_{2.5}$ components: sulfate, nitrate, ammonium, BC and OM (note that we omit to mention $PM_{2.5}$ when referring to these components hereafter). Compared to the results with the coarse grid on July 5 (Figure 3-9 vs. Figure 3-11), CMAQ with the fine grid predicts higher sulfate concentrations (by ~5 μg m^{-3}) in southern Ohio and southeastern Indiana and higher OM concentrations (by ~5 μg m^{-3}) in southern Ohio, southeastern Indiana, eastern Kentucky and a small portion of northwestern Virginia. OM comprises a significant fraction of SOA from biogenic sources in this area, sulfate results from both gaseous and aqueous-phase oxidation of SO_2 and primary emissions from several power plants in the area. Compared to the coarse grid, the fine grid provides a better representation for the emissions of SO_2, primary sulfate and biogenic OM precursors, resulting in higher concentrations for sulfate and OM, thus higher $PM_{2.5}$ concentrations in this area. On July 6 (Figure 3-13 vs. Figure 3-15), CMAQ with the fine grid predicts much higher BC and OM concentrations (by 10-20 and 5-15 μg m^{-3}, respectively) than those predicted with the coarse grid, because of better representation of primary BC and OC emissions. This results in much higher $PM_{2.5}$ concentrations in the areas that cover Waverly and Memphis, TN. On July 7 (Figure 3-17 vs. Figure 3-19), CMAQ with the fine grid predicts a similar level of OM but lower sulfate concentrations (by 5-15 μg m^{-3}) in the southeastern corner of the southeastern U.S. domain, which mainly covers northern Georgia including Atlanta. As shown later in Figure 3-22 and 3-23, CMAQ with the fine grid tends to underpredict sulfate in the northern Georgia area. The contribution to sulfate from the gaseous oxidation of SO_2 by OH predicted by CMAQ with the fine grid on July 7 in northern Georgia is greater than that with the coarse grid, due to a finer resolution in SO_2 emissions. However, sulfate formation in that area on July 7 is dominated by the aqueous-phase oxidation of SO_2 by dissolved oxidants such as H_2O_2, due to the frequent presence of convective clouds. As shown in Figure 3-21, the H_2O_2 mixing ratios predicted by CMAQ with the fine grid are significantly lower (e.g., by nearly a factor of 2 in the Atlanta area) than those with the coarse grid on July 7, due to the nonlinearity of the H_2O_2 chemistry, which is also nonlinearly related to grid resolution. The lower H_2O_2 mixing ratios predicted by CMAQ with the fine grid lead to

24-hour average:H2O2a

CMAQ SOS–99 32km km domain
a=CONC.H2O2.0707.nc

July 7,1999 0:00:00
Min= 0.000 at (121,102), Max= 0.012 at (102,36)

b)

24-hour average:H2O2a

CMAQ SOS–99 08km km domain
a=CONC.sos08.0707

July 7,1999 0:00:00
Min= 0.001 at (16,98), Max= 0.011 at (43,15)
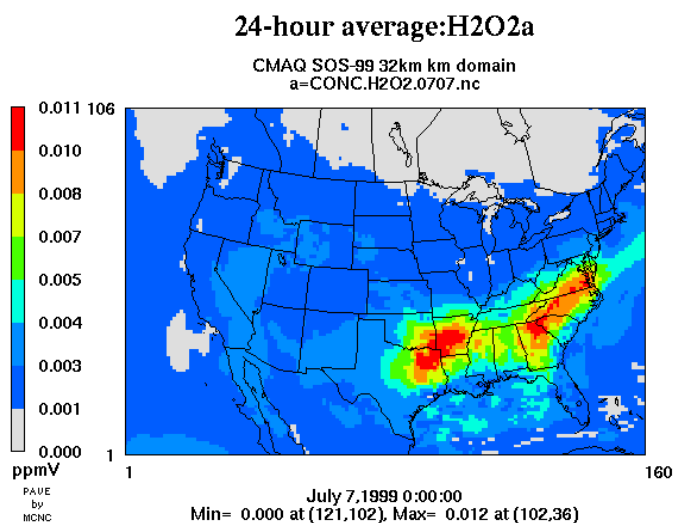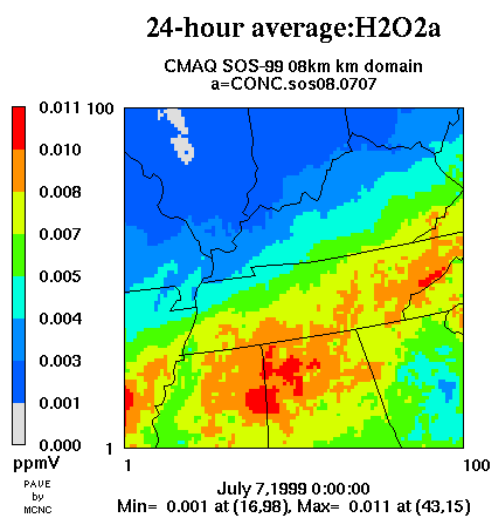
Figure 3-21.   The spatial distribution of 24-hour average mixing ratios of H_2O_2 predicted by CMAQ on July 7, 1999 with horizontal resolutions of (a) 32 km, (b) 8 km.

Observed

(Jefferson St., Atlanta)

a)

CMAQ

b)

d)

PMCAMX

c)

e)

Coarse Grid (32 km)   **Fine Grid (8 km)**

Figure 3-22.   The observed and predicted 24-hour average PM$_{2.5}$ chemical composition (in %) on July 5 at Jefferson Street, Atlanta, GA (a) CMAQ (32 km), (b) PM-CAMx (32 km), (b) CMAQ (8 km), and (d) PM-CAMx (8 km).

Observed
(Yorkville, GA)
a)
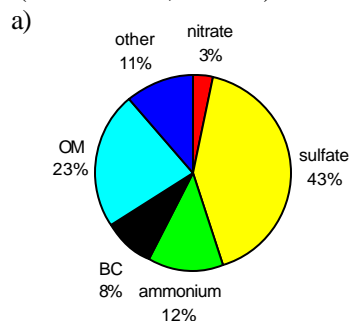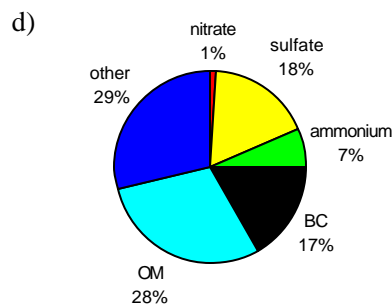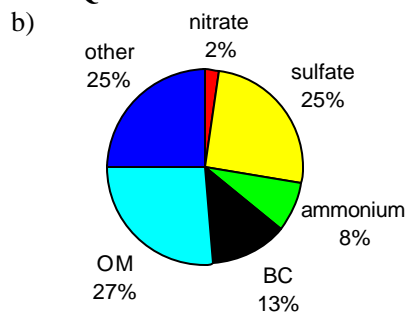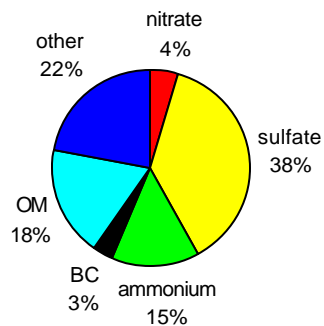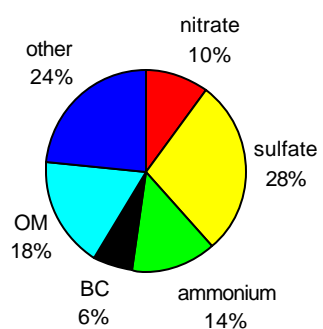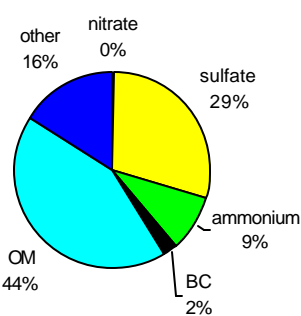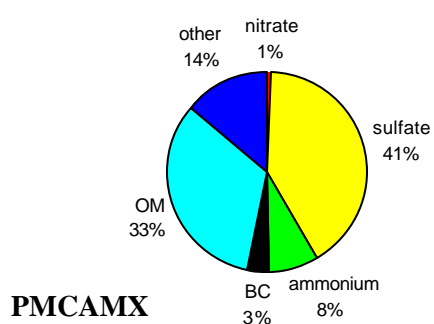
CMAQ

PMCAMX

Coarse Grid (32 km)   **Fine Grid (8 km)**

Figure 3-23.   The observed and predicted 24-hour average $PM_{2.5}$ chemical composition (in %) on July 5 at Yorkville, GA (a) CMAQ (32 km), (b) PM-CAMx (32 km), (b) CMAQ (8 km), and (d) PM-CAMx (8 km).

significantly lower sulfate formation through aqueous-phase oxidation of SO_2 by H_2O_2, causing lower sulfate concentrations than those predicted with the coarse grid.

3.1.2.3 Chemical Composition of PM$_{2.5}$ Over the U.S. and the Southeastern U.S.

Figures 3-9 to 3-20 show the concentrations of PM$_{2.5}$ and its chemical composition over the U.S. and the southeastern U.S. domains on July 5-7 predicted by the two models with both the fine and coarse grid resolutions. For the U.S. domain, among the five measurable PM species (i.e., sulfate, nitrate, ammonium, BC and OM), CMAQ (Figures 3-9, 3-13, and 3-17) predicts that sulfate and OM are the largest and the second largest contributors to PM$_{2.5}$ concentrations for the eastern and the southeastern U.S., nitrate and OM tend to dominate in California, where both NO$_x$ and VOC emissions from motor vehicles and industrial sources are high. PM-CAMx (Figures 3-10, 3-14, and 3-18) predicts that sulfate is the largest contributor to PM$_{2.5}$ concentrations for the eastern and southeastern U.S., followed by either OM (e.g., in the southeastern U.S. on July 6-7) or ammonium (e.g., over Kentucky and Tennessee on July 5-7) or both (e.g., in southern Virginia and North Carolina on July 5 and 7). PM-CAMx predicts high nitrate concentrations of 5-20 μg m^{-3} in several areas including southern Louisiana, and Los Angeles, CA on all three days; Houston, TX, Monroe, LA, and North Birmingham, AL on July 6-7; and Fort Worth, TX, Atlanta, GA, and the adjacent area of South Dakota, Nebraska, and Iowa on July 7.

For the southeastern U.S. domain, CMAQ (Figures 3-11, 3-15, and 3-19) predicts sulfate to be the largest contributor in the northern portion of the domain on July 5, the northeastern portion on July 6, and the eastern and southern portions on July 7. OM is predicted to be the second largest contributor in the eastern portion on July 5 and the eastern and southern portions on July 7. The contributions from BC, nitrate and ammonium are below 5 μg m^{-3} in many areas of the domain. For comparison, PM-CAMx (Figures 3-12, 3-16, and 3-20) predicts sulfate to be the largest contributor in the northern and eastern portions on July 5 and 6 and almost the entire domain except for a small area in the northern and southwestern portions of the domain on July 7. The second largest contributor is OM in a small area in the southeastern corner on July 6 or

ammonium in the northeastern portion on July 5-6 or both OM and ammonium in the southeastern portion on July 7. While the contributions from BC are below 5 μg m^{-3} in many areas of the domain, those from nitrate can be as high as 11 μg m^{-3} in several areas such as Louisville, KY on July 5 and Memphis, TN on July 6-7.

Figures 3-22 and 3-23 show the observed and predicted 24-hour average PM$_{2.5}$ chemical composition (in %) on July 5, 1999 at an urban site, Jefferson Street, Atlanta, GA (JST) and a rural site, Yorkville (YRK) in Georgia, respectively. Predictions with horizontal resolutions of 32 km and 8 km are shown. JST is an urban site located in downtown Atlanta. YRK is a rural site located about 70 km west of downtown Atlanta. This area is characterized by (1) a high frequency of air mass stagnation, warm temperatures, high humidities, and intense solar insolation during summer; (2) dense vegetation, which emits large amounts of isoprene that dominate VOC reactivity and other natural hydrocarbons during the hot summers; and (3) an anthropogenic emission mix dominated by cities and large point sources (e.g., several power plants) located in rural areas (Cowling et al., 1998). The stagnant and hot summer climatology inhibits the dispersion of pollutants and favors the accumulation of O$_3$ precursors near the ground. The high biogenic emissions make O$_3$ formation generally NO$_x$-sensitive during summertime (Pun et al., 2002). The VOC emission inventory in this area reflects a mix of anthropogenic and biogenic emissions. The observed mass fractions for sulfate and OM at both sites on July 5 are quite high, consistent with the emission characteristics in this area. PM$_{2.5}$ at JST, Atlanta was observed to consist of 43% sulfate, 12% ammonium, 8% BC, 23% OM, 3% nitrate and 11% other inorganic materials (OI) (e.g., crustal species). At JST, both models significantly underpredict the sulfate contribution (18% and 25% for the fine and coarse grids for CMAQ and 23% and 18% for the fine and coarse grids for PM-CAMx versus an observed value of 43%) and overpredict the contribution of OI (29% and 25% for the fine and coarse grids for CMAQ and 32% and 31% for the fine and coarse grids for PM-CAMx versus an observed value of 11%). CMAQ with the fine grid tends to underpredict the 24-hour average nitrate (1%) and ammonium (7%) contributions and overpredicts BC (17% versus 8%) and OM (28% versus 23%) contributions but it reproduces well the mass fractions of these species for the coarse grid simulation (2%, 8%, 13% and 27% for nitrate, ammonium, BC and OM,

respectively). PM-CAMx tends to underpredict the contributions of the 24-hour average OM (17% and 18% for the fine and coarse grids versus the observed value of 23%) and ammonium (7% and 9% for the fine and coarse grids versus the observed value of 12%) and overpredicts those of nitrate (3% and 8% for the fine and coarse grids versus the observed value of 3%) and BC (18% and 16% for the fine and coarse grids versus the observed value of 8%). Compared to the observations, CMAQ with the coarse grid gives the best results at JST among the four simulations.

At Yorkville, GA, $PM_{2.5}$ was observed to consist of 52% sulfate, 14% ammonium, 1% BC, 15% OM, 2% nitrate and 16% OI on July 5, 1999. As for JST, both models significantly underpredict sulfate fractions (29% and 41% for the fine and coarse grids for CMAQ and 38% and 28% for the fine and coarse grids for PM-CAMx). CMAQ reproduces well nitrate and OI contributions, but it significantly overpredicts the OM (44% and 33% for the fine and coarse grids) and BC (2% and 3% for the fine and coarse grids) fractions and underpredicts the ammonium contributions (9% and 8% for the fine and coarse grids). PM-CAMx reproduces well the contributions of ammonium and OM, but it significantly overpredicts those of nitrate (4% and 10% for the fine and coarse grids), BC (3% and 6% for the fine and coarse grids) and OI (22% and 24% for the fine and coarse grids). Compared to the observations, CMAQ with the coarse grid gives the best results at YRK among the four simulations.

Figures 3-24 and 3-25 show the observed and predicted 24-hour average $PM_{2.5}$ chemical compositions (in %) on July 6, 1999 at an urban site, Hendersonville (HEN), and a rural site, Dickson (DI) in Tennessee, respectively, with horizontal resolutions of 32 km and 8 km. HEN and DI are located about 15 km northeast and 45 km southwest of downtown Nashville. The chemical composition of $PM_{2.5}$ observed at HEN is quite different from that at JST, with much higher mass fractions for OM (43% vs. 23%) and OI (26% vs. 11%) but much lower mass fractions for sulfate (21% vs. 43%), ammonium (6% vs. 12%) and BC (2% vs. 8%). At HEN, both models significantly overpredict the sulfate fraction (36% and 44% for the fine and coarse grids for CMAQ and 35% and 34% for the fine and coarse grids for PM-CAMx), the ammonium fraction (14% and 13% for the fine and coarse grids for CMAQ and 17% and 18% for the fine and coarse grids for PM-CAMx), the nitrate fraction (3% and 6% for the fine and coarse grids for CMAQ and

Observed
(Hendersonville, TN)

a)

CMAQ

b)

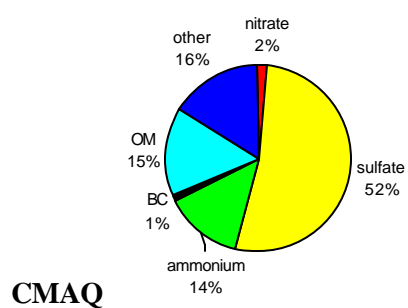
d)

PMCAMX

c)

e)
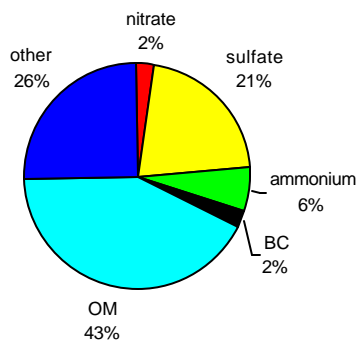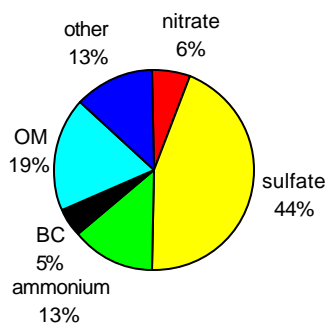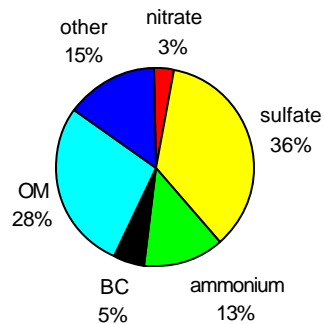
Coarse Grid (32 km) **Fine Grid (8 km)**

Figure 3-24.   The observed and predicted 24-hour average PM$_{2.5}$ chemical composition (in %) on July 6 at Hendersonville, TN (a) Observed, (b) CMAQ (32 km), (c) PM-CAMx (32 km), (d) CMAQ (8 km), and (e) PM-CAMx (8 km).

Observed
(Dickson, TN)
a)

CMAQ
b)

d)

PMCAMX
c)

e)
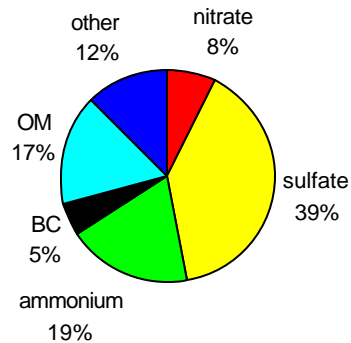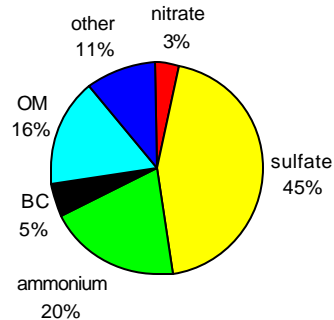
Coarse Grid (32 km)   **Fine Grid (8 km)**

Figure 3-25.   The observed and predicted 24-hour average PM$_{2.5}$ chemical composition (in %) on July 6 at Dickson, TN (a) Observed, (b) CMAQ (32 km), (c) PM-CAMx (32 km), (d) CMAQ (8 km), and (e) PM-CAMx (8 km).

7% and 15% for the fine and coarse grids for PM-CAMx) and the BC fraction (5% for both the fine and coarse grids for CMAQ and 6% and 5% for the fine and coarse grids for PM-CAMx). They both underpredict the OM fraction (28% and 19% for the fine and coarse grids for CMAQ and 17% and 14% for the fine and coarse grids for PM-CAMx). CMAQ also significantly underpredicts the OI fraction (15% and 13% for the fine and coarse grids for CMAQ). PM-CAMx significantly underpredicts the OI fraction for both the fine and coarse grid simulations (18% and 14%, respectively). Compared to the observations, all four simulations failed to correctly reproduce the chemical composition of $PM_{2.5}$ at Hendersonville, TN.

At Dickson, TN, the observed PM2.5 composition on July 6, 1999 was overwhelmingly dominated by OM and OI (44% and 39%, respectively), it contained only 9% sulfate, 6% ammonium, 2% nitrate and 0% BC. Both models significantly overpredict the sulfate fraction (44% and 54% for the fine and coarse grids for CMAQ and 45% and 39% for the fine and coarse grids for PM-CAMx), the ammonium fraction (9% and 11% for the fine and coarse grids for CMAQ and 20% and 19% for the fine and coarse grids for PM-CAMx), and the BC fraction (4% and 3% for the fine and coarse grids for CMAQ and 5% for both fine and coarse grids for PM-CAMx). They both significantly underpredict the OI fraction (10% and 9% for the fine and coarse grids for CMAQ and 16% and 17% for the fine and coarse grids for PM-CAMx) and the OM fraction (32% and 22% for the fine and coarse grids for CMAQ and 16% and 17% for the fine and coarse grids for PM-CAMx). While CMAQ reproduces well the nitrate fraction (1.1% and 0.7% for the fine and coarse grid simulations), PM-CAMx significantly overpredicts the nitrate fraction (3% and 8% for the fine and coarse grids). Compared to the observations, all four simulations failed to correctly reproduce the chemical composition of $PM_{2.5}$ at Dickson, TN.

Figure 3-26 shows the observed and predicted 24-hour average $PM_{2.5}$ chemical compositions (in %) on July 7, 1999 at Great Smoky Mountains National Park (GRSM), TN. The observed $PM_{2.5}$ composition at this site was dominated by sulfate and OI (39% and 35%, respectively); it contained 17% OM, 7% ammonium, 2% BC and 0% nitrate. Both models accurately reproduce the mass fraction for BC, but they both significantly overpredict that of ammonium (13 and 11% for the fine and coarse grids for CMAQ and

Observed

(Great Smoky Mt., TN)

(a)

CMAQ

(b)

(d)

PMCAMX

(c)

(e)
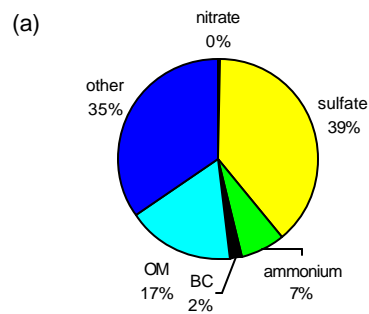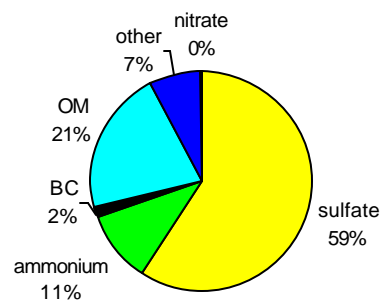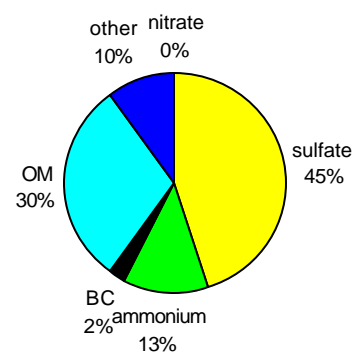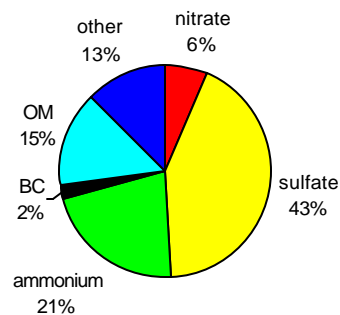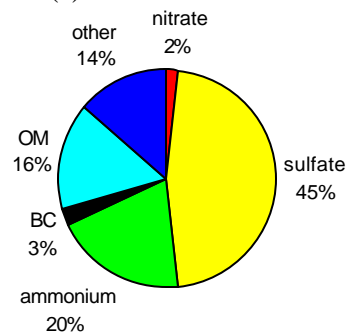
Coarse Grid (32 km)   **Fine Grid (8 km)**

Figure 3-26.   The observed and predicted 24-hour average PM$_{2.5}$ chemical composition (in %) on July 7 at Great Smoky Mountains National Park, TN (a) Observed, (b) CMAQ (32 km), (c) PM-CAMx (32 km), (d) CMAQ (8 km), and (e) PM-CAMx (8 km).

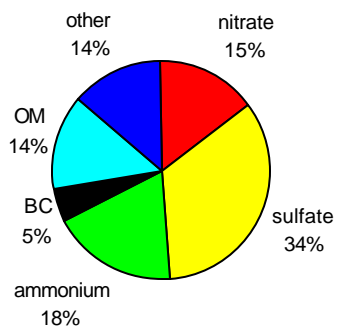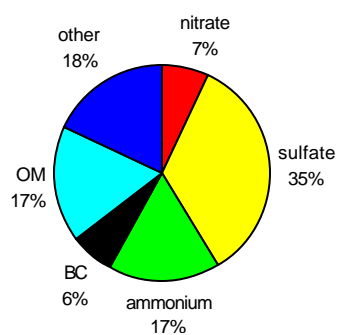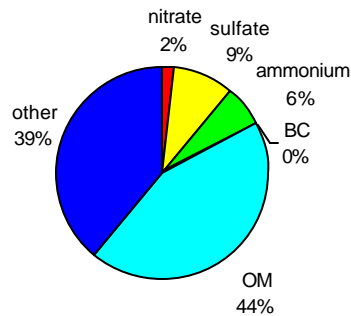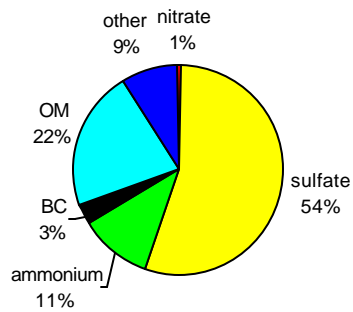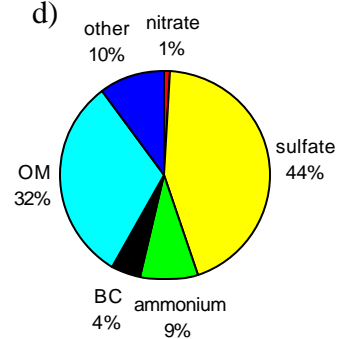20% and 21% for the fine and coarse grids for PM-CAMx) and underpredict the OI fraction (10% and 7% for the fine and coarse grids for CMAQ and 14% and 13% for the fine and coarse grids for PM-CAMx). CMAQ significantly overpredicts the OM fraction (30% and 21% for the fine and coarse grids) and the sulfate fraction (45% and 59% for the fine and coarse grids). PM-CAMx reproduces well the fractions of OM (16% and 15% for the fine and coarse grids) and sulfate (45% and 43% for the fine and coarse grids) but it overpredicts that of nitrate (2% and 6% for the fine and coarse grids). Compared to the observations, PM-CAMx with the fine grid gives the best results at GRSM among the four simulations.

3.2 Temporal Distributions of O_3 and $PM_{2.5}$ at Selected Sites

3.2.1 Temporal Distributions of O_3

Figures 3-27 and 3-28 show the time series of observed and predicted O_3 mixing ratios at Jefferson Street, Atlanta, GA and Yorkville, GA, respectively, with horizontal resolutions of 32 km and 8 km. The measured O_3 mixing ratios from the SEARCH network are available at JST from 1:00 am July 1 to 2:00 p.m., July 6, 1999. The observed peak O_3 mixing ratios at JST were 26-54 ppb on July 1-4 (i.e., low O_3 days) and 101-111 ppb on July 5-6 (high O_3 days). The observed peak O_3 mixing ratios typically occurred in the mid afternoon between 2 p.m. and 4 p.m. (July 4 is an exception with two peaks, the first peak of 45.8 ppb occurred at 11:00 a.m., and the second peak of 46.6 ppb occurred at 5:00 p.m.). For the coarse grid simulations (Figure 3-27 (a)), PM-CAMx significantly overpredicts daytime and peak O_3 mixing ratios (up to factors of 8 and 3.8, respectively) for all days. The daytime and peak O_3 mixing ratios predicted by CMAQ are overpredicted (up to factors of 6 and 4.0, respectively) on July 1-2 and 4 and the peak O_3 mixing ratio is underpredicted (by 17%) on July 6. However, those on July 3-4 are in good agreement with the observations. The times of the peak O_3 predicted by both CMAQ and PM-CAMx are either the same as the observed peak times or off by 1-3 hours. For the fine grid simulations (Figure 3-27 (b)), CMAQ predicts the daytime and peak O_3 mixing ratios that are closer to the observations than those predicted with the

JST, 32 km domain

JST, 8 km domain

Figure 3-27.   The time series of observed and predicted O$_3$ mixing ratios on July 1-9, 1999 at Jefferson Street, Atlanta with horizontal resolutions of (a) 32 km (b) 8 km.

YRK, 32 km domain

YRK, 8 km domain

Figure 3-28.   The time series of observed and predicted O_3 mixing ratios on July 1-9, 1999 at Yorkville, Georgia with horizontal resolutions of (a) 32 km (b) 8 km.

coarse grid (within factors of 4.0 and 2.4, respectively, for low O_3 days and 43% and 35%, respectively, for high O_3 days). The peak O_3 mixing ratios predicted by PM-CAMx are also closer to the observation (within a factor of 3 for low O_3 days and 30% for high O_3 days) than those predicted with the coarse grid, but it predicts several peaks on some days (e.g., July 2 and 6) with the peak times for the highest peak values significantly off the observations (e.g., delayed by 6 hours on July 2). In addition, other daytime and nighttime O_3 mixing ratios predicted by PM-CAMx during most of the days on July 1-9 are much higher than the observations and those predicted by CMAQ.

The measured O_3 mixing ratios are available at the rural site (i.e., Yorkville, see Figure 3-28) on July 1-9. The observed peak O_3 mixing ratios at YRK were 39-75 ppb on July 1-4 and 9 (i.e., low O_3 days) and 81-97 ppb on July 5-8 (high O_3 days). The observed peak O_3 mixing ratios typically occurred in the early-to-late afternoon between 1 p.m. and 5 p.m. For the coarse grid simulations (Figure 3-28 (a)), PM-CAMx significantly overpredicts the peak O_3 mixing ratios (by a factor of up to 3.5) and other daytime and nighttime O_3 mixing ratios (by up to factors of 8.3 and 31, respectively) throughout the simulation period. CMAQ overpredicts the peak O_3 mixing ratios on July 1-2 and 7 by up to 57% but underpredicts those on July 5-6 and 8-9 by up to -21%. CMAQ overpredicts both daytime and nighttime O_3 mixing ratios on July 1-2 and 7-8 (by up to factors of 4 and 27, respectively). CMAQ underpredicts O_3 mixing ratios during high O_3 periods on July 5-6 and 8-9 (i.e., between noon-6 p.m. on July 5, noon-2 p.m. on July 6, 2-3 p.m. on July 8 and 11 a.m.-2 p.m. on July 9) by up to -31% but reproduces well the temporal variation of O_3 mixing ratios on July 3-4. Compared to the observations, the times of peak O_3 predicted by PM-CAMx are either 1 hour ahead or 1-5 hours delayed, and those predicted by CMAQ are either the same or delayed by 1-6 hours. For the fine grid simulations (Figure 3-28 (b)), both models predict O_3 mixing ratios that are in closer agreement to the observations at YRK than those predicted with the coarse grid with exceptions on July 7 for CMAQ and July 4 for PM-CAMx. PM-CAMx overpredicts both daytime and nighttime O_3 mixing ratios (by up to factors of 4.7 and 24.4, respectively). CMAQ overpredicts the daytime O_3 mixing ratios on July 1-2, 4 and 7 by up to a factor of 4.4 and underpredicts those on July 3, 5-6, 8-9 by up to 50%. It also overpredicts nighttime O_3 mixing ratios on July 1-2, 4 and 6-7 by up to a factor of 26

and underpredicts those on July 5 by up to 23%. The times of peak O_3 predicted by PM-CAMx are either 1-2 hours ahead or 1-6 hours delayed, and those predicted by CMAQ are either the same as the observed peak times or delayed by 1-5 hours.

3.2.2 Temporal Distributions of PM$_{2.5}$

Figures 3-29 and 3-30 show the time series of observed and predicted PM$_{2.5}$ concentrations at Jefferson Street, Atlanta, GA and Yorkville, GA. Results with both horizontal resolutions of 32 km and 8 km are shown. The measured PM$_{2.5}$ concentrations were obtained using the Tapering Element Oscillating Microbalance (TEOM) on July 1-6 during SEARCH. The observed PM$_{2.5}$ concentrations ranged from 3.9 to 52 μg m^{-3}, with high concentrations (> 25 μg m^{-3}) occurring on July 1-2 and 5-6 (i.e., high PM days) and low concentrations occurring on July 3-4. Unlike O_3 mixing ratios, the peak PM$_{2.5}$ concentrations could occur at anytime (e.g., 5 p.m. on July 1, 8 p.m. on July 2, and 6 a.m. on July 3) and could appear several times (e.g., July 5-6) in a day, depending on the ambient chemical and meteorological conditions. For the coarse grid simulations (Figure 3-29 (a)), both CMAQ and PM-CAMx fail to reproduce the temporal variation of PM$_{2.5}$. PM-CAMx significantly underpredicts the peak PM$_{2.5}$ concentrations on July 1-2 and overpredicts those on July 5, 7 and 8. CMAQ tends to overpredict PM$_{2.5}$ concentrations on low PM days but underpredicts those on high PM days. For the fine grid simulations (Figure 3-29 (b)), PM-CAMx significantly underpredicts PM$_{2.5}$ concentrations on July 1 and overpredicts those during afternoon/evening periods on July 2, 4, 5 and 6. CMAQ underpredicts PM$_{2.5}$ concentrations on July 1-2, 3 (0:00 a.m. to 6:00 p.m.), 5 (11:00 a.m. to 12:00 a.m.) and 6 and overpredicts those on July 4 (0:00 a.m. to 5:00 p.m.) but reproduces those well during the period of 5:00 p.m., July 4 through 10:00 a.m., July 5. PM-CAMx predicts several significant spikes in the PM$_{2.5}$ concentrations (e.g., in the afternoon on July 2, the morning on July 5, and the evening on July 6) that are inconsistent with the observed values. Overall, CMAQ captures the magnitudes of PM$_{2.5}$ and some temporal variation trends better than PM-CAMx.

The TEOM-measured PM$_{2.5}$ concentrations are available at Yorkville on July 1-9 during SEARCH. The observed PM$_{2.5}$ concentrations ranged from less than 3.4 to 57 μg

(a)

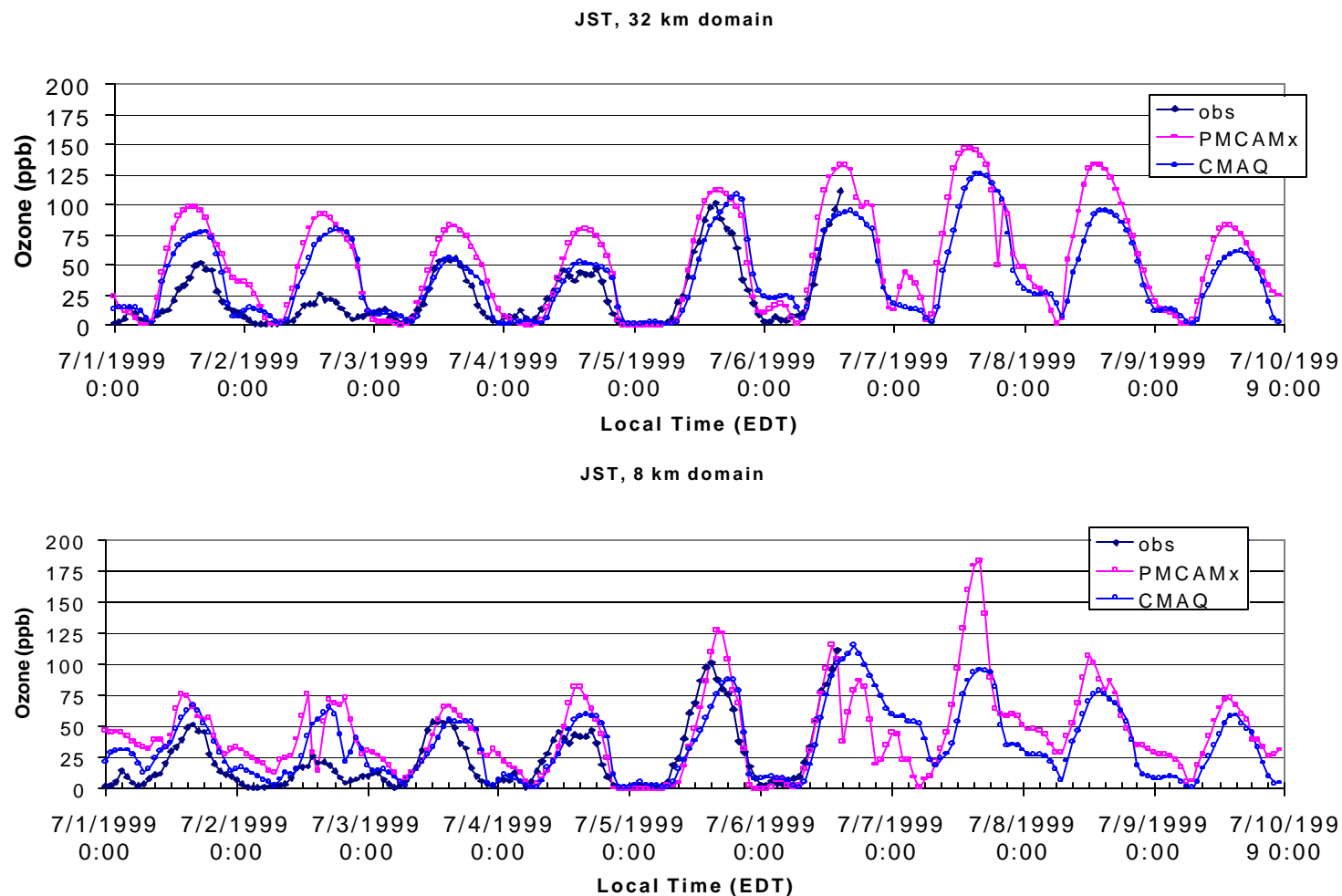**JST, 32 km domain**

(b)

JST, 8 km domain
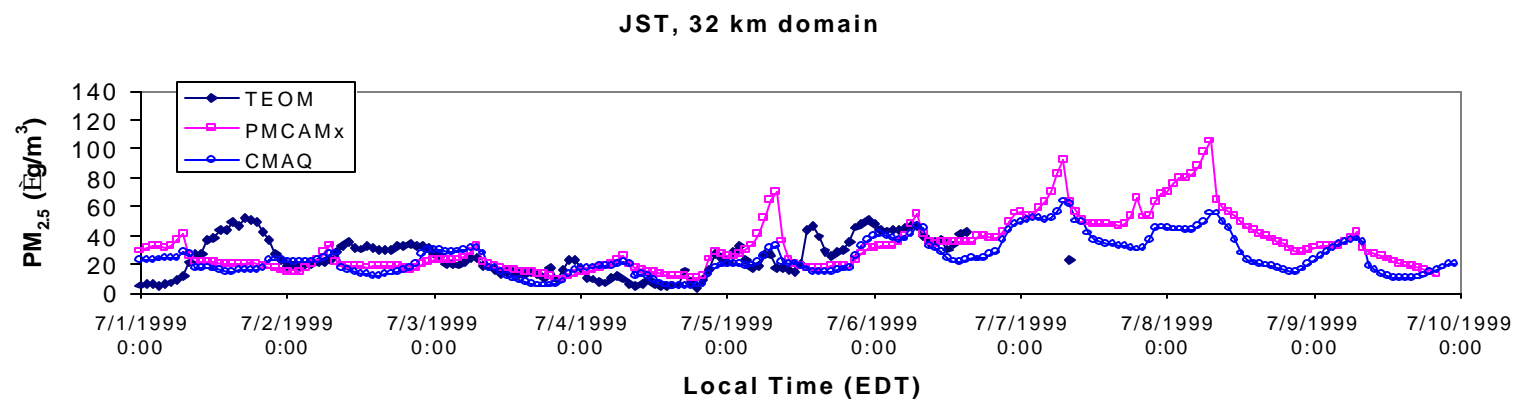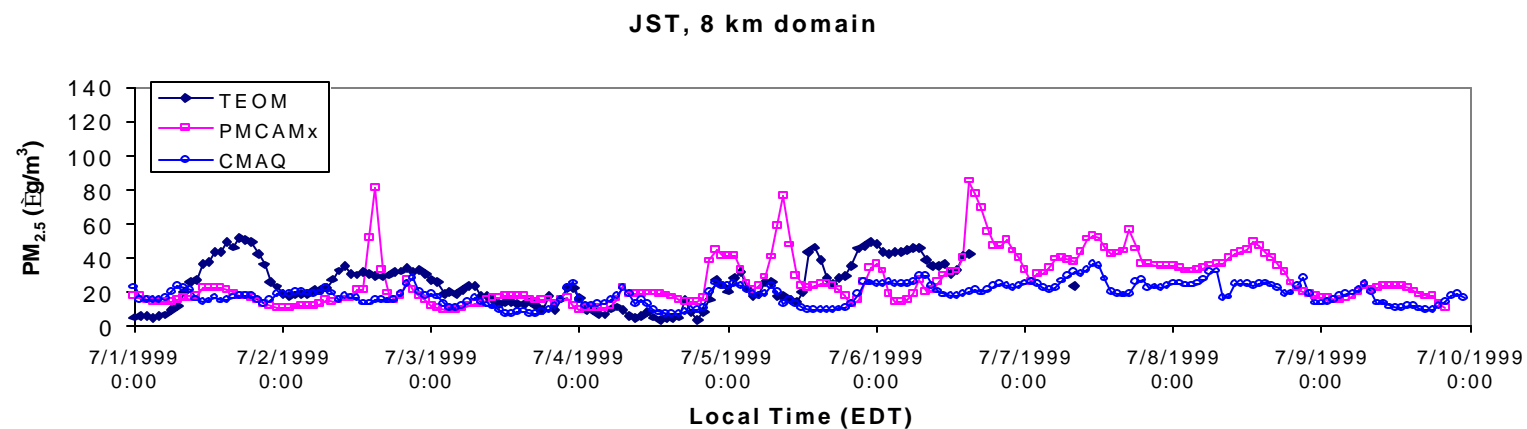
Figure 3-29.   The time series of observed and predicted PM$_{2.5}$ concentrations on July 1-9, 1999 at Jefferson Street, Atlanta with horizontal resolutions of (a) 32 km (b) 8 km.
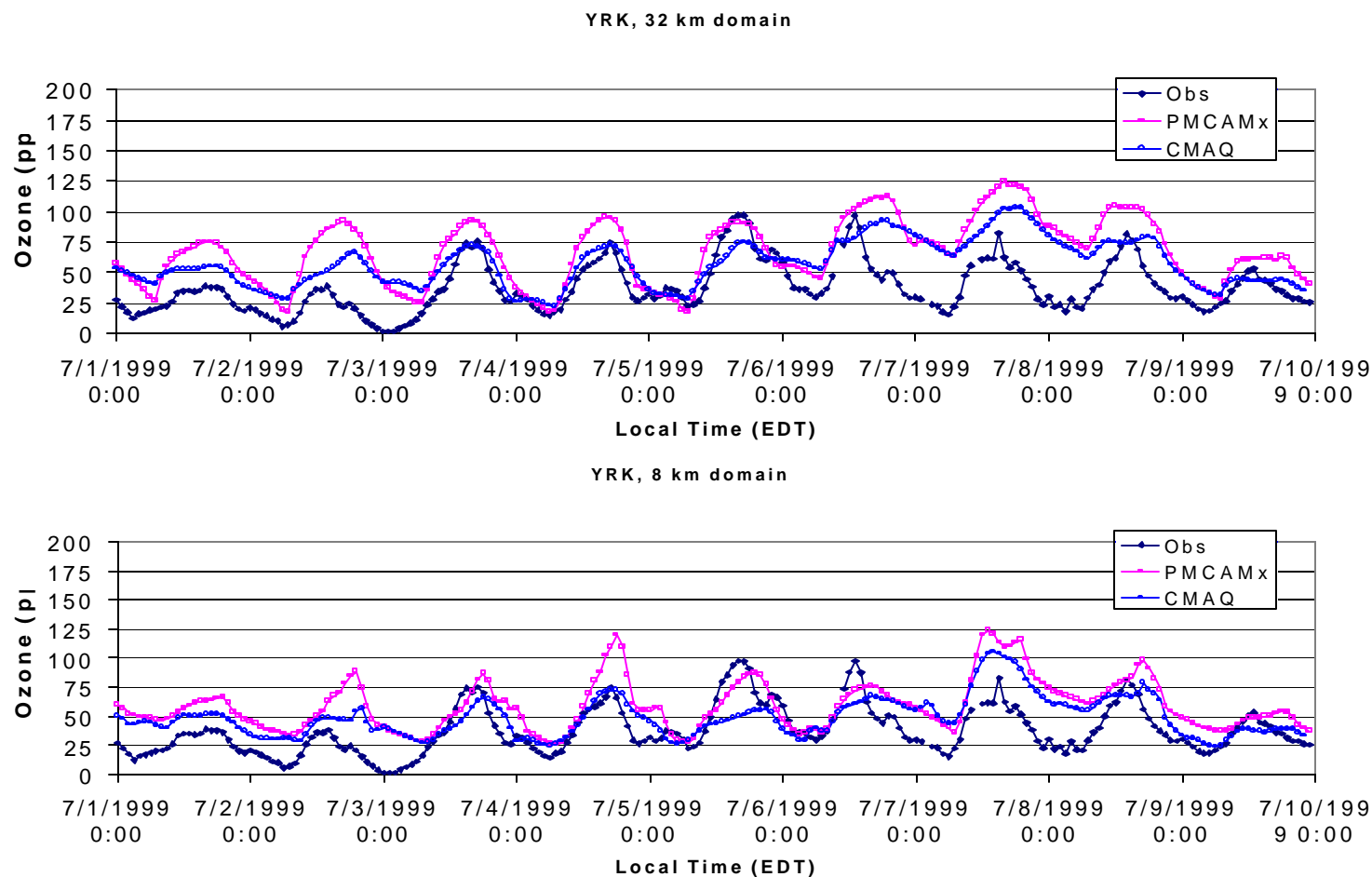
(a)

YRK, 32 km domain

(b)

YRK, 8 km domain
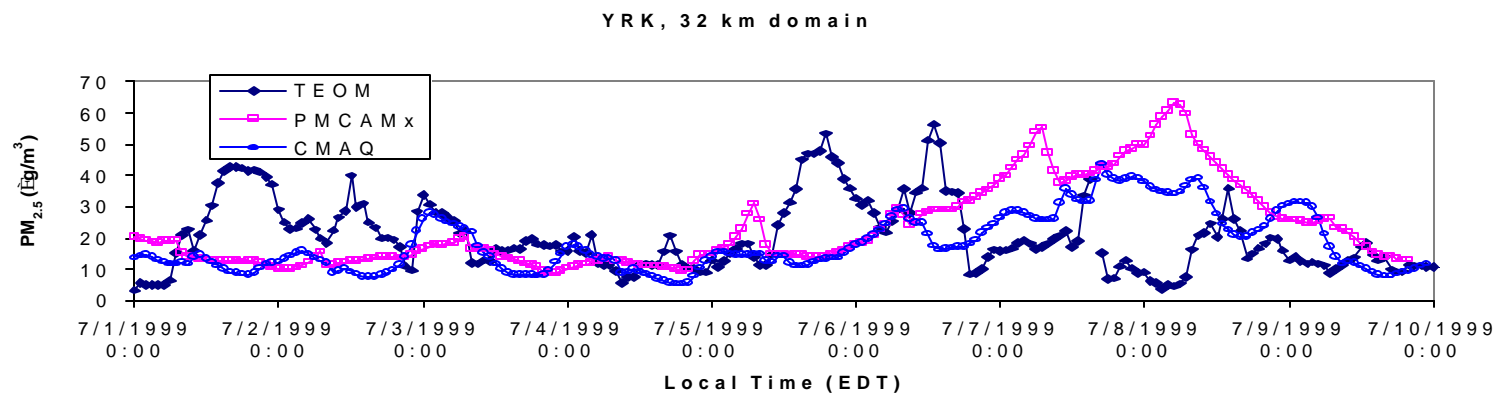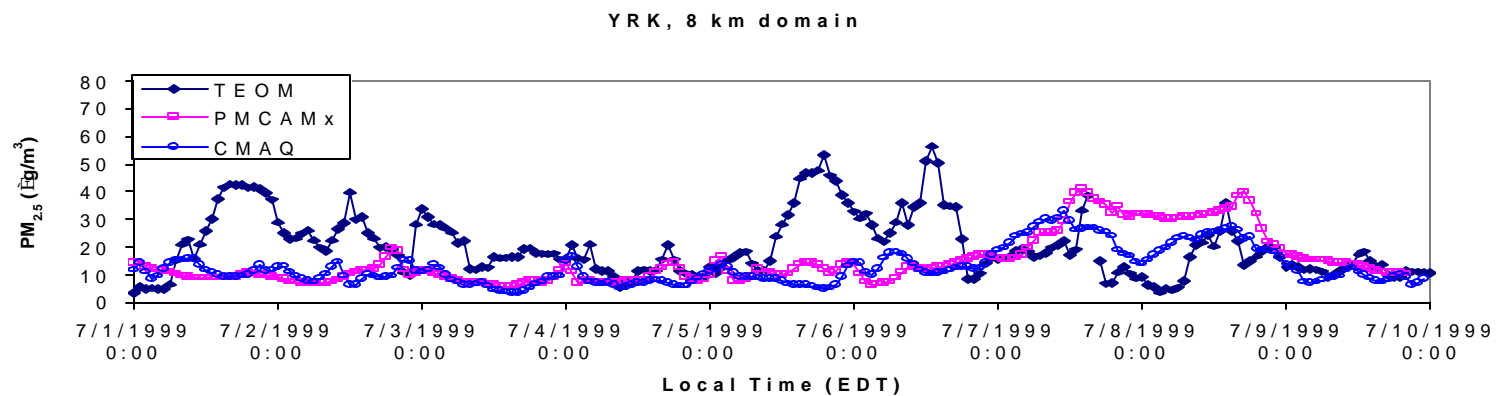
Figure 3-30.   The time series of observed and predicted PM$_{2.5}$ concentrations on July 1-9, 1999 at Yorkville, Georgia with horizontal resolutions of (a) 32 km (b) 8 km.

m^{-3}, with high concentrations (> 25 μg m^{-3}) occurring on July 1-3 and 5-8 (i.e., high PM days) and low concentrations occurring on July 4 and 9. Unlike the urban site, Yorkville has one peak PM$_{2.5}$ concentration during each day (except for July 4 during which two peaks occurred, at 1:00 a.m. and 5 p.m.), which usually occurred between noon to 7 p.m. For the coarse grid simulations (Figure 3-30 (a)), PM-CAMx significantly underpredicts the PM$_{2.5}$ concentrations on most of the high PM days (e.g., July 1-3 and July 5-6) and overpredicts those on July 4, 7-9. CMAQ also underpredicts PM$_{2.5}$ concentrations on most of the high PM days (e.g., July 1-2 and 5-6) and overpredicts most of the PM$_{2.5}$ concentrations between 7:00 p.m., July 6 through 8:00 a.m., July 9. Compared to the coarse grid simulation, PM-CAMx with the fine grid resolution gives even larger underpredictions in PM$_{2.5}$ concentrations on July 1-3 and 5-6 but closer agreement with the observations on July 7-9 (Figure 3-30 (b)). The CMAQ results with the fine grid are closer to the observations compared to the results with the coarse grid during 5:00 p.m., July 7 to July 9 but generally become even worse on the rest of the days especially on July 2-3.

3.3 Performance Evaluation

The model performance is evaluated following the protocol developed by Seigneur et al. (2002). Our evaluation focuses on the coefficient of determination (r^2), the gross error, the gross bias, the mean normalized gross error (MNGE), and the mean normalized bias (MNB) for the O$_3$ and PM predictions at the monitoring sites. For O$_3$, we use hourly O$_3$ measurements taken at 145 routine monitoring sites. Hourly PM$_{10}$ measurements from the AIRS data base are aggregated to 24-hr averages at 5 sites within the southeastern U.S. domain for use in the PM$_{10}$ evaluation. For PM$_{2.5}$ and its chemical composition, we use the measurements taken from the routine monitoring network of the Interagency Monitoring of Protected Visual Environments (IMPROVE) at four sites (Mammoth Cave National Park (MACA), KT, Great Smoky Mountains National Park (GRSM), TN, Shining Rock Wilderness Area (SHRO), TN and Sipsey Wilderness Area (SIPS), AL), the 1998-1999 Southern Oxidants Study (SOS) at three sites (Dickson (DI), Hendersonville (HEN), Cornelia Fort (CF)), and the Southeastern Aerosol Research and

Characterization study (SEARCH) at four sites (Jefferson Street (JST), Atlanta, GA; Yorkville (YRK), GA; Birmingham (BHM), AL, and Centreville (CTR), AL).

3.3.1 Evaluation of O_3 Predictions

Figures 3-31 and 3-32 show the scatter plots of the simulated vs. the observed hourly O_3 mixing ratios for all the data pairs on July 1-9, 1999. The results from both models with a 32 km horizontal resolution are shown in Figure 3-31 and those with a 8 km horizontal resolution are shown in Figure 3-32. A cut off value of 40 ppb in the observed O_3 mixing ratios was used. A high coefficient of determination (close to 1), a slope close to 1 and a low y-intercept indicate good agreement between simulated and observed values. O_3 mixing ratios are mostly overpredicted by PM-CAMx and are either overpredicted or underpredicted by CMAQ. The coefficients of determination for both models with both the fine and coarse grids are low (0.16 for both the fine and coarse grids for CMAQ and 0.08 and 0.12 for the fine and coarse grids for PM-CAMx). Compared to the coarse grid simulations, the correlation between the simulated and observed values is slightly better (with a greater slope) for CMAQ and worse (with lower r^2 and more outliers) for PM-CAMx when a fine grid is used.

Table 3-1 shows the model performance statistics for 1-hr average O_3 mixing ratios predicted by CMAQ and PM-CAMx with the fine and coarse grids averaged over 145 sampling sites on July 1-9, 1999. The statistical values were calculated using two cut off values, 40 ppb and 60 ppb. The mean observed O_3 mixing ratio over 145 sites is 57.2 ppb for a cut off value of 40 ppb and 73.3 ppb for a cut off value of 60 ppb. For the coarse grid simulations, CMAQ predicts the mean O_3 mixing ratio of 69.2 ppb for the lower cut off value and 75.8 ppb for the higher cut off value, whereas PM-CAMx predicts higher mean O_3 mixing ratios (78.4 ppb for the lower cut off value and 84.7 ppb for the higher cut off value). MNGE and MNB are 17% and 5% for CMAQ and 24% and 17% for PM-CAMx for the higher cut off value. The MNGE and MNB are much higher for both models for the lower cut off value of 40 ppb (31% and 25% for CMAQ and 46% and 42% for PM- CAMx), indicating that both models, especially PM-CAM have worse predictions for the O_3 mixing ratio ranges of 40-60 ppb. Compared to the coarse grid

(a)
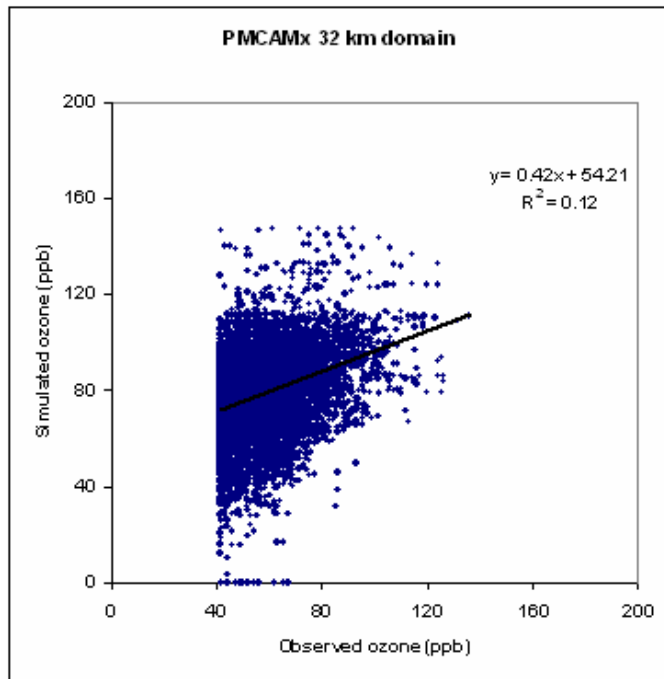
(b)
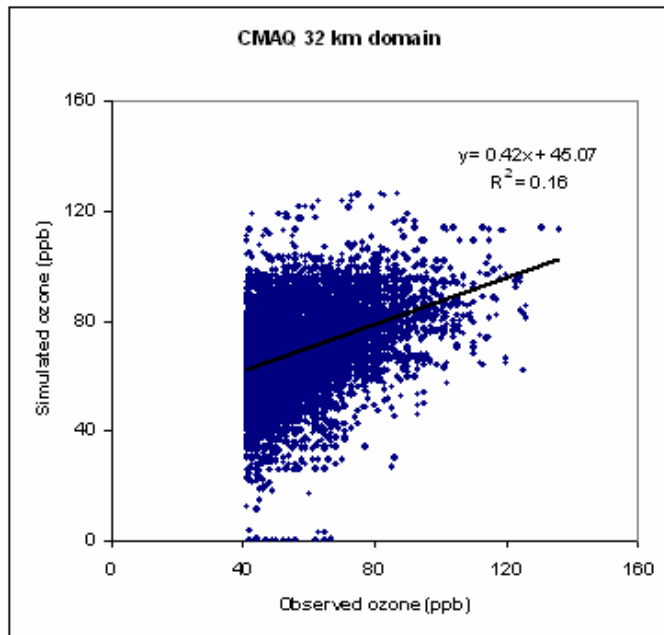
Figure 3-31.   The simulated vs. the observed O_3 mixing ratios on July 1-9, 1999 with a horizontal resolution of 32 km. The simulated O_3 mixing ratios shown are from (a) CMAQ, (b) PM-CAMx, with a cut off value of 40 ppb.

(a)
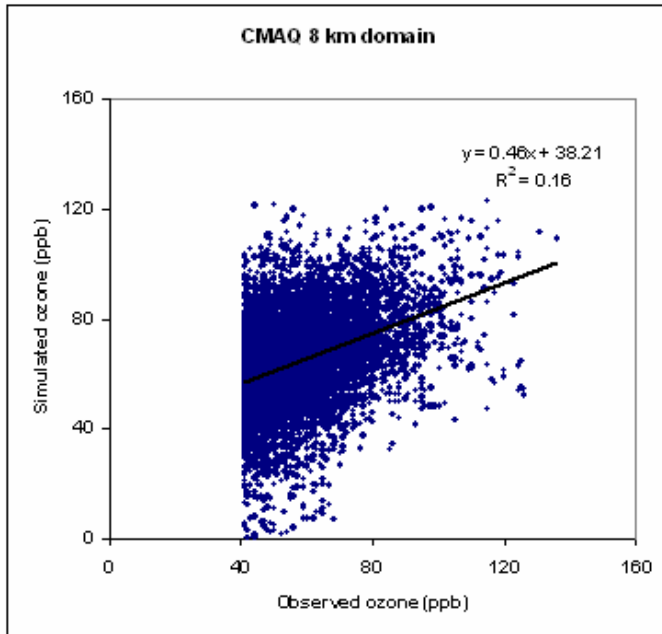
(b)
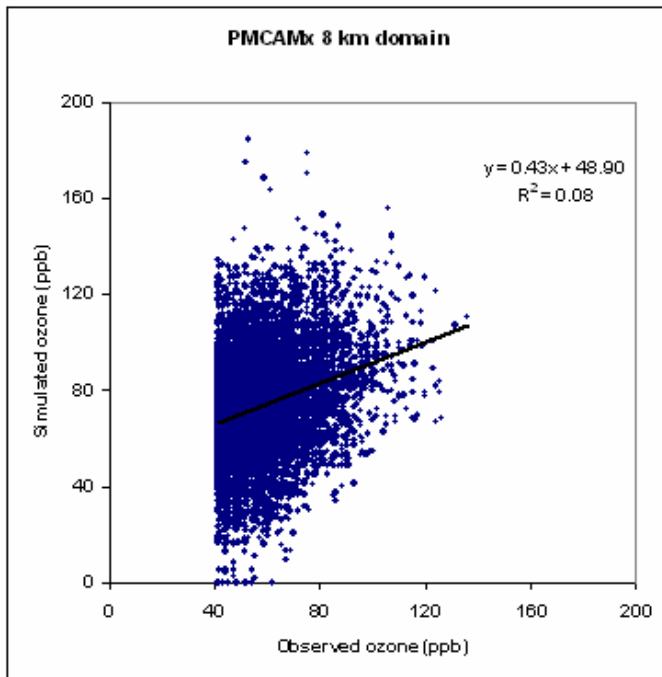
Figure 3-32.   The simulated vs. the observed O_3 mixing ratios on July 1-9, 1999 with a
horizontal resolution of 8 km. The simulated O_3 mixing ratios shown are
from (a) CMAQ, (b) PM-CAMx, with a cut off value of 40 ppb.

Table 3-1. Performance statistics for the hourly average concentrations of O_3 on July 1-9, 1999 for CMAQ and PM-CAMx simulations with 32 km and 8 km horizontal resolutions.

Grid (km)	Cut-off (ppb)	Data Pair	Mean observation	Mean prediction		Gross error		Bias		Mean normalized gross error (MNGE)		Mean Normalized bias (MNB)	
				CMAQ	PM-CAMx	CMAQ	PM-CAMx	CMAQ	PM-CAMx	CMAQ	PM-CAMx	CMAQ	PM-CAMx
32	40	10071	57.2	69.2	78.4	16.4	23.9	12.0	21.2	31.2	45.8	24.9	41.8
	60	3313	73.3	75.8	84.7	12.1	17.1	2.5	11.4	16.9	24.2	4.8	16.9
8	40	10071	57.2	64.3	73.4	14.2	21.6	7.1	16.2	26.5	40.8	15.6	32.6
	60	3313	73.3	71.6	79.9	12.5	17.0	-1.8	6.5	17.0	24.2	-1.2	10.2

simulation, both models with the fine grid predict the mean O_3 mixing ratios that are in better agreement with observations, with 64.3 ppb and 73.4 ppb for the lower cut off value for CMAQ and PM-CAMx, respectively, and 71.6 ppb and 79.9 ppb for the higher cut off value for CMAQ and PM-CAMx, respectively. Correspondingly, MNGE and MNB are lower, with 17% and 1% for CMAQ and 24% and 10% for PM-CAMx for the higher cut off value, and 27% and 16% for CMAQ and 41% and 33% for PM-CAMx for the lower cut off value. The U.S. EPA-recommended MNGE and MNB for O_3 predictions are 35% and 15%, respectively. While the performance of CMAQ in predicting O_3 with both fine and coarse grids is generally consistent with the EPA's recommendation for both low and high cut-off values, PM-CAMx does not meet the recommended performance standards for the cut-off O_3 value of 40 ppb.

3.3.2 Evaluation of PM Predictions

Figures 3-33 to 3-39 show the scatter plots of the simulated vs. the observed 24-hour average concentrations of PM_{10}, $PM_{2.5}$ and $PM_{2.5}$ chemical components for all the data pairs on July 1-9, 1999. As shown in Figure 3-33, CMAQ tends to underpredict PM_{10} concentrations, whereas PM-CAMx tends to overpredict PM_{10}. The coefficients of determination are very low (0.0 and 0.05 for the coarse and fine grids, respectively) for CMAQ. Those for PM-CAMx are even lower (0.01 and 0.04 for the coarse and fine grids, respectively), indicating little correlation between the simulated and observed PM_{10} concentrations. The $PM_{2.5}$ concentrations are either overpredicted or underpredicted by both models (see Figure 3-34). The coefficients of determination are low for predictions from both models, with 0.19 and 0.09 for the coarse and fine grids, respectively, for CMAQ and 0.15 and 0.11 for the coarse and fine grids, respectively, for PM-CAMx. For sulfate (Figure 3-35), the slopes are relatively high for both models with the coarse grid (0.68 for CMAQ and 0.7 for PM-CAMx), but both have low r^2 values (0.26 for CMAQ and 0.27 for PM-CAMx). While CMAQ with both grids tends to underpredict nitrate and ammonium (Figures 3-36 and 3-37), PM-CAMx with the coarse grid tends to significantly overpredict both nitrate and ammonium. For BC (Figure 3-38), the model predictions with the fine grid show better agreement with the observations than those

Figure 3-33.   The simulated vs. the observed PM_{10} concentrations on July 1-9, 1999.

The simulated PM_{10} concentrations shown are from: (a) CMAQ, 32 km

(top left), (b) PM-CAMx, 32 km (bottom left), (c) CMAQ, 8 km (top

right), (d) PM-CAMx, 8 km (bottom right).

$y = 0.41x + 9.63$
$R^2 = 0.19$

$y = 0.20x + 10.88$
$R^2 = 0.09$

$y = 0.58x + 10.76$
$R^2 = 0.15$

$y = 0.38x + 10.51$
$R^2 = 0.11$

Figure 3-34.   The simulated vs. the observed $PM_{2.5}$ concentrations on July 1-9, 1999.

The simulated $PM_{2.5}$ concentrations shown are from: (a) CMAQ, 32 km

(top left), (b) PM-CAMx, 32 km (bottom left), (c) CMAQ, 8 km (top

right), (d) PM-CAMx, 8 km (bottom right).
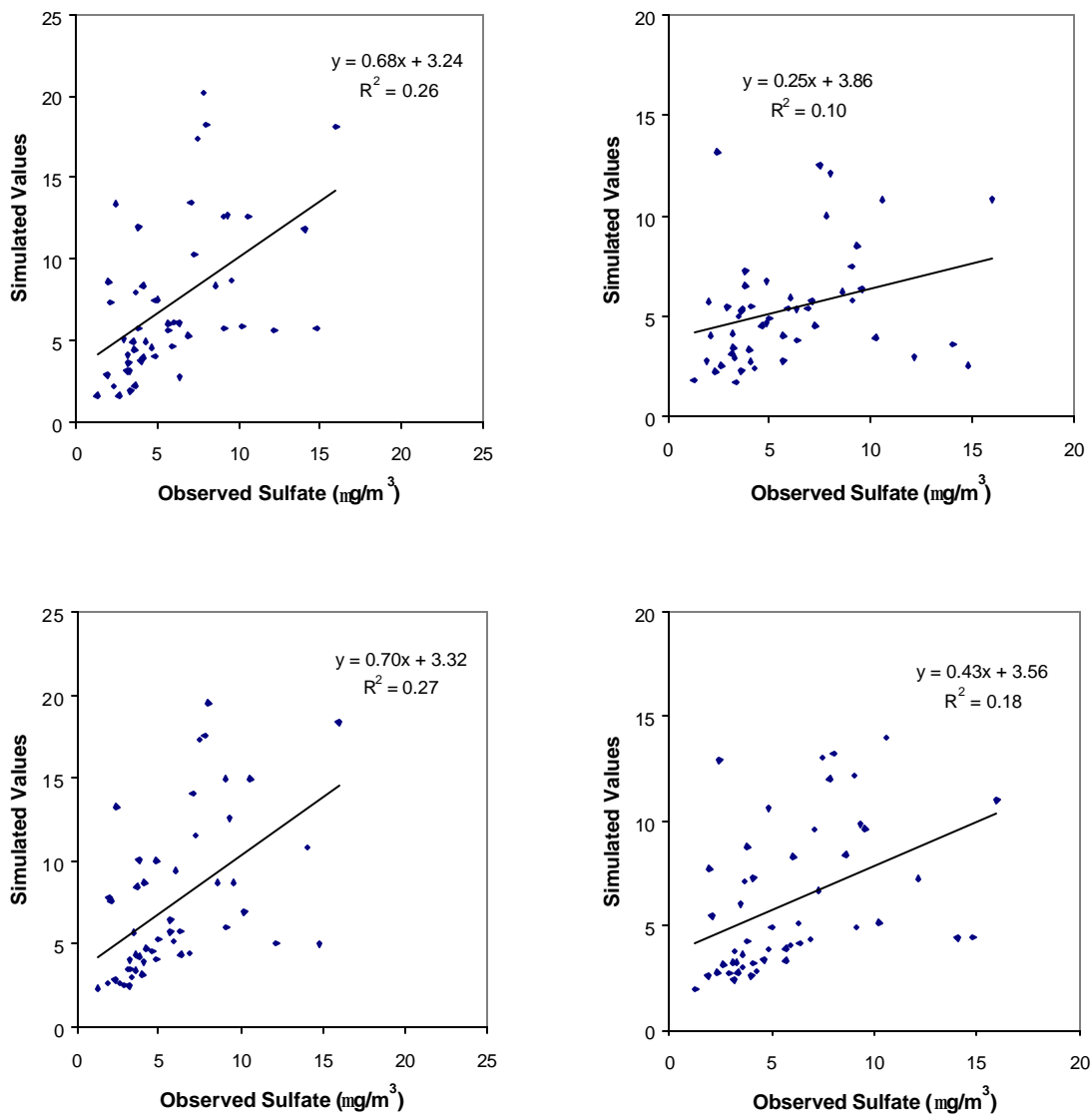
Figure 3-35.   The simulated vs. the observed sulfate concentrations on July 1-9, 1999.
The simulated sulfate concentrations shown are from: (a) CMAQ, 32 km
(top left), (b) PM-CAMx, 32 km (bottom left), (c) CMAQ, 8 km (top
right), (d) PM-CAMx, 8 km (bottom right).
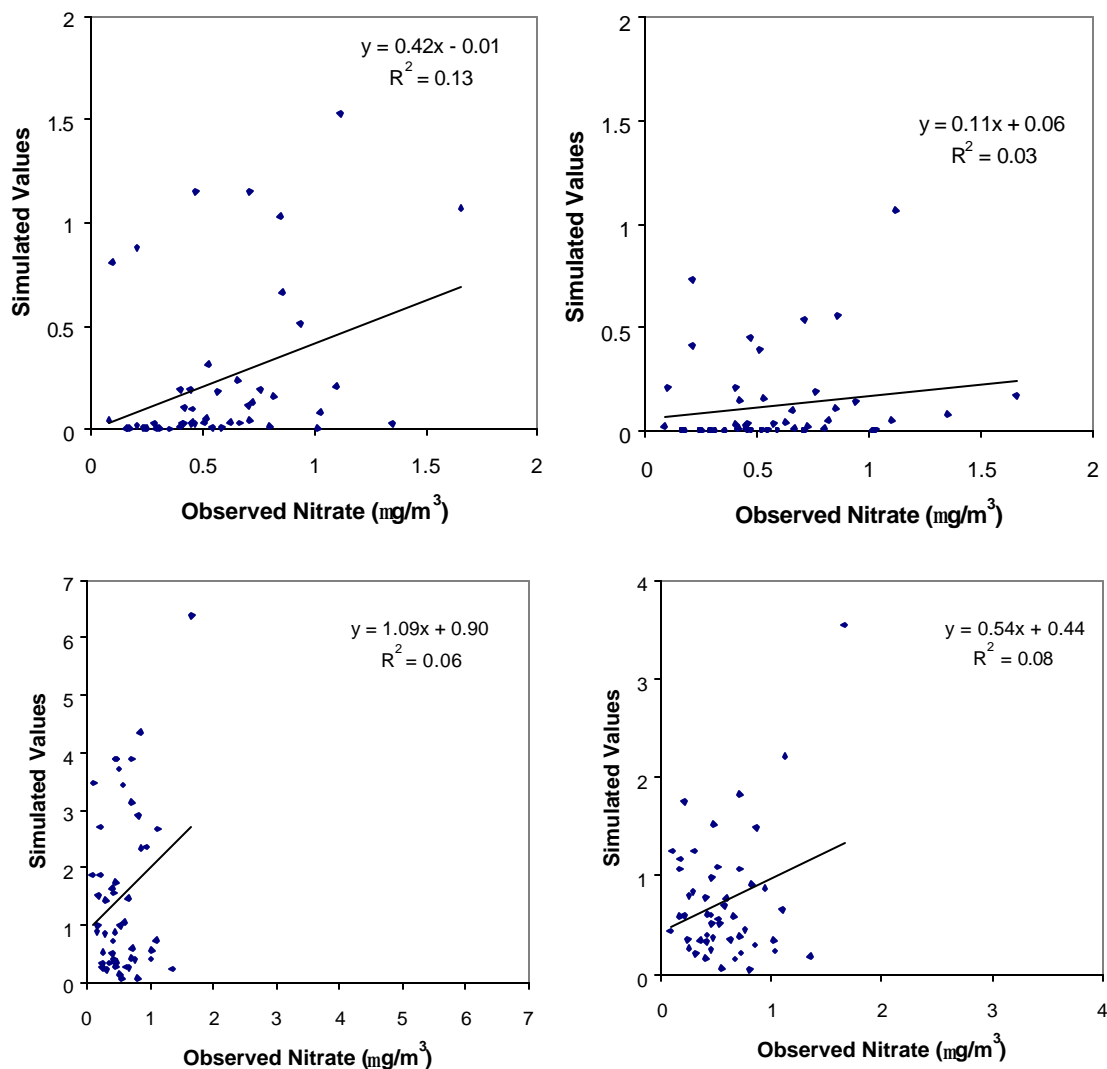
Figure 3-36. The simulated vs. the observed nitrate concentrations on July 1-9, 1999.

The simulated nitrate concentrations shown are from: (a) CMAQ, 32 km

(top left), (b) PM-CAMx, 32 km (bottom left), (c) CMAQ, 8 km (top right),

(d) PM-CAMx, 8 km (bottom right).
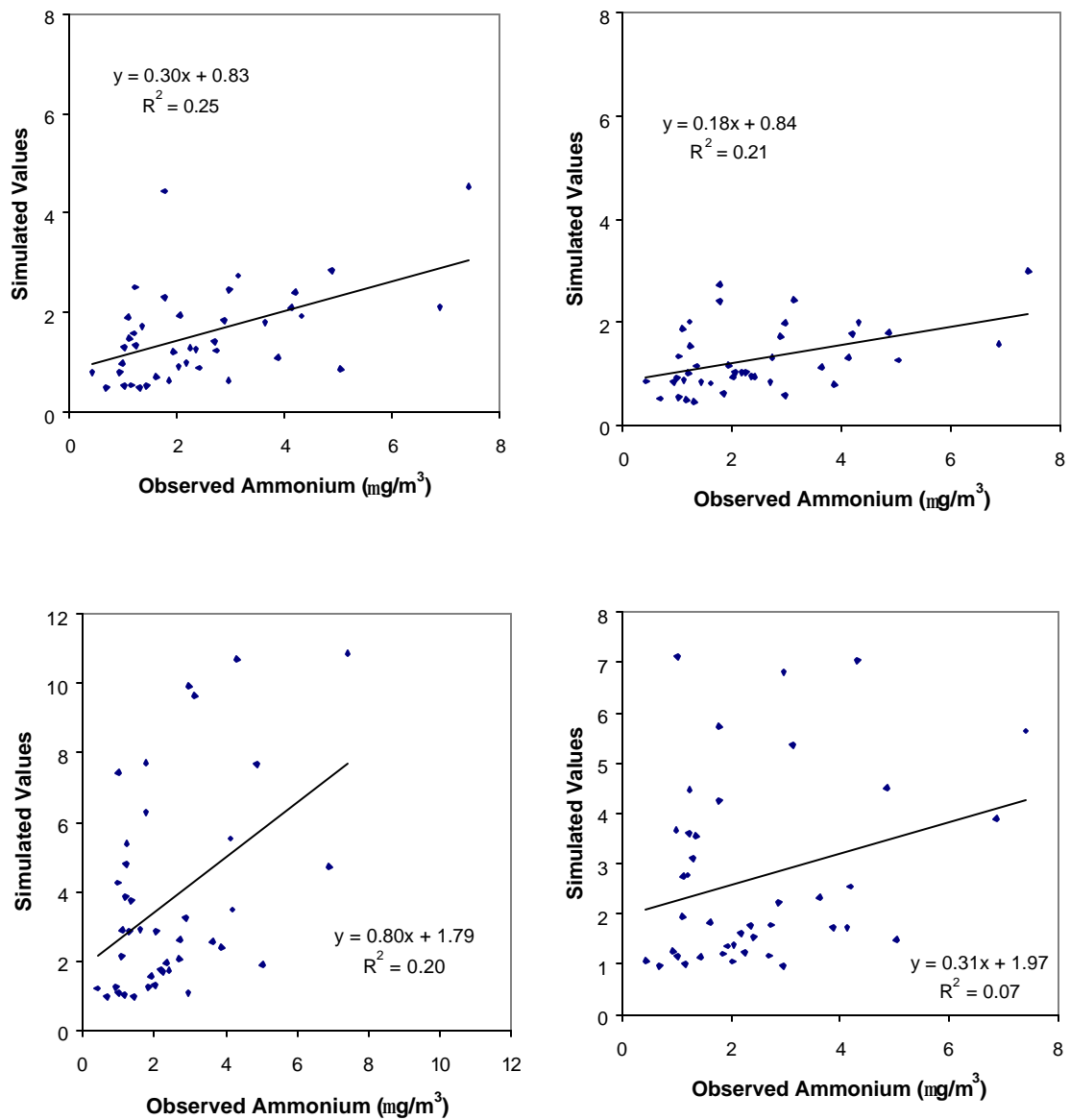
Figure 3-37. The simulated vs. the observed ammonium concentrations on July 1-9, 1999. The simulated ammonium concentrations shown are from: (a) CMAQ, 32 km (top left), (b) PM-CAMx, 32 km (bottom left), (c) CMAQ, 8 km (top right), (d) PM-CAMx, 8 km (bottom right).
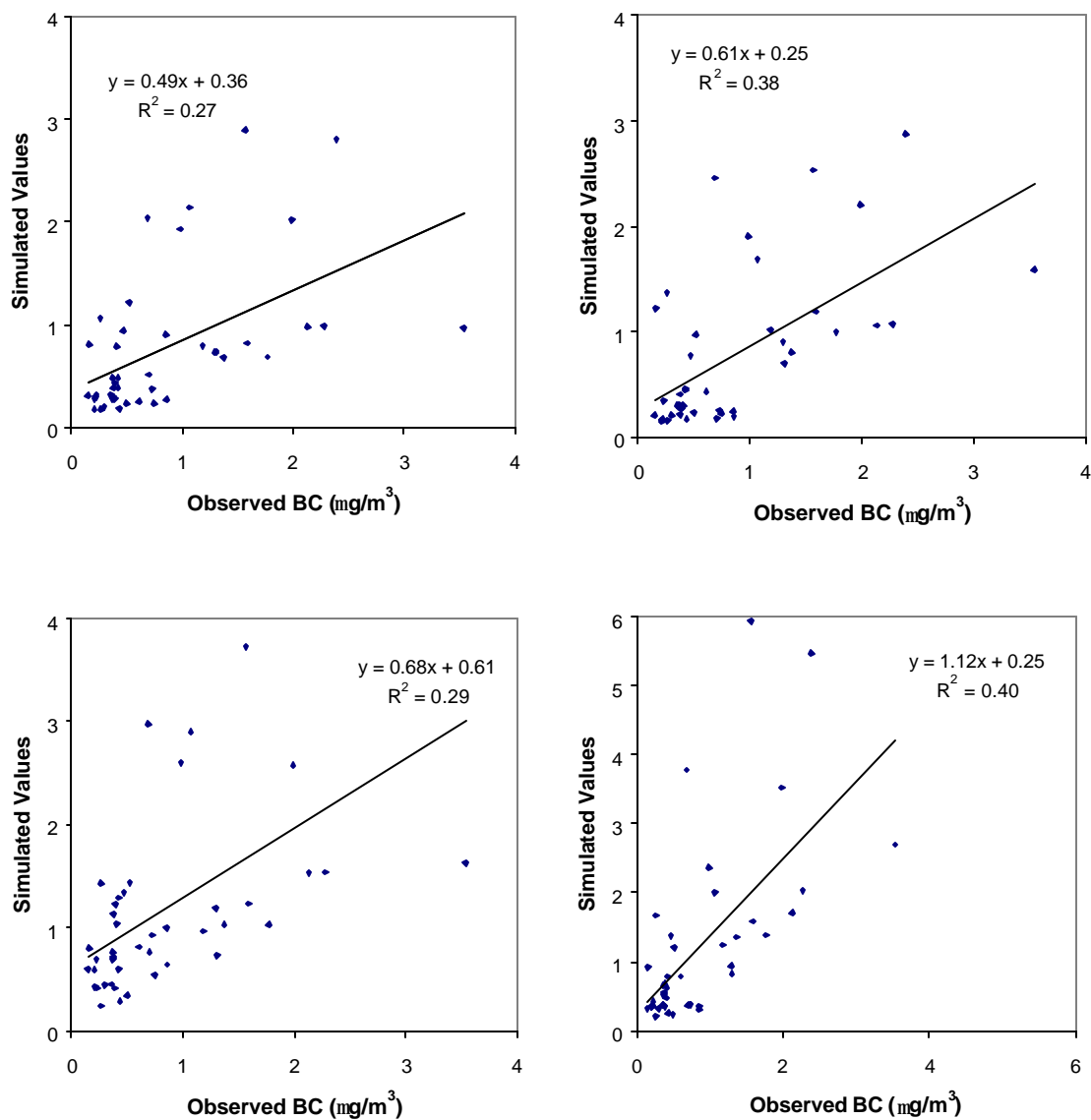
Figure 3-38.   The simulated vs. the observed BC concentrations on July 1-9, 1999. The

simulated BC concentrations shown are from: (a) CMAQ, 32 km (top

left), (b) PM-CAMx, 32 km (bottom left), (c) CMAQ, 8 km (top right), (d)
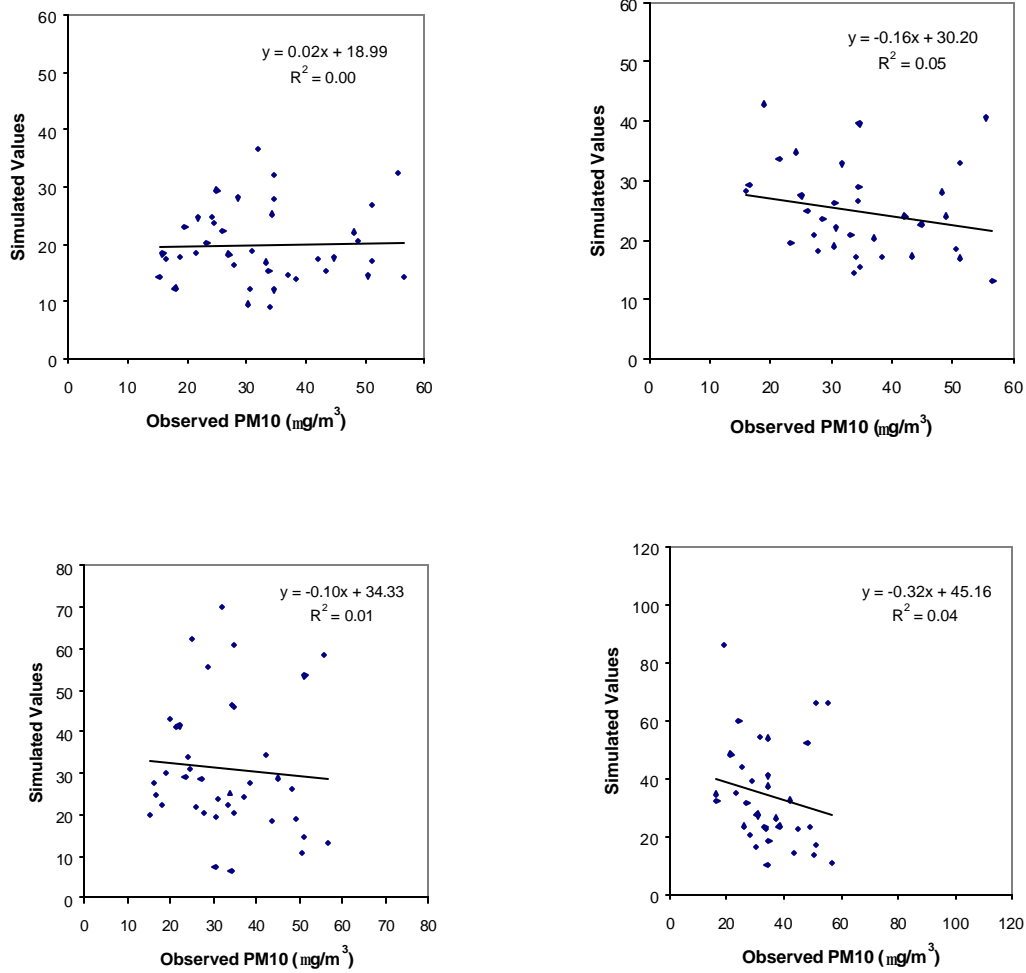
PM-CAMx, 8 km (bottom right).
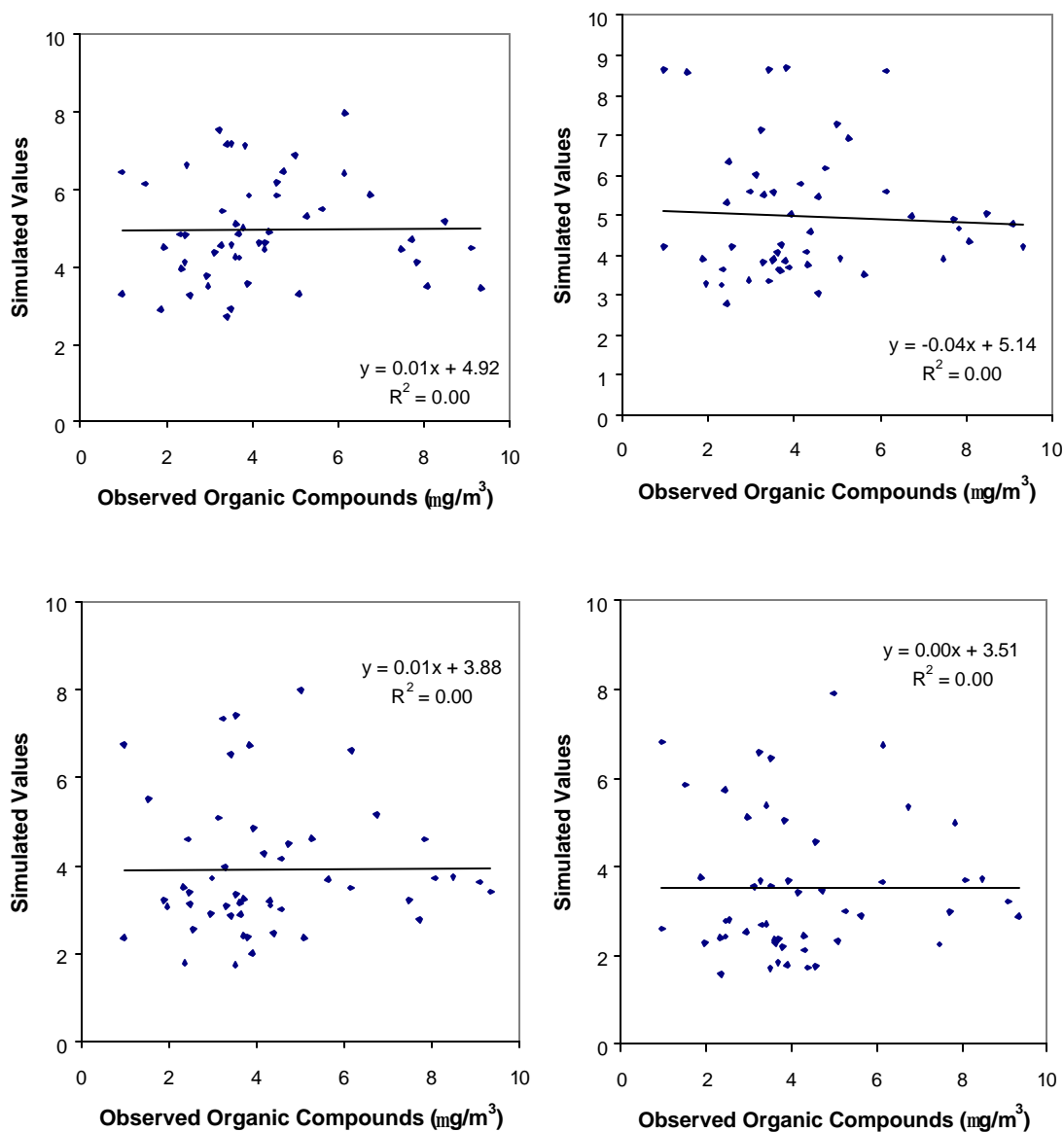
Figure 3-39. The simulated vs. the observed OM concentrations on July 1-9, 1999. The simulated OM concentrations shown are from: (a) CMAQ, 32 km (top left), (b) PM-CAMx, 32 km (bottom left), (c) CMAQ, 8 km (top right), (d) PM-CAMx, 8 km (bottom right).
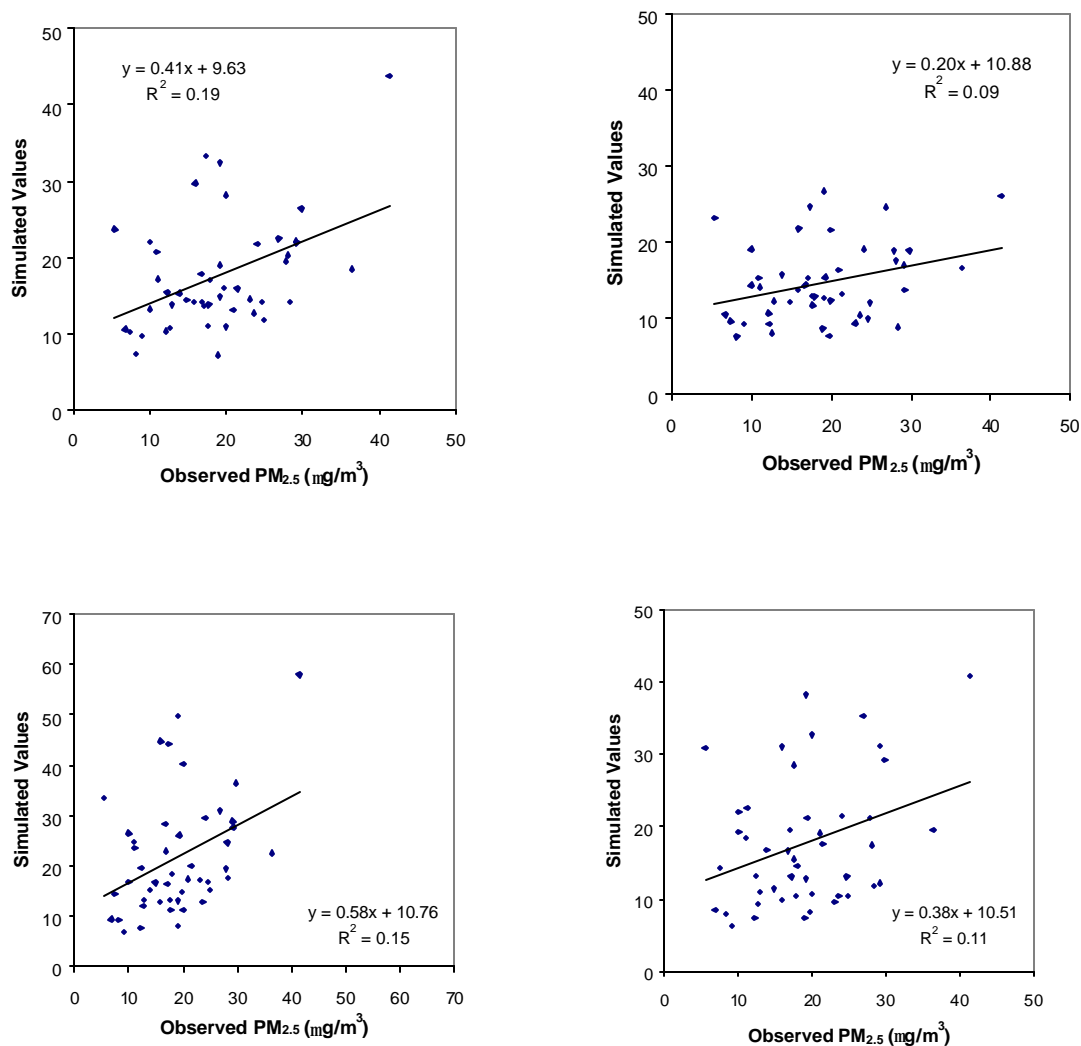
with the coarse grid for both models, as a result of better representation of BC emissions when the fine horizontal resolution is used. For OM (Figure 3-39), a poor agreement is found between the observed values and the simulated values of both models with both the fine and coarse grids.

Tables 3-2 and 3-3 show the model performance statistics for the 24-hr average concentrations of PM_{10}, $PM_{2.5}$, and $PM_{2.5}$ chemical components predicted by CMAQ and PM-CAMx with 32 km and 8 km horizontal resolutions, respectively. The values shown are the mean values averaged over all the selected sampling sites (11 sites for $PM_{2.5}$, 5 and 4 sites for PM_{10} for the coarse and fine grid simulations, respectively) on July 1-9, 1999. The mean observed concentrations are 32.9 $\mu g\ m^{-3}$ for PM_{10}, 18.9 $\mu g\ m^{-3}$ for $PM_{2.5}$, 5.9 $\mu g\ m^{-3}$ for sulfate, 0.6 $\mu g\ m^{-3}$ for nitrate, 2.4 $\mu g\ m^{-3}$ for ammonium, 0.9 $\mu g\ m^{-3}$ for BC and 4.3 $\mu g\ m^{-3}$ for OM. For the coarse grid simulations, CMAQ tends to underpredict PM_{10} (by 40%), $PM_{2.5}$ (by 8%), nitrate (by -67%), ammonium (by -33%) and BC (by 11%) and overpredict sulfate (by 19%) and OM (by 16%). PM-CAMx tends to underpredict PM10 b7 6% and OM by 9% and overpredict other species, by 14% for $PM_{2.5}$, 27% for sulfate, 150% for nitrate, 54% for ammonium and by 33% for BC. CMAQ predicts the MNGEs of $\leq 50\%$ and MNBs of -33 to 6% for PM_{10}, $PM_{2.5}$ and ammonium and MNGEs of 61-99% and MNBs of -48 to 49% for other PM components. By contrast, PM-CAMx predicts MNGEs and MNBs of 52% and 7% for PM_{10}, 56% and 30% for $PM_{2.5}$ and 58-338% and 19-305% for PM components, indicating significant overpredictions of the concentrations of PM and its components.

The significant overpredictions in PM predictions by PM-CAMx may be attributed to several major reasons including (1) the lack of wet removal for PM species in the current version of PM-CAMx; (2) a likely underprediction in the vertical mixing during the daytime (as discussed before, the vertical diffusion scheme used in PM-CAMx tends to underpredict vertical mixing, leading to overpredictions in mixing ratios of NO_x, NH_3 and other PM precursors, thus overpredictions in PM concentrations); and (3) uncertainties in the gas/particle partitioning under some conditions. Both CMAQ and PM-CAMx give the largest MNGEs for nitrate, a highly volatile species, whose formation may be sensitive to the abundance of HNO_3 (i.e., NO_x-limited), NH_3 (i.e., NH_3-limited) or ambient water vapor (i.e., H_2O-limited), depending on the chemical and

Table 3-2. Performance statistics for the 24-hr average concentrations of PM_{10}, $PM_{2.5}$, and $PM_{2.5}$ chemical components on July 1-9, 1999 for CMAQ and PM-CAMx simulations with a 32 km horizontal resolution.

Species	Data Pair	Mean observation	Mean prediction		Gross error		Bias		Mean normalized gross error (MNGE)		Mean Normalized bias (MNB)	
			CMAQ	PM-CAMx	CMAQ	PM-CAMx	CMAQ	PM-CAMx	CMAQ	PM-CAMx	CMAQ	PM-CAMx
PM_{10}	39	32.9	19.8	31.0	14.2	16.5	-13.2	-1.9	36.9	51.7	-32.6	7.2
$PM_{2.5}$	47	18.9	17.4	21.6	6.4	8.4	-1.5	2.8	39.7	56.4	5.5	30.4
Sulfate	50	5.9	7.3	7.5	2.9	3.0	1.4	1.6	60.9	60.1	41.2	44.1
Nitrate	50	0.6	0.2	1.5	0.5	1.2	-0.3	1.0	99.4	337.8	-47.5	305.4
Ammonium	41	2.4	1.6	3.7	1.2	2.1	-0.9	1.3	49.0	111.5	-20.6	87.5
BC	44	0.9	0.8	1.2	0.5	0.6	-0.1	0.3	64.4	106.9	17.7	88.7
OM	51	4.3	5.0	3.9	2.0	1.9	0.7	-0.3	65.4	57.6	48.5	19.4

Table 3-3. Performance statistics for the 24-hr average concentrations of PM_{10}, $PM_{2.5}$, and $PM_{2.5}$ chemical components on July 1-9, 1999 for CMAQ and PM-CAMx simulations with an 8 km horizontal resolution.

Species	Data Pair	Mean observation	Mean prediction		Gross error		Bias		Mean normalized gross error (MNGE)		Mean Normalized bias (MNB)	
			CMAQ	PM-CAMx	CMAQ	PM-CAMx	CMAQ	PM-CAMx	CMAQ	PM-CAMx	CMAQ	PM-CAMx
PM_{10}	34	34.9	25.0	34.2	14.8	17.9	-9.8	-0.7	42.7	58.7	-17.3	14.4
$PM_{2.5}$	47	18.9	15.2	17.6	6.7	7.6	-3.7	-1.2	37.7	49.7	-6.5	9.0
Sulfate	50	5.9	5.2	6.1	2.4	2.6	-0.7	0.2	44.8	51.7	8.7	22.9
Nitrate	50	0.6	0.2	0.7	0.5	0.5	-0.4	0.2	97.8	138.0	-49.5	98.6
Ammonium	41	2.4	1.3	2.7	1.4	1.6	-1.1	0.3	50.4	90.1	-30.7	49.7
BC	44	0.9	0.8	1.2	0.5	0.6	-0.1	0.4	71.3	88.2	19.8	63.8
OM	51	4.3	5.4	3.5	2.3	2.1	1.2	-0.7	83.9	60.1	68.2	10.3

meteorological conditions at a specific location. Both CMAQ and PM-CAMx use a bulk equilibrium approach for gas/particle mass transport, in which the same thermodynamic equilibrium module (i.e., ISORROPIA) is used to calculate partitioning and the mass changes for the condensed species are distributed among two lognormally-distributed modes for fine PM in CMAQ and ten particle size sections in PM-CAMx. As shown in Figure 3-40, ISORROPIA in both models tends to predict unrealistically high nitrate concentrations under some ambient conditions. The spikes accentuate in terms of both magnitude and frequency of occurrence when coarse grid resolution and/or multiple size sections are used, due possibly to inaccuracy in the activity coefficients used for PM species. ISORROPIA uses activity coefficients in a precalculated look-up table, which may not cover all chemical regimes, especially those for highly acidic aerosols. We conclude that the treatment of wet removal for PM species, a better scheme for vertical mixing such as the scheme that uses the TKE and an on-line calculation for the aerosol activity coefficients may significantly improve the PM predictions in PM-CAMx. While the on-line calculation for PM activity coefficients can be implemented easily in ISORROPIA, a new MM5 simulation for the July 1999 episode will need to be conducted to output TKE values that can be used to generate vertical diffusion coefficients for input into PM-CAMx.

The number of data pairs used for the evaluations of PM_{10} for the fine grid simulations is less than that used for the coarse grid simulations (34 vs. 39). This is because one site is located very close to the southern boundary of the fine grid domain and is thus excluded in the PM_{10} evaluation for the fine grid simulations. Compared to the coarse grid simulations, CMAQ with the fine grid gives closer agreement to the observations for PM_{10} (underpredited by 28%) and sulfate (underpredicted by 12%) and slightly worse underpredictions for $PM_{2.5}$ (by 20%), ammonium (by -46%), and overprediction for OM (by 26%). The PM-CAMx simulation with the fine grid significantly improves the PM predictions for all species except PM_{10} and BC. The overprediction (by 14%) changes to an underprediction (by 7%) for $PM_{2.5}$. The overpredictions are reduced from 27% to 3% for sulfate, 150% to 17% for nitrate, 54% to 13% for ammonium when the fine grid is used. CMAQ predicts MNGEs of $\leq$ 50% and MNBs of -31 to 9% for PM_{10}, $PM_{2.5}$, sulfate and ammonium and MNGEs of 71-98% and
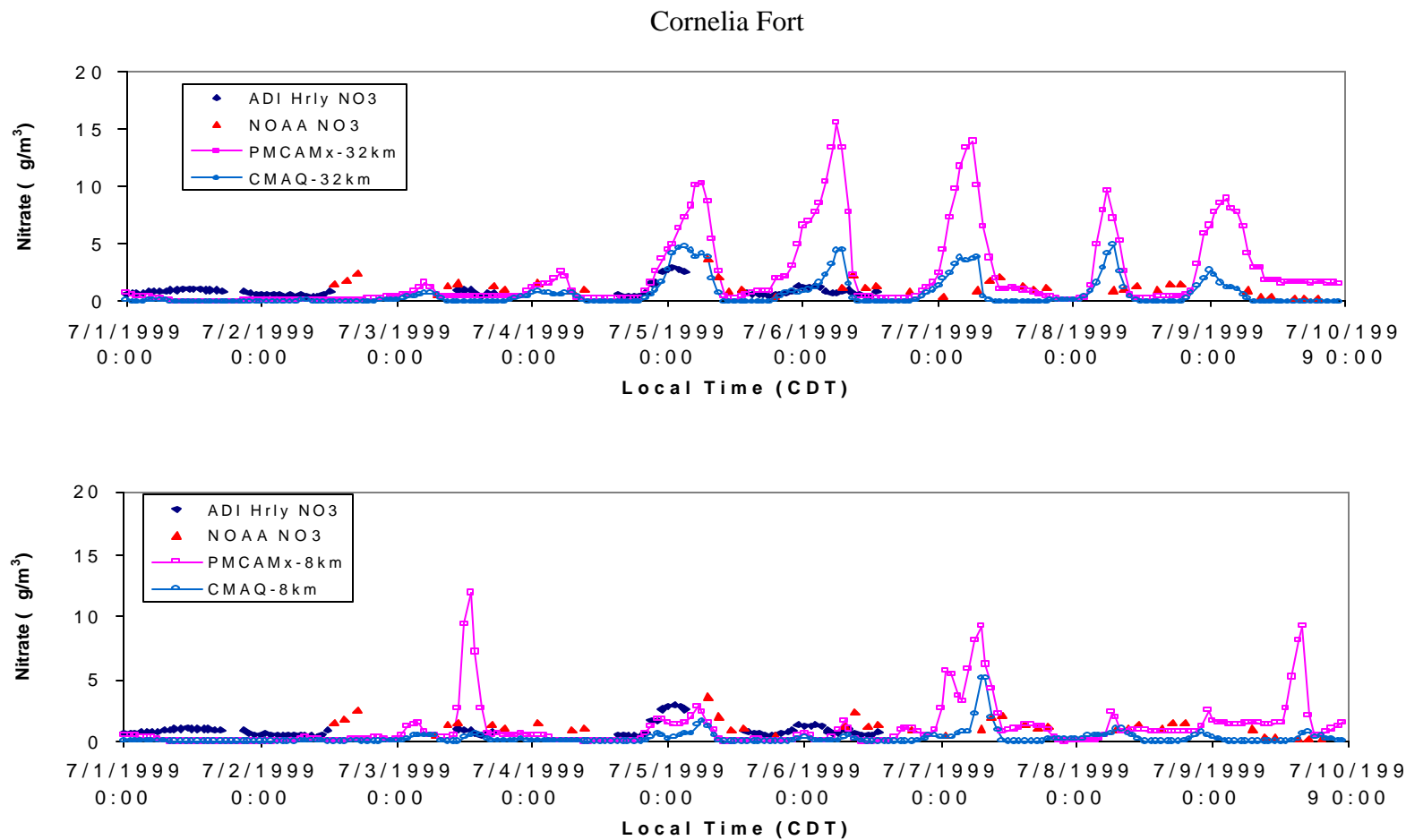
Cornelia Fort

Figure 3-40.   The time series of observed and predicted PM$_{2.5}$ nitrate concentrations on July 1-9, 1999 at Cornelia Fort, TN with horizontal resolutions of (a) 32 km (top), (b) 8 km (bottom).

MNBs of -50 to 68% for other PM components. These results are consistent with performance that can currently be expected from PM models (Seigneur, 2001; Seigneur and Moran, 2003). PM-CAMx predicts MNGEs and MNBs of 59% and 14% for PM_{10}, 50% and 9% for $PM_{2.5}$ and 51-138% and 23-99% for PM -components. Compared to the coarse grid simulation, the errors in PM predictions by PM-CAMx with the fine grid due to underpredictions in vertical mixing are less significant, since less overpredictions in $PM_{2.5}$ concentrations occurred when the fine grid is used. The lack of wet removal for PM species and possible inaccuracies in activity coefficients, however, still cause large overpredictions for concentrations of PM and its components for the PM-CAMx simulation with the fine grid.

3.4. Comparison of Computational Requirements

Both CMAQ and PM-CAMx simulations were conducted on 2-GHz Linux computers. The total CPU time and disk requirements for the simulation of the June 29-July 10 1999 episode are summarized in Table 3-4. For the coarse grid simulation, the CPU time for 12-day CMAQ simulation is 4.7 days, which is about a factor of 2.5 faster than PM-CAMx (11.7 days). For the fine grid simulation, the CPU time for CMAQ is 4 days, which is about a factor of 2.2 faster than PM-CAMx (8.6 days). PM-CAMx requires more memory than CMAQ, primarily due to the use of more PM size sections (i.e., 10 sections in PM-CAMx vs. 3 modes in CMAQ). CMAQ requires more disk space for input and output files than PM-CAMx. However, one must note that the size of outputs from both models are user-dependent. In this particular study, the output files from CMAQ include files for 3-D instantaneous (i.e., output at the last time step for each hour) and hourly-average concentrations of gaseous and particulate species, files for 3-D hourly dry and wet depositions of gaseous and particulate species and a file containing model diagnostic information. These output files are in netCDF format that can be read and viewed by PAVE. The output files from PM-CAMx are less comprehensive; they include files for 3-D instantaneous (i.e., output at the last hour for each day for a restart run for the next day) and hourly-average concentrations of gaseous and particulate species, a diagnostic file containing a tabular summary of the hourly gas and particle

Table 3-4. Computational requirements for CMAQ and PM-CAMx.

	CMAQ		PM-CAMx	
	32-km	8 km	32-km	8 km
Run Time (CPU days)[1]	4.7	4	11.7	8.6
Memory (MB)	305	190	606	524
Input (GB)	16.9	9.7	8.0	5.3
Output (GB)	31.7	18.7	8.1	16.2

1. The runtimes are for a 2 GHz Linux computer with the Portland Group FORTRAN90 compiler.

deposition rates, and a mass budget file showing the contributions of each major model process to the total budget. The concentration output files are in UAM-IV binary format that can also be read and viewed by PAVE.

4. SUMMARY AND RECOMMENDATIONS

The performance of CMAQ and PM-CAMx was evaluated for the June 29 through July 10, 1999 SOS episode. The spatial distributions of O_3 predicted by CMAQ and PM-CAMx with the two grids are quite different, especially over the eastern and southeastern U.S., where PM-CAMx tends to overestimate O_3 mixing ratios. The overpredictions in O_3 mixing ratios are likely caused by underpredictions in vertical mixing during the daytime in PM-CAMx, which lead to the mispredicted temporal and spatial abundance of O_3 precursors such as NO_x and VOCs. Differences in other aspects of model formulation such as aqueous-phase chemistry, subgrid-scale convective transport and vertical advection scheme may also contribute to the differences in the predicted abundance in O_3 and its precursors.

The spatial variations of $PM_{2.5}$ and PM_{10} concentrations in the rural areas from the western to the eastern U.S. predicted by both models are generally similar. The two models, however, differ significantly in their predictions over some urban/suburban areas in the U.S., especially in the southeastern, eastern and central U.S. Those differences between the $PM_{2.5}$ and PM_{10} predictions by the two models with the fine and coarse grids can be explained by differences in the predicted PM composition in the corresponding areas.

For the U.S. domain, CMAQ predicts that sulfate and OM are the largest and the second largest contributors to $PM_{2.5}$ concentrations for the eastern and southeastern U.S., nitrate and OM tend to dominate in California. PM-CAMx predicts that sulfate is the largest contributor to $PM_{2.5}$ concentrations for the eastern and southeastern U.S., followed by either OM or ammonium or both. PM-CAMx predicts high nitrate concentrations of 5-20 $\mu g\ m^3$ in several areas including Houston, TX, southern Louisiana, Monroe, LA, Los Angeles, CA, Fort Worth, TX, Atlanta, GA, North Birmingham, AL, and the adjacent area of South Dakota, Nebraska, and Iowa.

For the southeastern U.S. domain, CMAQ predicts sulfate to be the largest contributor in the northern portion of the domain on July 5, the northeastern portion on July 6, and the eastern and southern portions on July 7. OM is predicted to be the second largest contributor in the eastern portion on July 5 and the eastern and southern portions

on July 7. The concentrations of BC, nitrate and ammonium are below 5 μg m^{-3} in many areas of the domain. PM-CAMx predicts sulfate to be the largest contributor in the northern and eastern portions on July 5 and 6 and almost the entire domain except for a small area in the northern and southwestern portions of the domain on July 7. The second largest contributor is OM in a small area in the southern corner on July 6 or ammonium in the northeastern portion on July 5-6 or both OM and ammonium in the southeastern portion on July 7. While the concentrations of BC are below 5 μg m^{-3} in many areas of the domain, those of nitrate can be as high as 11 μg m^{-3} in several areas including Louisville, KY on July 5 and Memphis, TN on July 6-7.

Both CMAQ and PM-CAMx with the coarse grid tend to overpredict the daytime and peak O$_3$ mixing ratios. Better agreement between the observed and predicted O$_3$ temporal distributions is obtained for both models with the fine grid. The peak O$_3$ times predictions by both CMAQ and PM-CAMx with both grids were a few hours off the observed peak O$_3$ times on some days. Both CMAQ and PM-CAMx fail to reproduce correctly the observed temporal distribution of PM$_{2.5}$ and its chemical components.

For the coarse grid simulation, CMAQ predicts MNGEs and MNBs of 17% and 5% for observed O$_3$ mixing ratios > 60 ppb and 31% and 25% for observed O$_3$ mixing ratios > 40 ppb. PM-CAMx predicts MNGEs and MNBs of 24% and 17% for observed O$_3$ mixing ratios > 60 ppb and 46% and 42% for observed O$_3$ mixing ratios > 40 ppb. Both models show better performance for the fine grid than for the coarse grid. CMAQ predicts MNGE and MNB of 17% and -1% and PM-CAMX predicts MNGE and MNB of 24% and 10% for observed O$_3$ mixing ratios > 60 ppb. CMAQ predicts MNGE and MNB of 27% and 16% and PM-CAMx predicts MNGE and MNB of 41% and 33% for observed O$_3$ mixing ratios > 40 ppb. While the performance of CMAQ in predicting O$_3$ with both the fine and coarse grids is generally consistent with the EPA's recommendation for both low and high cut off values, PM-CAMx does not meet EPA's recommended performance values when the low cut off O$_3$ concentration of 40 ppb is used.

For PM predictions, CMAQ with the coarse grid predicts MNGEs of ≤ 50% and MNBs of -33 to 6% for PM$_{10}$, PM$_{2.5}$ and PM$_{2.5}$ ammonium and MNGEs of 61-99% and MNBs of -48 to 49% for other PM components. CMAQ with the fine grid predicts

MNGEs of $\leq 50\%$ and MNBs of -31 to 9% for PM_{10}, $PM_{2.5}$, $PM_{2.5}$ sulfate and $PM_{2.5}$ ammonium and MNGEs of 71-98% and MNBs of -50 to 68% for other PM components. The predictions of $PM_{2.5}$ nitrate have the largest MNGEs and MNBs. These statistics for CMAQ with both grids are generally consistent with the performance currently exxpected from PM models. There are, however, significant uncertainties in the chemical composition of $PM_{2.5}$ that will require further diagnostic investigations. In particular, spikes were sometimes predicted in nitrate concentrations due possibly to the inaccuracies in the aerosol activity coefficients under some conditions. An on-line calculation for the aerosol activity coefficients may improve the nitrate predictions in CMAQ.

PM-CAMx with the coarse grid predicts MNGEs and MNBs of 52% and 7% for PM_{10}, 56% and 30% for $PM_{2.5}$ and 58-338% and 19-305% for PM components. PM-CAMx with the fine grid predicts MNGEs and MNBs of 59% and 14% for PM_{10}, 50% and 9% for $PM_{2.5}$ and 51-138% and 23-99% for PM components. The predictions of $PM_{2.5}$ nitrate have the largest MNGEs and MNBs. Although the PM-CAMx simulation with the fine grid significantly improves the PM predictions, large overpredictions still remain for most PM species, especially for nitrate (by 50%) and ammonium (by 33%). The significant overpredictions in PM predictions by PM-CAMx may be attributed to several major reasons including (1) the lack of wet removal for PM species in the current version of PM-CAMx; (2) a likely underprediction in the vertical mixing during the daytime; (3) the uncertainties in the gas/particle partitioning under some conditions in PM-CAMx. The treatment of wet removal for PM species, a better scheme for vertical mixing and an on-line calculation for the aerosol activity coefficients may significantly improve the PM predictions in PM-CAMx.

5. REFERENCES

Binkowski, F.S. and U. Shankar, 1995. The regional particulate matter model, 1: Model description and preliminary results, *J. Geophys. Res.,* **100**, 26191-26209.

Byun and Ching (1999). Science algorithms of the EPA Models-3 Community Multiscale Air Quality (CMAQ) Modeling System. EPA/600/R-99/030, U.S. Environmental Protection Agency, Research Triangle Park, NC.

Capaldo, K.P., C. Pilinis, and S.N. Pandis, 2000. A computationally efficient hybrid approach for dynamic gas/aerosol transfer in air quality models, *Atmos. Environ.*, **34**, 3617-3627.

Cowling E.B., W.L. Chameides, C.S. Kiang, F.C. Fehsenfeld and J.F. Meagher, 1998. Introduction to special section: Southern Oxidants Study Nashville/Middle Tennessee Ozone Study, *J. Geophys. Res.*, **103**, 22,209-22,212.

Emery, C. 2002. Private communication, ENVIRON, Novato, CA.

ENVIRON, 2000, User's Guide: Comprehensive Air Quality Model with Extensions (CAMx), Version 3.00, ENVIRON International Corporation, 101 Rowland Way, Suite 220, Novato, CA 94945.

ENVIRON, 2002, Aerosol Modeling with PMCAMx, Supplement to CAMx v3.00 User's Guide, June.

EPA, 2001. Draft Guidance for Demonstrating Attainment of Air Quality Goals for PM2.5 and Regional Haze, U.S. Environmental Protection Agency, Research Triangle Park, NC.

Harrington, D.Y. and S.M. Kreidenweis, 1998. Simulation of sulfate aerosol dynamics, I. Model description, *Atmos. Environ.*, **32**, 1691-1700.

Jang, J.-C. C., H.E. Jeffries, D. Byun and J.E. Pleim, 1995. Sensitivity of Ozone to Model grid Resolution – I. Application of High-Resolution Regional Acid Deposition Model, *Atmos. Environ.*, **29**, 3085-3100.

Pandis, S.N., A.S. Wexler, J.H. Seinfeld, 1993. Secondary organic aerosol formation and transport – II. Predicting the ambient secondary organic aerosol size distribution, *Atmos. Environ.*, **27A**, 2403-2416.

Pun, B.K., S.-Y. Wu, and C. Seigneur, 2002. Contribution of biogenic emissions to the formation of ozone and particulate matter in the Eastern United States*, Environ. Sci. Technol.*, **36**, 3586-3596.

Russell, L.M., S.N. Pandis, J.H. Seinfeld, 1994. Aerosol production and growth in the marine boundary layer, *J. Geophys. Res.* **99**, 20989-21003.

Seigneur, C. and M. Moran, 2003. Chemical Transport Models, Chapter 8, *in* Particulate Matter Science for Policy Makers: A NARSTO Assessment, EPRI 1007735, P.H. McMurry, M. Shepherd and J. Vickery, eds.

Seigneur, C., B. Pun, and Y. Zhang, 2002. Modeling protocol for the performance evaluation of CMAQ and PM-CAMx for the July 1999 SOS Episode, report prepared for Coordinating Research Council, Alpharetta, GA. Document Number CP131-02-01.

Seigneur, C., 2001. Current status of air quality models for particulate matter, *J. Air Waste Manage. Assoc*., **51**, 1508-1521.

Seigneur, C., B. Pun, P. Pai, J. F. Louis, P. Solomon, C. Emery, R. Morris, M. Zahniser, D. Worsnop, P. Koutrakis, W. White and I. Tombach, 2000. Guidance for the performance evaluation of three-dimensional air quality modeling systems for particulate matter and visibility, *J. Air Waste Manage. Assoc*., **50**, 588-599.

Seinfeld, J.H., 1986. Atmospheric Chemistry and Physics of Air Pollution, Wiley, New York.

Smagorinsky, J., 1963. General circulation experiments with the primitive equations: 1. The basic experiment, *Mon. Wea. Rev*., **91**, 99-164.

TVA, 2003. MM5 Meteorological Simulation on Nashville 1999 SOS Episode, draft report, TVA.

Yarwood, G. 2002. Private communication, ENVIRON, Novato, CA.